

CHARACTERISATION OF OPTICAL FIBRE AMPLIFIERS:

**amplifiers for the 632.8 nm He-Ne wavelength in
praseodymium-doped ZBLAN.**

A thesis submitted

by

Bill Petar Petreski

for the degree of

DOCTOR OF PHILOSOPHY

Optical Technology Research Laboratory,

Department of Applied Physics,

Victoria University of Technology

February, 1997.



FTS THESIS
621.3692 PET
30001005084886
Petreski, Bill Petar
Characterisation of optical
fibre amplifiers :
amplifiers for the 632.8 nm

Declaration

I, **Bill Petar Petreski**, declare that the thesis titled,

“Characterisation of optical fibre amplifiers: amplifiers for the 632.8 nm He-Ne wavelength in praseodymium-doped ZBLAN”

is my own work and has not been submitted previously, in whole or in part, in respect of any other academic award.

A handwritten signature in black ink, appearing to read 'Bill Petreski', with a long horizontal stroke extending to the right.

Bill Petreski,

dated the 3rd day of February, 1997

Acknowledgments

I would firstly like to thank Prof. David Booth for giving me the opportunity and having confidence in my ability and the Department of Applied Physics for the provision of a Postgraduate Scholarship.

I am very grateful to Mr. Ken Clarke of Telstra Research Laboratory for his willingness and discussion in all matters of this research and for making available praseodymium-doped bulk glasses and fibre. The helpful assistance of Dr. Min Gu and Mr. Steven Schilders, during the collaborative work in the imaging laboratory, is appreciated. I would also like to thank my fellow post-graduate students for their friendship and assistance when it was required.

Of the technical staff, I would most like to thank Mr. Alex Shelamoff and Mr. Tibor Kovacs for their helpful assistance with the design of electronic apparatus. From the mechanical workshop I would like to thank Mr. Mark Kivinen and Mr. Donald Ermel for their helpful consultation and construction of necessary equipment. In addition I would like to thank all the other academic, technical and administrative staff from the Department of Applied Physics, Victoria University.

I would like to thank Dr. Michael Murphy for his ideas, supervision and guidance during the initial stages of this research. I acknowledge Dr. Stephen Collins for his consistent contribution in his role as secondary supervisor. Primarily, I would like to thank my supervisor, Dr. Peter Farrell for all his support, guidance and encouragement he has given over the years I have worked with him. He has played an important part in the development of this work since taking over the role of primary supervisor.

Finally, I would like to thank my family including my father Petar, mother Gorica, sister Karolina and Stefka, Bill and Benjamin who really made it possible. Deepest appreciation is given to Leanne for her encouragement and patience during the duration of this PhD program.

Abstract

An investigation of small-signal amplification on the ${}^3\text{P}_0 \rightarrow {}^3\text{F}_2$ transition in a praseodymium-doped fluorozirconate optical fibre at the 632.8 nm He-Ne wavelength, has been conducted. The optical gain is fundamentally related to the spectroscopic characteristics of praseodymium-doped in a fluorozirconate glass host together with optical fibre parameters, that determine the physical characteristics of the waveguide. These parameters have been experimentally determined independently of the gain and used to model the performance of the amplifier.

The components integral to the optical fibre amplifier include the praseodymium-doped fluorozirconate optical fibre, the optical pump laser and the He-Ne signal laser. Ground state ions were excited into the ${}^3\text{P}_0$ state of praseodymium using an argon-ion laser tuned to 476.5 nm. The small signal gain, on the ${}^3\text{P}_0 \rightarrow {}^3\text{F}_2$ transition, was measured as a function of length, input signal power and input pump power. A slope efficiency of 0.15 dB/mW was realised with a maximum of 14 dB gain reported.

The spectroscopic parameters that influence the optical gain on the ${}^3\text{P}_0 \rightarrow {}^3\text{F}_2$ transition in praseodymium-doped fluorozirconate glass were measured. The branching ratio, for the ${}^3\text{P}_0 \rightarrow {}^3\text{F}_2$ transition, was measured to be 15%. The fluorescence lifetime of the ${}^3\text{P}_0$ state, measured for varying dopant concentrations ranging from 2.8×10^{25} ions/m³ to 67×10^{25} ions/m³, was found to vary between 49 μs and 33 μs respectively. The emission cross-section (σ_s^e) at the signal

wavelength was calculated to be $2.1 \pm 0.2 \times 10^{-24} \text{ m}^2$ at 632.8 nm while the absorption cross-section (σ_p^a) at the pump wavelength (476.5 nm) was calculated to be $0.14 \pm 0.02 \times 10^{-24} \text{ m}^2$.

The waveguiding properties that influence the small signal gain were also measured. The intensity spot-sizes ($\omega_{s,p}$) of the fundamental mode for the pump and signal beams were determined from Gaussian approximations given by the Marcuse polynomial ($\omega_s = 1.67 \text{ }\mu\text{m}$, $\omega_p = 1.54 \text{ }\mu\text{m}$), from Bessel function solutions ($\omega_s = 1.75 \text{ }\mu\text{m}$, $\omega_p = 1.65 \text{ }\mu\text{m}$) and from near field measurements ($\omega_s = 1.6 \pm 0.1 \text{ }\mu\text{m}$, $\omega_p = 1.47 \text{ }\mu\text{m}$) of the mode profile.

From fluorescence lifetime measurements and a rate equation analysis of the level dynamics, values for a cross-relaxation parameter ($\alpha_{cr} = 2.6 \pm 0.1 \times 10^{-23} \text{ m}^3/\text{s}$) and the lifetime in the limit of zero concentration ($\tau(\rho \rightarrow 0) = 49.8 \pm 0.3 \text{ }\mu\text{s}$) were obtained. The concentration profile and the absolute concentration of the praseodymium-doped fluorozirconate optical fibre were determined by using spatially resolved fluorescence lifetime measurements with a confocal microscope. These measurements are novel in that they rely directly on concentration-dependent processes in the material and as a result do not require calibration of optical equipment.

The spectroscopic and physical parameters of the amplifier components were measured independently of the gain and used to model the performance of the amplifier. The behaviour of the amplifier was consistent with the predictions of the model. Indeed, the agreement between the calculated gain, using the measured parameters, and the measured gain indicates that the important processes that

influence the gain characteristics of the amplifier have been included. The importance of the work presented in this Thesis is that much of the existing amplifier technology has been extended for possible application in the expanding field of optical fibre sensor systems.

Table of Contents

	Page
DECLARATION.....	i
ACKNOWLEDGMENTS.....	ii
ABSTRACT.....	iv
TABLE OF CONTENTS.....	vii
CHAPTER 1. INTRODUCTION.	
1.1 Introduction.....	1-2
1.1.1 Introduction.....	1-2
1.1.2 Applications of optical fibre amplifiers.....	1-3
1.1.3 Types of optical amplifiers.....	1-6
1.2 Historical overview.....	1-9
1.3 Scope of thesis.....	1-12
CHAPTER 2. MODELLING OF OPTICAL FIBRE AMPLIFIERS.	
2.1 Introduction.....	2-2
2.2 Idealised three- and four-level amplifier/laser systems.....	2-3
2.3 Propagation of pump and signal beams in an optical fibre.....	2-10
2.4 Analytic approximations for the small signal gain coefficient.....	2-17
2.4.1 Introduction.....	2-17
2.4.2 Approximation for a four-level system.....	2-18

2.4.3 Approximation for a three-level system.....	2-21
2.5 Conclusion.....	2-23

**CHAPTER 3. SPECTROSCOPIC CHARACTERISATION OF
PRASEODYMIUM-DOPED FLUOROZIRCONATE
GLASS SAMPLES**

3.1 Introduction.....	3-2
3.2 Material properties of rare-earth-doped glass.....	3-3
3.3 Attenuation measurements.....	3-8
3.4 Measurement of radiative transitions.....	3-15
3.5 Calculation of non-radiative transitions	3-25
3.6 Measurement of the fluorescence lifetime of the 3P_0 state.....	3-29
3.6.1 Introduction.....	3-29
3.6.2 Laser beam modulation.....	3-31
3.6.3 Experimental measurements and results.....	3-34
3.7 Calculation of absorption and emission cross-sections.....	3-41
3.8 Ion-ion interactions in praseodymium.....	3-46
3.8.1 Introduction.....	3-46
3.8.2 Cross-relaxation and energy transfer in praseodymium.....	3-49
3.8.3 Rate equation model.....	3-52
3.8.4 Effects on gain.....	3-58
3.9 Conclusion.....	3-60

**CHAPTER 4. CHARACTERISATION OF PRASEODYMIUM DOPED
FIBRE PARAMETERS**

4.1 Introduction.....	4-2
4.2 Measurement of the mode profile and determination of the intensity spot-size.....	4-3
4.2.1 Introduction.....	4-3
4.2.2 Confocal scanning images of the mode profile.....	4-6
4.2.3 Determination of the intensity spot-size from the mode profile.....	4-10
4.3 Measurement of the concentration profile.....	4-14
4.3.1 Introduction.....	4-14
4.3.2 Experimental measurements and results.....	4-17
4.4 Conclusion	4-23

**CHAPTER 5. AMPLIFICATION AT THE 632.8 nm He-Ne
WAVELENGTH IN PRASEODYMIUM-DOPED
FLUOROZIRCONATE OPTICAL FIBRE**

5.1 Introduction.....	5-2
5.2 General experimental arrangement.....	5-3
5.3 Measurement of small signal gain.....	5-9
5.4 Rate equation model and calculation of gain.....	5-18
5.5 Conclusion.....	5-26

CHAPTER 6 *CONCLUSION AND FUTURE WORK*

6.1 Conclusion..... 6-2
6.2 Future work..... 6-8

REFERENCES R-1

APPENDICES

A.1 List of figures..... A-2
A.2 List of tables..... A-6
A.3 List of symbols..... A-7

PUBLICATIONS

P.1 Journal articles..... P-2
P.2 International conference publications..... P-3
P.3 National conference publications..... P-5
P.4 Other publications..... P-6

This Thesis describes optical characterisation of rare-earth-doped optical fibre amplifiers. An investigation of small-signal amplification on the ${}^3P_0 \rightarrow {}^3F_2$ transition in a praseodymium-doped fluorozirconate optical fibre at the 632.8 nm He-Ne wavelength, has been conducted.

As found by other authors, the single-pass small-signal gain is dependent upon the spectroscopic parameters of the rare-earth-ion and the waveguiding properties of the optical fibre. The spectroscopic parameters that influence the optical gain on the ${}^3P_0 \rightarrow {}^3F_2$ transition in praseodymium-doped fluorozirconate glass are the absorption cross-section at the pump wavelength (σ_p^a), emission cross-section at the signal wavelength (σ_s^e), the branching ratio of the ${}^3P_0 \rightarrow {}^3F_2$ transition (β), the lifetime of the 3P_0 state (τ) and ion-ion interactions such as cross relaxation described by the cross-relaxation parameter (α_{cr}). For the ${}^3P_0 \rightarrow {}^3F_2$ transition, the branching ratio was measured to be about 15%. The fluorescence lifetime of the 3P_0 state, measured for varying dopant concentrations ranging from 2.6×10^{25} ions/m³ to 61×10^{25} ions/m³, was found to vary between 49 μ s and 33 μ s respectively. From fluorescence lifetime measurements and a rate equation analysis of the level dynamics, values for a cross-relaxation parameter (α_{cr}) and the lifetime in the limit of zero concentration ($\tau(\rho \rightarrow 0)$) were also obtained. The cross-relaxation parameter was calculated to be $2.8 \pm 0.1 \times 10^{-23}$ m³/s and was obtained from a least squares fit of Equation 3.8.3.7 to the lifetime measurements as a function of concentration. From the same least squares fit, the lifetime in the limit of zero concentration was determined to be 49.8 ± 0.3 μ s. From the fluorescence lifetime measurements and measurement of the branching ratio of the ${}^3P_0 \rightarrow {}^3F_2$ transition, the absorption and

emission cross-sections were calculated using Fuchtbauer-Ladenburg analysis. The emission cross-section was calculated to be about $2.4 \pm 0.2 \times 10^{-24} \text{ m}^2$ at 632.8 nm while the absorption cross-section at the pump wavelength (476.5 nm) was calculated to be $0.15 \pm 0.02 \times 10^{-24} \text{ m}^2$.

The waveguiding properties that influence the small-signal are the intensity spot-size of the fundamental mode and the dopant ion distribution. The intensity spot-sizes ($\omega_{s,p}$) of the fundamental mode for the pump and signal beams were determined from Gaussian approximations given by the Marcuse polynomial ($\omega_s = 1.67 \text{ }\mu\text{m}$, $\omega_p = 1.54 \text{ }\mu\text{m}$), from Bessel function solutions ($\omega_s = 1.75 \text{ }\mu\text{m}$, $\omega_p = 1.65 \text{ }\mu\text{m}$) and from near field measurements ($\omega_s = 1.6 \pm 0.1 \text{ }\mu\text{m}$, $\omega_p = 1.47 \text{ }\mu\text{m}$) of the mode profile. The concentration profile and the absolute concentration of the praseodymium-doped fluorozirconate optical fibre were determined by using spatially resolved fluorescence lifetime measurements with a confocal microscope. The measurements presented in this Thesis are novel in that they rely directly on concentration-dependent processes in the material and as a result do not require calibration. The results indicate to some extent that the dopant ion distribution is radially constant.

Measurements of the small-signal amplification at 632.8 nm have been performed on a number of fibre samples. The best results indicate a slope efficiency of 0.15 dB/mW with upto 14 dB net gain reported. Apart from experimental measurements, the gain was also evaluated theoretically by using many of the spectroscopic parameters and the fibre waveguiding parameters. Evidently the calculated gain compared well with the measured gain. Indeed, the agreement between the calculated gain, using the measured parameters, and the measured gain

indicates that the important processes that influence the gain characteristics of the amplifier have been included.

The work conducted in this Thesis complements other work on optical fibre amplifiers.

Chapter 1

INTRODUCTION

- 1.1 Introduction
 - 1.1.1 Introduction
 - 1.1.2 Applications of optical fibre amplifiers
 - 1.1.3 Types of optical amplifiers
- 1.2 Historical overview
- 1.3 Scope of thesis

1.1 INTRODUCTION

1.1.1 INTRODUCTION

In the past two decades there has been considerable investment into research and development of optical fibre technology for communication systems. Optical fibre is an attractive medium mainly because of its larger bandwidth, lower attenuation and its ability to carry higher data rates over longer distances compared to other transmission media [Agrawal G.P., 1992]. Optical fibre technology has also been developing in other application areas, most noticeably in the area of sensors [Culshaw B. and Dakin J., 1988/1989]. One attraction of optical fibre sensors is the possibility of incorporating many of them in a multiplexed system [Gambling W.A., 1993], thereby allowing either a number of parameters to be measured or a single parameter to be measured at several different points in a network. Since optical fibre systems incorporating sensors are not unlike those in communications networks, much of the technology developed for communication systems may also be applied to sensing systems.

Comparatively recent developments in optical fibre communication are the praseodymium-doped-fibre amplifier (PrDFA) [Ohishi Y. *et al.*, 1991; Durteste Y. *et al.*, 1991; Carter S. *et al.*, 1991; Sugawa T. and Miyajima Y., 1991; Miyajima Y. *et al.*, 1991] and the erbium-doped-fibre-amplifier (EDFA) [Mears R.J. *et al.*, 1987; Whitley T.J., 1988; Shimizu M. *et al.*, 1990; Suzuki K. *et al.*, 1990; Horiguchi M. *et al.*, 1990; Desurvire E., 1994a & ba & b]. These devices are used to amplify light, in the second (around 1310 nm) and the third (around 1550 nm) communication

windows respectively, so that the inevitable attenuation and power division in multiport couplers may be overcome.

Optical amplifier technology may also be applied to sensor systems. However, for optical systems, including sensor systems, it is often preferable to use visible wavelength sources as they offer certain sensitivity advantages over infrared (IR) laser diodes and the convenience of lower cost silicon detectors. The 632.8 nm He-Ne laser is attractive and widely used because it is inexpensive and it offers good frequency and intensity stability and a high degree of coherence. Consequently, an optical fibre amplifier that will increase the system power budget in such a system is required, and is the subject of these investigations.

1.1.2 APPLICATIONS OF OPTICAL AMPLIFIERS

An optical amplifier can increase the amplitude of a propagating signal wave. The need for such a device arises because of intrinsic (Rayleigh scattering and absorption) and extrinsic (caused by connections and splices) losses in optical fibre systems and as a result of multiplexing or power division in networked systems. Furthermore, attenuation and power division limit the performance of an optical fibre system because the receiver has a minimum useful power input and the transmitter a maximum power output.

A power amplifier (Figure 1.1.2.1), an in-line amplifier (Figure 1.1.2.2) and a pre-amplifier (Figure 1.1.2.3) are three main applications for an optical fibre amplifier. Power amplifier is a term adopted for an optical fibre amplifier that is used immediately after the signal source. A power amplifier can increase an intrinsically small signal, where poor coupling of the signal source to the fibre system or a

degraded transmitter performance is apparent. In a multiplexed system, a power amplifier can be used prior to power division in multiport couplers. The signal amplitude can be amplified in proportion to the power division.

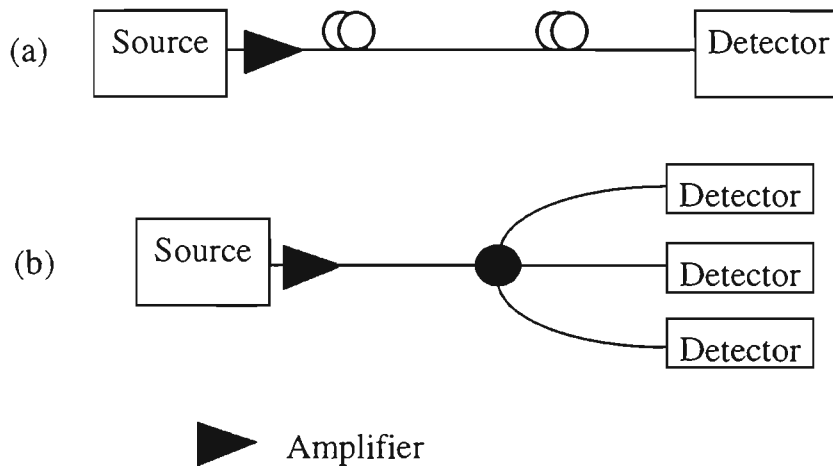


Figure 1.1.2.1 *An optical amplifier (triangle) immediately after the signal source (power amplifier) in (a) a simple system and (b) a multiplexed system.*

The transmission distance of an optical signal is mainly limited by attenuation. However an in-line optical fibre amplifier (Figure 1.1.2.2) can be positioned at intervals such that the signal power never drops below a certain level. Many amplifiers may be distributed along a transmission line for long haul applications. The main application of an in-line amplifier is in communication systems since sensor systems are not usually associated with long haul applications.

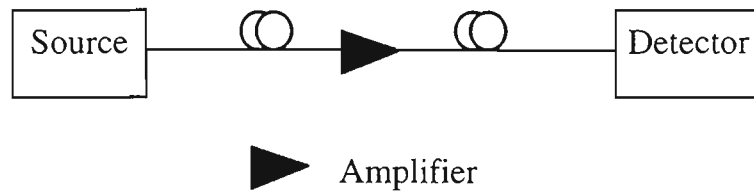


Figure 1.1.2.2 *In-line amplifier : used in long haul applications to maintain signal power.*

An amplifier positioned immediately prior to detection is referred to as a pre-amplifier (Figure 1.1.2.3). The purpose is to amplify a signal which has been diminished by transmission losses. An increased signal level can also result in an increased detector sensitivity. This configuration may also be applied to multiplexed systems (Figure 1.1.2.3 (b)).

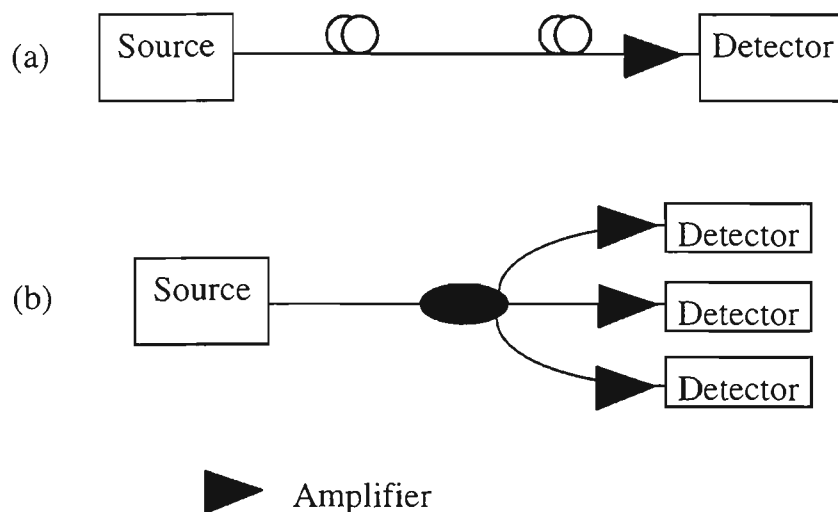


Figure 1.1.2.3 *Pre-amplifier immediately before detection (a) can increase the detector sensitivity and (b) in a multiplexed system.*

1.1.3 TYPES OF OPTICAL AMPLIFIERS

For fibre based applications optical amplifiers may be considered in three classes namely; semiconductor amplifiers, non-linear fibre amplifiers, and rare-earth-doped fibre amplifiers. The principles of operation of a semiconductor amplifier are based on a process that allows conversion of electrical energy into light. Light emission in semiconductor materials occurs during the recombination of an electron in the conduction band with a hole in the valance band [Jones W.B., 1988; Cheo P.K., 1990]. The optical gain spectrum is dependent upon the bandgap of the material (which defines the wavelength at which maximum gain is obtained) and the bias current supplied to the device (which defines the envelope of the gain). The electrical energy may be transferred to the propagating signal beam resulting in single pass amplification.

There are two non-linear processes which have been used to amplify light namely, stimulated Raman scattering (SRS) and stimulated Brillouin scattering (SBS). Both processes are based on non-linear light scattering (scattering with shifted wavelength) in an optical fibre.

The physical process involved in Raman scattering is the interaction of light with optical phonons [Stolen R. H. and Ippen E.P., 1973; Yasuhiro A., 1988]. The signal gain characteristics are determined by the optical (Raman) phonon spectra, which is defined by the fibre material. In the stimulated Raman scattering process, light at frequency ν_0 is scattered into a red-shifted component at frequency ν' (Stokes light) with a certain gain coefficient $g_R(\nu_0 - \nu')$. The frequency difference is referred to the Stokes or Raman shift ($\Delta\nu_R$) (for example in fused silica

$\Delta\nu_R = 440 \text{ cm}^{-1}$ [France P.W., 1991]). Raman amplification can occur at any wavelength as long as an appropriate pump laser is available.

Stimulated Brillouin scattering can also be used to amplify light in optical fibre [Ippen E.P. and Stolen R.H., 1972; Offenberger A.A. *et al.*, 1993]. Stimulated Brillouin scattering manifests itself as a backward travelling scattered wave, the frequency of which is shifted by an amount corresponding to the acoustic frequency. The signal gain characteristics are thus determined by acoustic (Brillouin) phonon spectra of the medium. When the input pump power exceeds some threshold value, most of this light can be converted into lower frequency Stokes light. The frequency difference between the input light wave and the generation of Stokes light is called the Brillouin shift ($\Delta\nu_B$), which is equal to the acoustic phonon frequency. For example, for fused silica $\Delta\nu_B \approx 11 \text{ GHz}$ at $1.55 \mu\text{m}$ [Atkins C.G. *et al.*, 1986] and $\Delta\nu_B \approx 13 \text{ GHz}$ at $1.32 \mu\text{m}$ [Cotter D., 1982].

Another type of optical amplifier is one based on rare-earth-doped fibre [Digonnet M.J.F., 1993; Desurvire E., 1994a & b]. With the appropriate pumping a rare-earth-doped fibre can be used as a gain medium. Generally, the pump energy must match that of an absorption transition of the rare-earth. By absorbing pump energy, ground-state ions are excited to higher energy levels allowing a population inversion to build in the metastable level. From this higher energy level the ions can relax to the ground state or to lower lying intermediate levels either radiatively or non-radiatively. Non-radiative decay reduces the efficiency of a laser level. Radiative decay takes one of two forms: spontaneous or stimulated emission, and for both cases a photon is emitted. Spontaneous emission always takes place when ions are in an

excited state. However, energy released by stimulated emission may be transferred to the propagating signal wave, amplifying it through the medium. The important property of stimulated emission is that the generated electromagnetic wave is coherent with that of the signal. That is, it has the same phase and polarisation characteristics.

A rare-earth-doped fibre amplifier generally includes a small number of components; an appropriate optical pump source, a length of rare-earth-doped fibre and a signal light source (Figure 1.1.3.4). These devices are attractive because they combine the excellent properties of laser materials and high energy confinement of an optical fibre waveguide and their configuration is compatible with standard optical fibre. A common form of optical fibre amplifier system incorporates an optical fibre coupler (Figure 1.1.3.4). Optical fibre couplers and wavelength division multiplexers are important devices in any optical fibre system as they provide beam splitting and combining “in-fibre”, avoiding difficulties with bulk optics and thus have low excess and insertion loss.

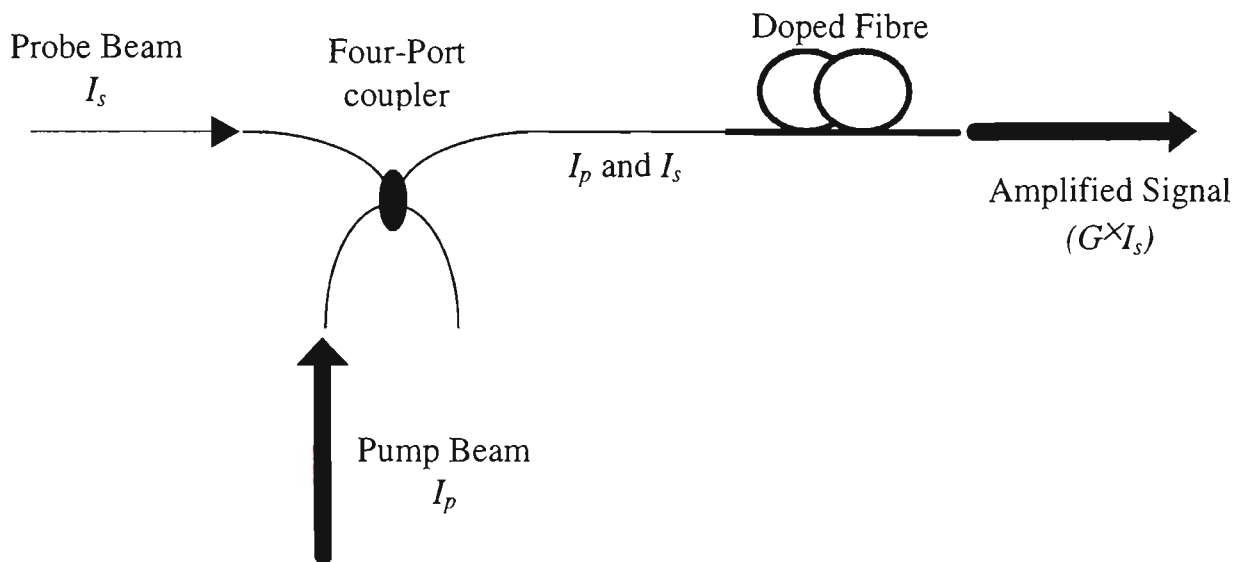


Figure 1.1.3.1 Typical optical fibre amplifier arrangement incorporating a rare-earth-doped fibre, directional coupler and pump and probe (signal) lasers. The probe is amplified by a factor (G).

1.2 HISTORICAL OVERVIEW

Investigations into optical fibre amplifiers began with the demonstration of the first fibre laser. This laser operated at $1.06 \mu\text{m}$ in neodymium-doped silica and had a core diameter of 0.3 mm [Snitzer E., 1961]. The main motivation for this configuration was that the waveguiding effects associated with the fibre allowed a maximum intensity to be maintained over a greater distance than is possible in a bulk material. Then, in the mid-1960's, Charles Koester and Elias Snitzer used neodymium-doped fibre to amplify $1.06 \mu\text{m}$ radiation from a neodymium glass laser

source [Koester C.J. and Snitzer E., 1964]. This fibre amplifier had a large core diameter ($\sim 10 \mu\text{m}$), was optically pumped by a flash-lamp and operated in a pulsed mode. Later a neodymium glass fibre was used as a power amplifier for a He-Ne laser emitting at $1.0621 \mu\text{m}$ [Holst G.C. *et al.*, 1969]. The fibre used in the experiment had a $15 \mu\text{m}$ core diameter and increased the He-Ne output from $230 \mu\text{W}$ to 0.6 W (34 dB net gain). The amplified light preserved the coherence of the He-Ne laser.

Research into optical fibre communications had increased significantly by 1970 with major emphasis placed on constructing single-mode optical fibres [Kapron F.P. *et al.*, 1970]. It was shortly after this time that advances in the fabrication of low-loss silica fibre made long distance optical communications a practical reality [Payne D.N. and Gambling W.A., 1974]. Fibre dispersion and attenuation became important factors, with major emphasis placed on the low loss wavelength of $1.5 \mu\text{m}$ and the low dispersion wavelength of $1.31 \mu\text{m}$. These became commonly referred to as the second ($1.31 \mu\text{m}$) and third ($1.5 \mu\text{m}$) communications windows.

It wasn't until the mid 1980's, however, that a research group led by David N. Payne at the University of Southampton, England, showed that erbium-doped silica fibres could exhibit optical gain at the communications systems wavelength of $1.5 \mu\text{m}$. After demonstrating laser action in erbium-doped fibres [Mears R.J. *et al.*, 1986], this group successfully constructed the first erbium-doped fibre amplifier [Mears R.J. *et al.*, 1987]. From 1988 compact laser diode sources were used to optically pump erbium-doped fibre amplifiers [Whitley T.J., 1988; Shimizu M. *et al.*, 1990; Suzuki K. *et al.*, 1990; Horiguchi M. *et al.*, 1990]. For its most essential

aspects, the theoretical analysis of erbium-doped fibre amplifiers was established by 1990 [Desurvire E. *et al.*, 1987; Oshlansky R., 1988; Armitage J.R., 1988; Bjarklev A. *et al.*, 1989; Morkel P.R. and Laming R.I., 1989; Marcerou J.F. *et al.*, 1990; Peroni M. and Tamburrini M., 1990; Saleh A.A.M. *et al.*, 1990; Digonnet M.J.F., 1990; Pedersen B. *et al.*, 1990].

However, most installed fibre optic systems were optimised for 1.31 μm since at this wavelength standard silica fibres have a minimum level of chromatic dispersion. As a consequence amplifiers at 1.31 μm were sought. Early work on an amplifier for the second communications window was in neodymium-doped silica glass on the ${}^4\text{F}_{3/2} \rightarrow {}^4\text{I}_{13/2}$ transition centred on 1.32 μm . However, the gain was limited because the ${}^4\text{F}_{3/2} \rightarrow {}^4\text{I}_{13/2}$ transition suffers from excited state absorption (ESA) at the signal wavelength [Morkel P.R. *et al.*, 1988]. This led to investigations into alternative glass hosts and to the first use of neodymium-doped fluorozirconate optical fibre for amplifier applications [Miniscalco W.J. *et al.*, 1988; Brierly M. and Millar C.A., 1988]. Before this the brittle nature of fluorozirconate glass prevented the construction of useful optical fibres. In a fluorozirconate glass fibre the excited state absorption wavelength shifted to shorter values allowing some gain to be obtained from 1.31 μm to 1.38 μm [Miyajima Y. *et al.*, 1990; Brierly M. *et al.*, 1990]. However, this also introduced another problem in that the increased efficiency of the ${}^4\text{F}_{3/2} \rightarrow {}^4\text{I}_{11/2}$ competing transition (which corresponds to 1.05 μm emission) limited the overall performance at 1.31 μm so that only relatively low gains could be obtained.

The other rare-earth candidate for 1.31 μm amplifier applications is praseodymium. Initial investigation of praseodymium-doped silica based fibres indicated that multiphonon decay would prevail and prohibit radiative emission at 1.31 μm [Percival M.R. *et al.*, 1989]. Later fluorescence measurements of praseodymium in a fluorozirconate glass indicated that there was sufficient emission at 1.31 μm to warrant further investigation [Ohishi Y. *et al.*, 1991; Carter S.F. *et al.*, 1991; Durteste Y. *et al.*, 1991]. The lower phonon energy of fluorozirconate glass as compared to silica glass diminishes the phonon decay rate sufficiently to obtain gain on the $^1G_4 \rightarrow ^3H_5$ transition [Ohishi Y. *et al.*, 1983; Davey S.T. and France P.W., 1989; France P.W., 1990; Aggrawal I.D. and Lu G., 1991; Davey S.T. *et al.*, 1991; Smart R. *et al.*, 1991].

1.3 SCOPE OF THESIS

Although praseodymium-doped fluorozirconate fibres are well known for amplifier applications in the second communications window, lasing has also been reported by many authors at visible wavelengths [Allain J.Y. *et al.*, 1991; Smart R.G. *et al.*, 1991; Zhao Y. and Poole S., 1994; Zhao Y. *et al.*, 1994; Tropper A.C. *et al.*, 1994]. In 1991 Allain *et al.* reported CW lasing at many visible wavelengths in praseodymium-doped fluorozirconate optical fibre. Of particular interest here is that efficient lasing was possible on the $^3P_0 \rightarrow ^3F_2$ transition around 635 nm, where the tuning range is sufficiently broad to offer the possibility of useful amplification at the 632.8 nm He-Ne wavelength. Since an optical amplifier is an integral part of a fibre

laser a single pass amplifier is also possible. Reported in this Thesis is an investigation of single-pass small-signal amplification at the 632.8 nm He-Ne wavelength using praseodymium-doped fluorozirconate optical fibre as the amplifying medium. The work presented in this Thesis has been divided into six chapters beginning with the introduction. The second chapter deals with the modelling of rare-earth-doped fibre amplifiers in general. Presented in Chapter 3 is an experimental investigation of the spectroscopic properties of praseodymium-doped fluorozirconate glass. An experimental investigation of the optical fibre parameters relevant to the praseodymium amplifier are given in Chapter 4. An experimental investigation of the optical gain in praseodymium-doped fibre is given in Chapter 5 and compared with the calculated gain. Chapter 6 is the conclusion.

To assess the ultimate potential of an amplifier a rate equation model that represents the optical pumping and gain process is essential. In Chapter 2 idealised four- and three-level models are used to describe the gain in the limits of low pump and high pump powers. Chapter 2 steps back from considering specific amplifier/laser systems and gives an outline of the essential methods used in the modelling of active fibre devices and comments upon many of the approximations that have been used in these analyses.

To achieve basic understanding of an optical fibre amplifier, it is also necessary to study the spectroscopic properties of the rare-earth-ions doped in the glass host (Chapter 3). The attenuation spectrum and the emission (fluorescence) spectrum are two important spectroscopic measurements. Experimental investigations of the attenuation spectrum of praseodymium-doped in fluorozirconate glass are given in Section 3.3. In Section 3.4 a pump laser is used to excite ground

state ions into higher levels from which fluorescence can be observed. The fluorescence spectrum determines the wavelengths of light that can be amplified. Beside the radiative transitions from the 3P_0 state there is also a component of non-radiative decay to the closest state 1D_2 , which has been investigated in Section 3.5. Another important parameter, related to the gain, is the fluorescence lifetime of a level. The results of lifetime measurements of the 3P_0 state in praseodymium are given in Section 3.6. This parameter is also an integral component for calculating the emission cross-section of the 3P_0 state. In Section 3.7 Fuchtbauer-Ladenburg analysis is used to calculate the emission cross-section of the 3P_0 state, in particular at 632.8 nm. The fluorescence lifetime was also measured for varying dopant concentrations where it was observed for the first time that the lifetime of the 3P_0 state decreases with increasing dopant concentration. This lifetime quenching is caused by an increased rate of cross-relaxation or energy transfer. A rate equation model, which was developed, indicating the relationship between the lifetime of the 3P_0 state and the dopant concentration, is given in Section 3.8. The spectroscopic parameters are required for accurate modelling and qualitative understanding of the optical properties of the amplifier material.

In Chapter 4 the optical fibre parameters that influence the overall performance of the 632.8 nm praseodymium-doped amplifier are investigated experimentally. These parameters include the intensity spot-size of the fundamental mode for both the pump and signal beams and the radial distribution or the concentration profile of praseodymium ions in the fibre core. The concentration profile is an essential parameter used in modelling optical fibre amplifiers. However, optimisation and modelling of optical fibre amplifiers has been limited by the lack of

information about the spatial structure of the dopant concentration. In Chapter 4 a novel technique, based on cooperative energy transfer between dopant ions, is used for spatially resolved, absolute determination of the rare-earth dopant concentration. These experiments are novel in that they rely directly on concentration-dependent processes in the material.

In Chapter 5 experimental results of optical amplification of a 632.8 nm He-Ne probe beam in praseodymium-doped fluorozirconate fibre are presented for the first time. A rate equation approach is used to model and understand the gain dynamics.

Final conclusion and future work is outlined in Chapter 6.

Chapter 2

MODELLING OF OPTICAL FIBRE AMPLIFIERS

- 2.1 Introduction
- 2.2 Idealised three- and four-level amplifier/laser systems
- 2.3 Propagation of pump and signal beams in an optical fibre
- 2.4 Analytic approximations for the small signal gain coefficient
 - 2.4.1 Introduction
 - 2.4.2 Approximation for a four-level system
 - 2.4.3 Approximation for a three-level system
- 2.5 Conclusion

2.1 INTRODUCTION

The principles involved in optical amplification can be described using either a classical or a quantum mechanical perspective [Marcuse D., 1980]. From a classical perspective, an optical amplifier acts as an electromagnetic wave booster that coherently increases the amplitude of each frequency component of the input signal. From a quantum mechanical viewpoint, an optical amplifier is a photon multiplier such that the average number of signal photons are multiplied by a certain factor, the gain.

However, another possibility is a semiclassical approach, in which the atomic system is quantised and the electric field interacting with matter is treated classically. In this case one assumes that the ions doping the medium can exist in at least two discrete energy states namely, an upper level (metastable level) and a lower level. When the atomic system is in thermal equilibrium practically all the ions exist in the ground level. To move the system away from thermal equilibrium an optical pump source may be used. The energy of the pump source must match the energy difference between the upper level (the pump level) and the ground level. Ground level ions that absorb energy delivered by the pump source are excited into the pump level. Such pumping can cause a substantial fraction of the ions to persist in the higher-energy metastable state.

A “signal” photon incident upon the pumped medium, with an energy equal to the difference in energy between the lower and upper level may promote de-excitation. De-excitation, through stimulated emission, creates a photon of equal energy and the same phase as the incident photon. Signal amplification is possible

because stimulated emission continues along the length of the inverted medium, and so one incident photon can be replicated many times.

Modelling of rare-earth-doped optical fibre amplifiers represents a theoretical understanding that makes use of several fundamental principles borrowed from classical electromagnetism, quantum mechanics and laser physics. In particular, idealised three- and four-level atomic systems are considered in Section 2.2. Here, a set of coupled differential equations (rate equations) have been derived for both a three- and four-level model. The ion populations of the levels can be determined using the steady-state solutions of these rate equations.

The amplification or gain in an optical fibre is determined by the evolution of the pump and signal power along the length of the fibre (Section 2.3). Using standard approximations, an analytical expression for the gain coefficient is given in Section 2.4. The gain is determined for both the low-pump and high-pump regimes.

2.2 IDEALISED THREE- AND FOUR-LEVEL AMPLIFIER/LASER SYSTEMS

Atomic systems typically involve a very large number of energy levels, with complex excitation processes and cascaded relaxation channels among all the levels. The operation of an actual amplifier/laser material is described properly only by a many-level system. However, for practical purposes, amplifiers and lasers can be conveniently classified into idealised four-level or three-level amplifier/ laser systems [Koechner W., 1992]. In this section idealised four- and three-level amplifier/laser

systems are described. The usual approach, namely using rate equation analysis to analyse the population dynamics of energy levels, has been adopted [Digonnet M.J.F. *et al.*, 1985; Barnard C. *et al.*, 1994].

For a four-level system shown in Figure 2.2.1 it is assumed that optical pumping causes a fraction of ground state ions to be raised into the intermediate pump state (level 4), from which ions decay via multiphonon relaxation rapidly into the metastable level (level 3). The transition rate is assumed to be very fast such that, $\tau_{43} \rightarrow 0$. The amplifier/laser transition and spontaneous emission takes place between level 3 and level 2. Following this, ions decay non-radiatively rapidly back to the ground level (level 1). The overall implications of these assumptions are that only the populations of the metastable level (N_3) and the ground level (N_1) are significant and that the sum of these is the total dopant concentration (ρ), that is

$$N_1 + N_3 = \rho. \quad (2.2.1)$$

The transition rates (Figure 2.2.1), for a four-level system are given in terms of the pump (I_p) and signal (I_s) mode intensity and absorption ($\sigma_{s,p}^a$) and emission ($\sigma_{s,p}^e$) cross-sections (the subscripts s and p indicate the signal or pump respectively). For a four-level system the pump (R_{14}) absorption rate and the signal (W_{32}) emission rate can be written as [Digonnet M.J.F., 1990]

$$R_{14} = \frac{\sigma_p^a I_p}{h\nu_p} \quad (2.2.2)$$

and

$$W_{32} = \frac{\sigma_s^e I_s}{h\nu_s} \quad (2.2.3)$$

respectively, where h is Planck's constant and $h\nu_p$ and $h\nu_s$ are the pump and signal photon energies respectively. The spontaneous radiative transition rate from some initial state i , A_i , is given by

$$A_i = \frac{1}{\tau_i} = \sum_j A_{ij} \quad (2.2.4)$$

where τ_i represents the total radiative lifetime, and A_{ij} the decay rate from the state i to the state j .

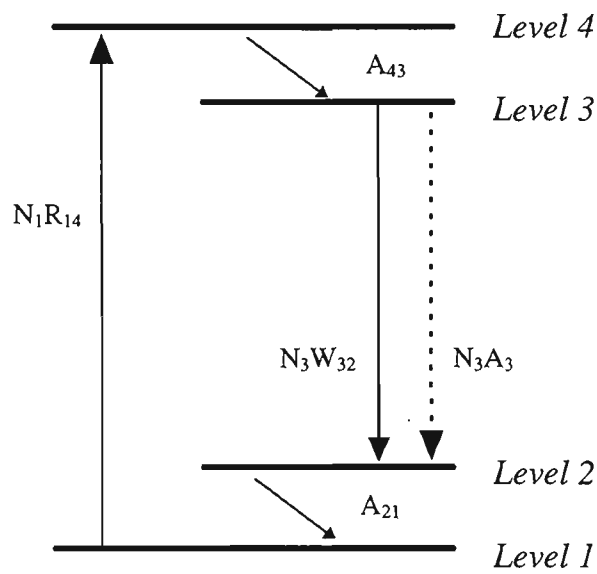


Figure 2.2.1 *Idealised four-level model. The pump level (level 4) is characterised by fast non-radiative decay into the metastable level (level 3). The amplifier/laser transition is between level 3 and level 2. Ions in level 2 are assumed to decay non-radiatively rapidly back to the ground level.*

The main difference between the pump and signal beams is that they interact with different atomic levels. A pump beam is defined as one that interacts with the ground level and the pump band and the signal beam is defined as one that interacts with the metastable level and the terminal (ie. lower) level.

For a four-level system the following rate equations can be used to describe the population densities of the relevant levels

$$\frac{dN_1}{dt} = -R_{14}N_1 + A_{21}N_2, \quad (2.2.5)$$

$$\frac{dN_2}{dt} = W_{32}N_3 + A_3N_3 - A_{21}N_2, \quad (2.2.6)$$

$$\frac{dN_3}{dt} = A_{43}N_4 - W_{32}N_3 - A_3N_3 \quad (2.2.7)$$

and

$$\frac{dN_4}{dt} = R_{14}N_1 - A_{43}N_4. \quad (2.2.8)$$

An idealised three-level amplifier/laser model, shown schematically in Figure 2.2.2, is a special case of the four-level model. The underlying difference is that for a three-level system the amplifier/laser transition terminates on the ground level. As a result signal reabsorption becomes prominent and is taken into account in this model (in the case of a four-level model signal reabsorption is neglected). For a three-level model the total population is also assumed to be divided between the metastable (which for this model is level 2) and the ground level (level 1) such that

$$N_1 + N_2 = \rho. \quad (2.2.9)$$

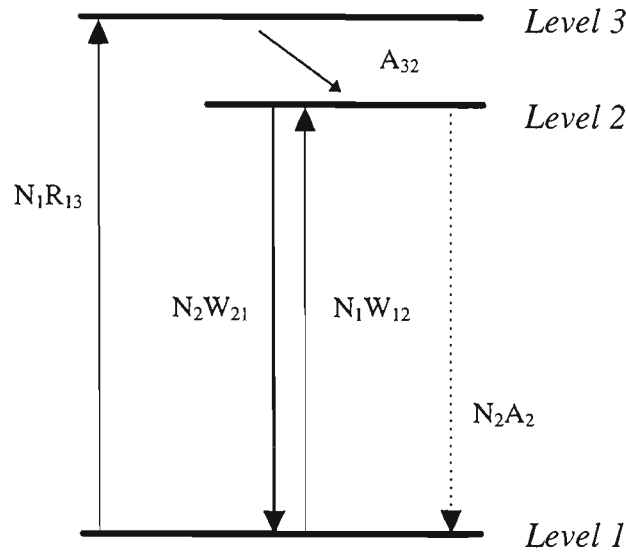


Figure 2.2.2 *Idealised three-level model. The pump level (level 3) is characterised by fast non-radiative decay into the metastable level (level 2). The amplifier/laser transition is between level 2 and the ground level.*

For a three-level system the pump (R_{13}) and signal (W_{12}) absorption rates and the signal (W_{21}) emission transition rate can be written as

$$R_{13} = \frac{\sigma_p^a I_p}{h\nu_p}, \quad (2.2.10)$$

$$W_{12} = \frac{\sigma_s^a I_s}{h\nu_s}, \quad (2.2.11)$$

$$W_{21} = \frac{\sigma_s^e I_s}{h\nu_s} \quad (2.2.12)$$

and the rate equations for a three-level system are given by

$$\frac{dN_1}{dt} = -R_{13}N_1 + A_2N_2 + W_{21}N_2 - W_{12}N_1, \quad (2.2.13)$$

$$\frac{dN_2}{dt} = A_{32}N_3 - A_2N_2 - W_{21}N_2 + W_{12}N_1 \quad (2.2.14)$$

and

$$\frac{dN_3}{dt} = R_{13}N_1 - A_{32}N_3. \quad (2.2.15)$$

Another underlying assumption, for both a four- and three-level amplifier/laser system, is that the pump emission rate is negligible. Furthermore, only the small signal gain is considered here. The definition of a small-signal implies that the metastable level is not severely depopulated by stimulated emission. For this case the signal intensity is considered to be small and the signal emission and absorption rates can also be neglected (ie., in the four-level system $W_{32} = 0$ and for the three-level system $W_{12} = W_{21} = 0$). With these considerations approximations for the steady-state population dynamics may be obtained.

For steady-state conditions the time-dependent differentials are set to zero ($\frac{dN_i}{dt} = 0$). Under this condition the population of the metastable state and the ground level can be obtained for both an idealised four-level and three-level system. For an idealised four-level system the approximations for the populations of the levels are

$$N_1 = \rho \cdot \frac{I}{I + \tau_3 R_{14}}, \quad (2.2.16)$$

$$N_2 = 0, \quad (2.2.17)$$

$$N_3 = \rho \cdot \frac{\tau_3 R_{14}}{I + \tau_3 R_{14}} \quad (2.2.18)$$

and

$$N_4 = 0. \quad (2.2.19)$$

The condition for population inversion (ΔN) is given by the relative population difference between the metastable level (level 3) and the lower laser level (level 2) given by

$$N_3 - N_2 = \rho \cdot \frac{\tau_3 R_{14}}{1 + \tau_3 R_{14}}. \quad (2.2.20)$$

The implication is that for four-level systems the threshold pump rates are low.

For a three-level system the populations of the levels are given by

$$N_1 = \rho \cdot \frac{I}{I + \tau_2 R_{13}}, \quad (2.2.21)$$

$$N_2 = \rho \cdot \frac{\tau_2 R_{13}}{I + \tau_2 R_{13}}, \quad (2.2.22)$$

$$N_3 = 0, \quad (2.2.23)$$

and the population inversion threshold is

$$N_2 - N_1 = \rho \cdot \frac{\tau_2 R_{13} - I}{\tau_2 R_{13} + I}. \quad (2.2.24)$$

That is, the pump rate has some threshold value in order to satisfy the population inversion condition. This condition is given for a three-level system as

$$R_{13} > \frac{I}{\tau_2} \quad (2.2.25)$$

Similarly for a four-level system

$$R_{14} > \frac{I}{\tau_3}. \quad (2.2.26)$$

2.3 PROPAGATION OF PUMP AND SIGNAL BEAMS IN AN OPTICAL FIBRE

In the previous section a rate equation analysis was used to describe the population dynamics of atomic levels for idealised four- and three-level laser systems. However, the population dynamics for the levels of an active laser material in an optical fibre medium (ie., having waveguiding properties) are significantly more complicated. In this section the waveguiding properties of optical fibres are considered with respect to their relationship to amplification in a fibre medium. An outline of the essential methods used in the modelling of optical fibre amplifiers is also given.

For the model we consider an optical fibre, the core which is made of an active laser material of length L . The fibre has a step index profile with core radius a and a numerical aperture NA . The numerical aperture describes the maximum half angle of acceptance (θ) for a light ray into an optical fibre and is given by

$$NA = n_0 \sin \theta = \sqrt{n_1^2 - n_2^2} \quad (2.3.1)$$

where n_0 is the refractive index of air ($n_0 \approx 1$) and n_1 and n_2 are the refractive indices of the core and the cladding respectively. The core of the fibre is assumed to be doped with $\rho(r, \phi, z)$ active ions per unit volume, and the cladding undoped. For the remainder of this thesis the active section is a fluorozirconate glass doped with the rare-earth-ions praseodymium in various densities.

The rare-earth-doped fibre is optically end-pumped with a laser source at the pump wavelength, λ_p . For amplifier applications, feedback is suppressed and the medium is assumed to be probed by a small signal (probe), at the signal wavelength λ_s , co-propagating with the pump beam.

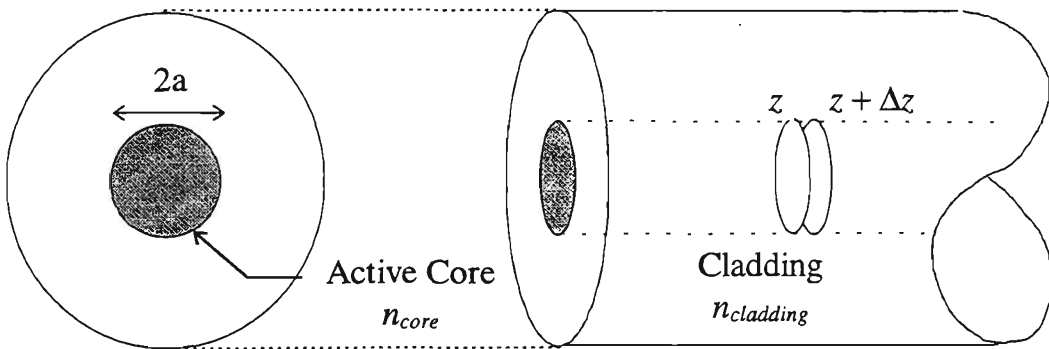


Figure 2.3.1 *An optical fibre with an active core region indicating the refractive index of the core (n_{core}) and the refractive index of the cladding ($n_{cladding}$).*

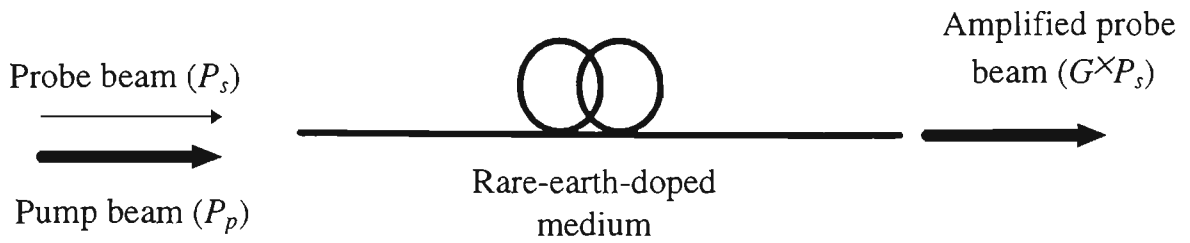


Figure 2.3.2 *An optical fibre amplifier configuration. The fibre is optically pumped with a pump beam of intensity P_p . The probe (signal) beam of intensity P_s is launched into the amplifier and is multiplied by a gain factor G .*

The amplification characteristics can be described sufficiently by the propagation of the pump and signal beams and their interaction along the length of the amplifying medium in the z direction. The difference in pump (or signal) intensity between planes z and $z+\Delta z$ in some rare-earth-ion doped medium (Figure 2.3.1), is given by [France P.W., 1991]

$$I(z + \Delta z, r, \phi) - I(z, r, \phi) = \left[\begin{array}{l} \text{(Rate of emissions per unit volume)} - \\ \text{(Rate of absorptions per unit volume)} \end{array} \right] \cdot \text{Photon energy} \cdot \Delta z - \alpha I(z, r, \phi) \Delta z, \quad (2.3.2)$$

where α describes losses in the system such as ground state absorption and attenuation in the medium. Ground state absorption is considered when the amplifier transition interacts with the ground level (as in the case of a three-level system) since

it may cause a substantial degree of signal reabsorption. This is of particular importance for an idealised three-level system. For a four-level system signal reabsorption is generally low and can be neglected. For simplicity attenuation due to the fibre material is neglected in these models.

The propagation of the pump and the propagation of the signal beam are essential for describing the single-pass gain in an optical fibre amplifier [Desurvire E. and Simpson J.R., 1989; Ohashi M., 1991; Pedersen B. *et al.*, 1991a]. Primarily, there are two approaches to consider for the propagation of the signal and pump beams. The simpler of these is the plane wave approximation where the transverse variation of the pump, signal and ion profiles are effectively ignored. This amounts to assuming a top-hat function for the pump and signal intensity mode shapes and a square rare-earth ion density profile.

For an idealised four-level system the propagation of the pump and signal beams respectively are given by

$$\frac{dI_p(z)}{dz} = -\sigma_p^a N_1(z) I_p(z), \quad (2.3.3)$$

and

$$\frac{dI_s(z)}{dz} = \sigma_s^e N_3(z) I_s(z). \quad (2.3.4)$$

For an idealised three-level system the propagation of the pump beam is given by Equation 2.3.3 and the propagation of the signal beam is now

$$\frac{dI_s(z)}{dz} = \sigma_s^e N_2(z) I_s(z) - \sigma_s^a N_1 I_s(z) \quad (2.3.5)$$

which takes into account ground state reabsorption of the signal.

However, in general the pump and signal beams in fibre will vary in intensity transverse to their direction of propagation and the rare-earth ion density may not be uniform across the fibre core. As a consequence the populations in all the excited rare-earth ion levels at position (r, ϕ, z) will depend on the pump and probe intensities at that same point and the local gain and absorption coefficients will also vary across the pump and signal beam profiles.

Using a cylindrical co-ordinate system appropriate for an optical fibre the propagation equations are given by [Digonnet M.J.F., 1990]

$$\int_{r=0}^{\infty} \int_{\phi=0}^{2\pi} \frac{dI_p(r, \phi, z)}{dz} r dr d\phi = - \int_{r=0}^{\infty} \int_{\phi=0}^{2\pi} (\sigma_p^u N_1(r, \phi, z)) I_p(r, \phi, z) r dr d\phi, \quad (2.3.6)$$

$$\int_{r=0}^{\infty} \int_{\phi=0}^{2\pi} \frac{dI_s(r, \phi, z)}{dz} r dr d\phi = \int_{r=0}^{\infty} \int_{\phi=0}^{2\pi} (\sigma_s^e N_3(r, \phi, z)) I_s(r, \phi, z) r dr d\phi, \quad (2.3.7)$$

for an idealised four-level system. For an idealised three-level system the pump propagation is the same as Equation 2.3.6 and the signal propagation equation is given by [Digonnet M.J.F., 1990]

$$\int_{r=0}^{\infty} \int_{\phi=0}^{2\pi} \frac{dI_s(r, \phi, z)}{dz} r dr d\phi = \int_{r=0}^{\infty} \int_{\phi=0}^{2\pi} \sigma_s^e N_2(r, \phi, z) I_s(r, \phi, z) r dr d\phi \quad (2.3.8)$$

$$- \int_{r=0}^{\infty} \int_{\phi=0}^{2\pi} \sigma_s^u N_1(r, \phi, z) I_s(r, \phi, z) r dr d\phi$$

For light propagating in a single-mode step-index optical fibre the field distribution is very nearly Gaussian in shape (higher order modes also exhibit Gaussian intensity distributions, multiplied by certain Hermite polynomials) [Marcuse D., 1992].

The intensity of the signal and pump beams are given by

$$I_s(r, \phi, z) = P_s(z)\psi_s(r, \phi) \quad (2.3.9)$$

and

$$I_p(r, \phi, z) = P_p(z)\psi_p(r, \phi) \quad (2.3.10)$$

respectively. The normalised distribution function for the pump and signal beams in an optical fibre are

$$\psi_p(r, \phi) = \frac{2}{\pi\omega_p^2} \exp\left[-2\frac{r^2}{\omega_p^2}\right] \quad (2.3.11)$$

and

$$\psi_s(r, \phi) = \frac{2}{\pi\omega_s^2} \exp\left[-2\frac{r^2}{\omega_s^2}\right] \quad (2.3.12)$$

respectively. In common with many fibre amplifier models, the dopant ion distribution is assumed to be constant following a top-hat function where

$$\rho(r, \phi, z) = \begin{cases} \rho & r \leq a \\ 0 & r > a \end{cases} \quad (2.3.13)$$

The overlap between pump and signal modes $\Gamma_{p,s}(r, \phi)$ can be described by the integral over all space of the product of the intensity distributions given by

$$\Gamma_{p,s} = 2\pi \int_{r=0}^a \psi_p(r)\psi_s(r)r dr . \quad (2.3.14)$$

The overlap between the pump beam and the fibre core is given by

$$\Gamma_p = 2\pi \int_{r=0}^a \psi_p(r) r dr, \quad (2.3.15)$$

the overlap between the signal beam and the fibre core is given by

$$\Gamma_s = 2\pi \int_{r=0}^a \psi_s(r) r dr. \quad (2.3.16)$$

The parameter ω is often called the beam radius, the spot-size or mode-field radius, and 2ω , the beam diameter. It characterises the radial distance at which the field amplitude drops to $1/e$ of its value on the axis and the power density is decreased to $1/e^2$ of its axial value. The quantity $\pi\omega^2 = A_{eff}$ is considered to be the effective area of the beam cross-section.

There are at least two definitions for the fibre mode spot-size; one due to Marcuse and the other due to Desurvire. Firstly, the Marcuse definition for the spot-size of a step-index single-mode optical fibre uses Gaussian approximations for the transverse field intensity and is a function of the core radius a , wavelength λ_i , normalised frequency parameter V_i , and the numerical aperture NA given by the Marcuse polynomial [Marcuse D., 1992]

$$\frac{\omega_i^{Marcuse}}{a} = 0.65 + \frac{1.619}{V_i^{3/2}} + \frac{2.879}{V_i^6} \quad (2.3.17)$$

where the normalised frequency, V_i , at either the pump or signal wavelength (denoted by the subscript p or s respectively) is given by

$$V_i = \frac{2\pi a}{\lambda_i} NA \quad (2.3.18)$$

The other definition for the mode spot-size is the Desurvire definition [Desurvire E. and Simpson J.R., 1990; Desurvire E., 1994a & b] and is given in terms of the modal field ψ (not the same as that used for the intensity in Equation 2.3.11 and Equation 2.3.12)

$$\omega^{Desurvire} = \left[\frac{1}{\pi} \int \psi_{mn}^2(r) dA \right]^{\frac{1}{2}} \quad (2.3.19)$$

This value for spot-size is, in the case of Bessel functions, different from the spot size at $1/e$ (as in the Gaussian approximation). Such an expression stems from the definition of pump and signal intensities in the fibre modes.

2.4 ANALYTIC APPROXIMATIONS FOR THE SMALL SIGNAL GAIN COEFFICIENT

2.4.1 INTRODUCTION

Approximate analytic expressions for the gain of an idealised four-level [Digonnet M.J.F. and Gaeta C.J., 1985; Digonnet M.J.F. *et al.*, 1989; Digonnet M.J.F., 1990; Whitley T.J. and Wyatt R., 1992; Fleming S.C., 1994; Whitley T.J. and Wyatt R., 1993] and three-level [Armitage J.R., 1988; Digonnet M.J.F. *et al.*, 1989; Barnard C. *et al.*, 1994] doped fibre amplifier have been previously derived by other authors.

As discussed in [Digonnet M.J.F. *et al.*, 1989], a simple rate equation/propagation equation analysis of a four- or three-level amplifier allows the derivation of a pair of coupled differential equations which describe the evolution of the pump and signal powers in a fibre amplifier in the small-signal regime. These

equations, which represent a generalisation of the widely used Digonnet equation [Digonnet M.J.F., 1990], enable a set of solutions for the propagation of the signal (that is the gain) to be obtained for the low pump power and the high pump power regimes [Whitley T.J. and Wyatt R., 1992; Whitley T.J. and Wyatt R., 1993; Fleming S.C., 1994].

2.4.2 APPROXIMATION FOR A FOUR-LEVEL SYSTEM

In the low pump power regime ($R_{14}\tau_3 \ll 1$) it is assumed that the depletion of the ground state population is negligible such that $N_1(r, \phi, z) = \rho$ and the population of the metastable level N_3 , in Equation 2.2.18 is given by

$$N_3(r, \phi, z) = \frac{\tau_3 \sigma_p^a}{h\nu_p} \rho \cdot P_p(z) \cdot \psi_p(r, \phi). \quad (2.4.2.1)$$

Using this result and Equation 2.3.13 and integrating over the fibre length the propagation equation (Equation 2.3.6) for the pump beam is given by

$$\int_{z=0}^L \frac{dP_p(z)}{P_p(z)} = -\sigma_p^a \int_{z=0}^L \rho \, dz \quad (2.4.2.2)$$

and the propagation of the signal beam is given by (Equation 2.3.7)

$$\int_{z=0}^L \frac{dP_s(z)}{P_s(z)} = \sigma_p^a \frac{\tau_3 \sigma_s^e}{h\nu_p} \rho \int_{z=0}^L P_p(z) \, dz \cdot \frac{\Gamma_{p,s}}{\Gamma_s}. \quad (2.4.2.3)$$

By substituting Equation 2.4.2.2 into Equation 2.4.2.3 the gain coefficient is given by

$$\int_{z=0}^L \frac{dP_s(z)}{P_s(z)} = g_{coeff}^{low} \cdot L = -\frac{\tau_3 \sigma_s^e}{h\nu_p} \int_{z=0}^L dP_p(z) \cdot \frac{\Gamma_{p,s}}{\Gamma_s}. \quad (2.4.2.4)$$

In Equation 2.4.2.2 and Equation 2.4.2.3 the product $\sigma_p^a \rho = \alpha_p$ is the exponential absorption coefficient at the pump wavelength. Equation 2.4.2.3 describes the exponential gain coefficient for the low pump power regime and has the following solution

$$\int_{z=0}^L \frac{dP_s(z)}{P_s(z)} = g_{coeff}^{low} \cdot L = \frac{\tau_3 \sigma_s^e}{h\nu_p} [P_p(0) - P_p(L)] \cdot \frac{\Gamma_{p,s}}{\Gamma_s}. \quad (2.4.2.5)$$

Equation 2.4.2.4 now becomes

$$g_{coeff}^{low} \cdot L = \frac{\tau_3 \sigma_s^e}{h\nu_p} [P_p(0) - P_p(L)] \cdot \frac{\Gamma_{p,s}}{\Gamma_s}. \quad (2.4.2.6)$$

The term $[P_p(0) - P_p(L)] = P_{abs}(L)$ is the absorbed pump power at position L along the fibre, so that Equation 2.4.2.6 becomes

$$g_{coeff}^{low} \cdot L = \frac{\tau_3 \sigma_s^e}{h\nu_p} P_{abs}(L) \cdot \frac{\Gamma_{p,s}}{\Gamma_s}. \quad (2.4.2.7)$$

The overlap integral is given by

$$\frac{\Gamma_{p,s}}{\Gamma_s} = \frac{2}{\pi(\omega_s^2 + \omega_p^2)} \frac{\left(1 - \exp \left[-2a^2 \left(\frac{\omega_s^2 + \omega_p^2}{\omega_s^2 \omega_p^2} \right) \right] \right)}{\left(1 - \exp \left[-\frac{2a^2}{\omega_p^2} \right] \right)} \quad (2.4.2.8)$$

In the high pumping regime ($R_{14} \tau_3 \gg 1$) it is assumed that most of the ground state ions may be excited into the upper level such that $N_3(r, \phi, z) = \rho$ and the population of the ground level N_1 in Equation 2.2.16 is given by

$$N_1(r, \phi, z) = \frac{h\nu_p}{\tau_3 \sigma_p^a} \cdot \frac{\rho}{P_p(z)} \frac{1}{\psi_p(r, \phi)}. \quad (2.4.2.9)$$

The propagation of the pump beam, from Equation 2.3.6 integrated over the fibre length, is given by

$$\int_{z=0}^L \frac{dP_p(z)}{P_p(z)} = -\frac{h\nu_p}{\tau_3} \int_{z=0}^L \frac{\rho}{P_p(z)} dz \cdot \frac{l}{\Gamma_p} \quad (2.4.2.10)$$

and the propagation of the signal beam, from Equation 2.3.7, is given by

$$\int_{z=0}^L \frac{dP_s(z)}{P_s(z)} = \sigma_s^e \int_{z=0}^L \rho dz. \quad (2.4.2.11)$$

By substituting Equation 2.4.2.10 into Equation 2.4.2.11 the gain coefficient is given by

$$g_{coeff}^{high} \cdot L = \int_{z=0}^L \frac{dP_s(z)}{P_s(z)} = -\frac{\tau_3 \sigma_s^e}{h\nu_p} \cdot \int_{z=0}^L dP_p(z) \cdot \Gamma_p \quad (2.4.2.12)$$

and hence, since $P_{abs}(L) = P_p(0) - P_p(L)$,

$$g_{coeff}^{high} \cdot L = \frac{\tau_3 \sigma_s^e}{h\nu_p} P_{abs}(L) \cdot \Gamma_p. \quad (2.4.2.13)$$

where

$$\Gamma_p = \left(1 - \exp\left[-\frac{2a^2}{\omega_p^2}\right] \right). \quad (2.4.2.14)$$

It is important to note here that the solution for the small signal gain in the high pump power regime (Equation 2.4.2.12) is different to that obtained in [Fleming S.C. *et al.*, 1991; Whitley T.J. and Wyatt R., 1992; Whitley T.J. and Wyatt R., 1993] where the small signal gain coefficient for the high pump regime is given by

$$g_{coeff}^{low} \cdot L = \frac{\tau_3 \sigma_s^e}{h\nu_p} P_{abs}(L) \cdot \frac{\Gamma_s}{\pi a^2}. \quad (2.4.2.15)$$

Here Γ_s is

$$\Gamma_s = \left(1 - \exp \left[-\frac{2a^2}{\omega_s^2} \right] \right). \quad (2.4.2.16)$$

The reason for this discrepancy is that the propagation equations used in this Thesis, as taken from [Digonnet M.J.F., 1990], are not consistent with those given in [Fleming S.C. *et al.*, 1991; Whitley T.J. and Wyatt R., 1992]. The difference in the final result is that the overlap integral is given as the overlap of the pump beam with the fibre core instead of the overlap of the signal beam with the fibre core. Nevertheless, the difference between these is small and the gain calculations are not expected to vary by any significant amount when the pump and signal wavelengths are close as they are in this case.

2.4.3 APPROXIMATION FOR A THREE-LEVEL SYSTEM

For an idealised three-level system in the low pump power regime ($R_{14}\tau_3 \ll 1$), it is assumed that the ground state population is not severely depopulated so that $N_1(r, \phi, z) = \rho$ and the population of the upper laser level N_2 , in Equation 2.2.22 is given by

$$N_2(r, \phi, z) = \frac{\tau_3 \sigma_p^a}{h\nu_p} \rho \cdot P_p(z) \cdot \psi_p(r, \phi) \quad (2.4.3.1)$$

The propagation equation for the pump beam, from Equation 2.3.6, is given by

$$\int_{z=0}^L \frac{dP_p(z)}{P_p(z)} = -\sigma_p^a \int_{z=0}^L \rho dz \quad (2.4.3.2)$$

and the propagation equation for the signal beam, from Equation 2.3.5, is given by

$$\int_{z=0}^L \frac{dP_s(z)}{P_s(z)} \cdot \Gamma_s = \int_{z=0}^L \left[\frac{\tau_2 \sigma_s^e}{h\nu_p} \right] \rho \sigma_p^a P_p(z) dz \cdot \frac{\Gamma_{p,s}}{\Gamma_s} - \sigma_s^a \int_{z=0}^L \rho dz \quad (2.4.3.3)$$

$$\int_{z=0}^L \frac{dP_s(z)}{P_s(z)} = g_{coeff}^{low} \cdot L = -\frac{\tau_2 \sigma_s^e}{h\nu_p} \cdot \frac{\Gamma_{s,p}}{\Gamma_s} \int_{z=0}^L dP_p(z) - \sigma_s^a \int_{z=0}^L \rho dz \quad (2.4.3.4)$$

$$g_{coeff}^{low} \cdot L = \frac{\tau_3 \sigma_s^e}{h\nu_p} [P_p(0) - P_p(L)] \cdot \frac{\Gamma_{s,p}}{\Gamma_s} - \alpha_s L \quad (2.4.3.5)$$

where $\alpha_s = \sigma_s^a \rho(z)$ is the absorption coefficient at the signal wavelength.

In the high pumping regime ($R_{14} \tau_3 \gg 1$) it is assumed that most of the ground state ions may be excited into the upper level such that $N_2(r, \phi, z) = \rho$ and the population of the ground level N_1 , in Equations 2.2.16 is given by

$$N_1(r, \phi, z) = \frac{h\nu_p}{\tau_3 \sigma_p^a} \cdot \frac{\rho}{P_p(z)} \frac{I}{\psi_p(r, \phi)}. \quad (2.4.3.6)$$

The propagation of the pump beam and the signal beam are given by

$$\int_{z=0}^L \frac{dP_p(z)}{P_p(z)} = -\frac{h\nu_p}{\tau_3} \int_{z=0}^L \frac{\rho}{P_p(z)} dz \cdot \frac{I}{\Gamma_p} \quad (2.4.3.7)$$

and

$$\int_{z=0}^L \frac{dP_s(z)}{P_s(z)} = \sigma_s^e \int_{z=0}^L \rho dz \quad , \quad (2.4.3.8)$$

$$-\frac{\sigma_s^a}{\sigma_p^a} \frac{h\nu_p}{\tau_2} \frac{P_s(z)}{P_p(z)} \frac{\rho}{\Gamma_s} \int_{\phi=0}^{2\pi} \int_{r=0}^a \frac{\psi_s(r, \phi)}{\psi_p(r, \phi)} r dr d\phi$$

respectively. The gain coefficient is given by

$$\int_{z=0}^L \frac{dP_s(z)}{P_s(z)} = g_{coeff}^{low} \cdot L = -\frac{\tau_2 \sigma_s^e}{h\nu_p} \cdot \frac{\Gamma_{s,p}}{\Gamma_s} \int_{z=0}^L dP_p(z) \quad (2.4.3.9)$$

$$-\frac{\sigma_s^a}{\sigma_p^a} \int_{z=0}^L \frac{dP_p(z)}{P_p(z)} \cdot \frac{\Gamma_p}{\Gamma_s} \int_{\phi=0}^{2\pi} \int_{r=0}^a \frac{\psi_s(r, \phi)}{\psi_p(r, \phi)} r dr d\phi$$

Finally, the intensity of the signal increases according to the amplification factor G given by the following equation

$$G = \frac{P_s(L)}{P_s(0)} = \exp[g_{coeff} \cdot L] \quad (2.4.3.10)$$

2.5 CONCLUSION

Using standard approximations, analytical expressions have been derived for the small-signal gain coefficient for idealised four-level and three-level atomic systems in the low and high pump power regimes. However, the models presented in this chapter do not account for excited state absorption, cross-relaxation, energy transfer or dopant ion distribution. Investigations of excited state absorption, cross-relaxation and energy transfer processes in praseodymium-doped fluorozirconate glass are discussed in Chapter 3. The distribution of praseodymium ions in a fibre core are discussed in Chapter 4.

Evidently, the gain coefficient is dependent on spectroscopic parameters and optical fibre waveguide parameters. Indeed many of the parameters which appear in the gain relationship can be measured independently. The spectroscopic parameters are discussed further in Chapter 3 while the optical fibre waveguide parameters are discussed in Chapter 4.

Chapter 3

SPECTROSCOPIC CHARACTERISATION OF PRASEODYMIUM-DOPED FLUOROZIRCONATE GLASS SAMPLES

- 3.1 Introduction
- 3.2 Material properties of rare-earth-doped glass
- 3.3 Attenuation measurements
- 3.4 Measurement of radiative transitions
- 3.5 Calculation of non-radiative transitions
- 3.6 Measurement of the fluorescence lifetime of the 3P_0 state
 - 3.6.1 Introduction
 - 3.6.2 Laser beam modulation
 - 3.6.3 Experimental measurements and results
- 3.7 Calculation of absorption and emission cross-section
- 3.8 Ion-ion interactions in praseodymium
 - 3.8.1 Introduction
 - 3.8.2 Cross-relaxation and energy transfer in praseodymium
 - 3.8.3 Rate equation model
 - 3.8.4 Effects on gain
- 3.9 Conclusion

3.1 INTRODUCTION

According to the models presented in Chapter 2 and in particular that described by Equation 2.4.2.11, the factors which influence the gain in an optical fibre are the emission cross-section at the signal wavelength (σ_s^e), the lifetime of the metastable level (τ), the absorbed pump power (P_{abs}) and the waveguiding properties of the optical fibre. Apart from the waveguiding properties these important parameters can be directly obtained by spectroscopic measurements.

The spectroscopic characteristics of praseodymium-doped in a fluorozirconate glass host play a fundamental role in the analysis and physical understanding of the optical properties of the material (Section 3.2). Spectroscopic studies of praseodymium have been reported in a variety of fluorozirconate glass hosts [Eyal M. *et al.*, 1985; Adam J.L. and Sibley W.A., 1985; Quimby R.S. *et al.*, 1992; Arauzo A.B. *et al.*, 1994; Jha A. *et al.*, 1995; Remillieux A. *et al.*, 1996], in a LaF₃ crystal host [Hegarty J. *et al.*, 1982; Shui T. *et al.*, 1982; Lai S.T. *et al.*, 1982; Lee L.S. *et al.*, 1984] and other glass hosts [German K.R. *et al.*, 1975; Newhouse M.A. *et al.*, 1994].

Spectroscopic measurements included in this chapter are the attenuation spectrum (Section 3.3), the radiative emission spectrum (Section 3.4) and the lifetime of the ³P₀ state (Section 3.6). In Section 3.7 these measurements are used to calculate the absorption cross-section at the pump wavelength (σ_p^a) and the emission cross-section at the signal wavelength (σ_s^e). Another purpose of Chapter 3 is to provide an understanding of the physical processes that are inherent to transitions arising from

the 3P_0 state. In particular radiative (Section 3.4) and non-radiative transitions (Section 3.5), cross-relaxation and energy transfer (Section 3.8) have been investigated.

For amplifier applications all of these important characteristics of praseodymium-doped fluorozirconate fibres are related fundamentally to these spectroscopic properties.

3.2 MATERIAL PROPERTIES OF RARE-EARTH-DOPED GLASS

Lanthanum (La) and the fourteen elements that follow in the periodic table (Figure 3.2.1) are collectively known as the lanthanide series of transition elements or more simply as the rare-earths. The other fourteen elements are cerium (Ce), praseodymium (Pr), neodymium (Nd), promethium (Pm), samarium (Sm), europium (Eu), gadolinium (Gd), terbium (Tb), dysprosium (Dy), holmium (Ho), erbium (Er), thulium (Tm), ytterbium (Yb) and lutetium (Lu). Figure 3.2.2 shows partial energy level diagrams of praseodymium, neodymium, and erbium in a LaF_3 crystal host [Kaminskii A.A., 1981]. These rare-earth-ions have been of particular interest for applications in communication systems.

All the rare-earth-ions have the same outer electron structure of $5s^2 5p^6 6s^2$, which are filled shells [Urquhart P., 1988]. The optical characteristics of rare-earth-ions are determined by the number of electrons occupying the inner $4f$ shell. Lanthanum has zero electrons while lutetium has fourteen $4f$ electrons. Absorption

and emission occur due to transitions within the $4f$ shell. Rare-earth-ions in their triply ionised configuration have one and two electrons removed from the $4f$ and $6s$ shells respectively. The outer $5s$ and $5p$ shells stay intact so that the remaining $4f$ electrons are shielded from perturbation by external fields. This property causes the $4f \rightarrow 4f$ transitions of rare-earth solid-state laser materials to exhibit relatively sharp lines, as compared to transition metals for instance. Furthermore, the spectroscopic characteristics of the $4f \rightarrow 4f$ transitions are weakly sensitive to the host material [Desurvire E., 1994a & b].

Silica- and fluorozirconate-based glasses are host materials commonly used for drawing rare-earth-doped optical fibre. Of particular interest in this Thesis are fluorozirconate optical fibres. Although many different fluorozirconate compositions have been reported in the literature the most stable and that preferred for fibre drawing is $\text{ZrF}_4(53\%)\text{-BaF}_2(22\%)\text{-LaF}_3(4\%)\text{-AlF}_3\text{-NaF}(18\%)$ [France P.W., 1990; Aggrawal I.D. and Lu G., 1991], commonly referred to as ZBLAN.

Although the initial attraction of fluorozirconate-based glass was the possibility of fabricating very low loss fibres (0.01 dB/km), they have proved themselves to be an important alternative to silica based for other reasons. Fluorozirconate glasses have two distinct advantages over silica based glasses. Firstly, fibres fabricated in ZBLAN glasses can be doped with higher rare-earth-ion concentrations than would be possible in silica-based glass. This is because the rare-earth dopant replaces La, which is an integral component of a fluorozirconate glass matrix, in the glass host [France P.W., 1990; Aggrawal I.D. and Lu G., 1991]. Secondly, fluorozirconate glass has a lower energy multiphonon edge than silica [Ohishi Y. *et al.*, 1983; Davey S.T. and France P.W., 1989; France P.W., 1990;

Aggrawal I.D. and Lu G., 1991; Davey S.T. *et al.*, 1991; Smart R. *et al.*, 1991]. This is because fluorozirconate glasses are composed of heavy metals and the bonding between the atoms is relatively weak resulting in phonon energies that are lower than those of silica. As a result the non-radiative relaxation rate, for a given energy gap, in ZBLAN glass is lower than that for a silica based glass. In non-radiative relaxation processes, an ion decays from an excited state to the next lowest state by emitting one or more vibrational quanta to the surrounding glass matrix. The probability for such a process decreases exponentially with the number of quanta needed to bridge the energy gap (Section 3.5). Since fluorozirconate glass has a lower vibrational quantum energy than silica glass the number of quanta needed to bridge a given energy gap is larger resulting in a lower non-radiative relaxation rate. Calculations of non-radiative relaxation rates between the 3P_0 state and the next lowest state 1D_2 are given in Section 3.5.

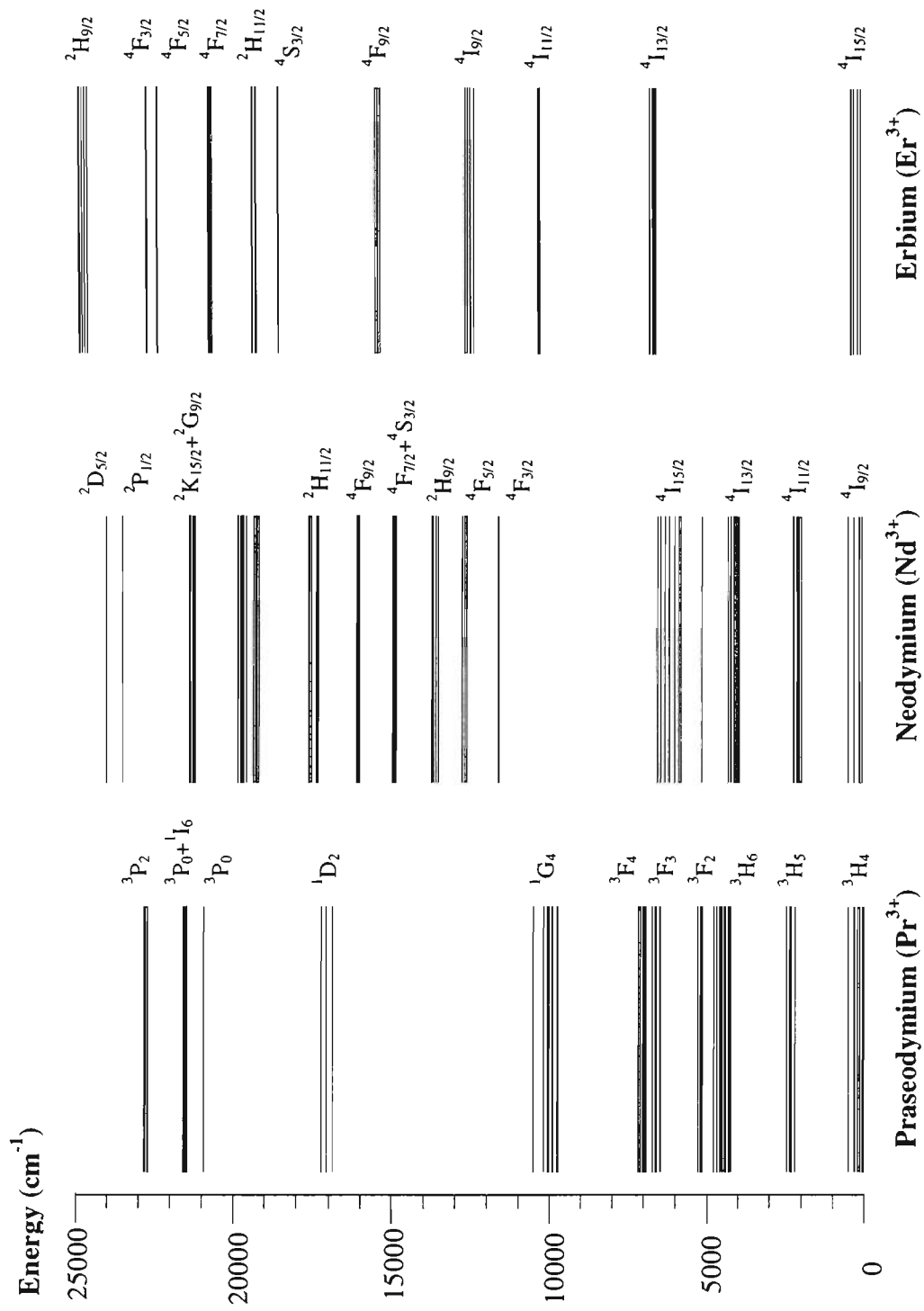


Figure 3.2.2 Partial energy level diagrams for praseodymium, neodymium and erbium [Kaminskii A.A., 1982]

3.3 ATTENUATION MEASUREMENTS

Figure 3.3.1 shows a simplified energy level diagram for praseodymium [Kaminskii A.A., 1982]. Considerable information on the electronic structure of rare-earth-ions may be obtained through spectroscopic measurements. Of particular importance is the measurement of the spectral attenuation. In Figure 3.3.1 the arrows represent the excitation of ions to the respective energy levels by photon absorption.

For low light intensities, as light propagates through a scattering medium the incident light, $I(0)$, is attenuated exponentially according to

$$\frac{I(L)}{I(0)} = \exp[-\alpha(\lambda)L] \quad (3.3.1)$$

where $I(L)$ is the intensity at position, L , along the medium. The absorption coefficient, $\alpha(\lambda)$, at a particular wavelength, λ , is a function of the total dopant concentration, ρ , the absorption cross-section, $\sigma_a(\lambda)$, and the overlap between the optical mode, $\Gamma_{overlap}$, and the praseodymium ions and is given by [Giles R.C. and Desurvire E., 1991]

$$\alpha(\lambda) = \sigma_a(\lambda)\rho\Gamma_{overlap} \quad (3.3.2)$$

The overlap function describes the relative overlap of the incident light to the ion distribution. Provided that a large optical beam is used with the sample glass, then the overlap integral is essentially unity and the absorption coefficient may be obtained directly.

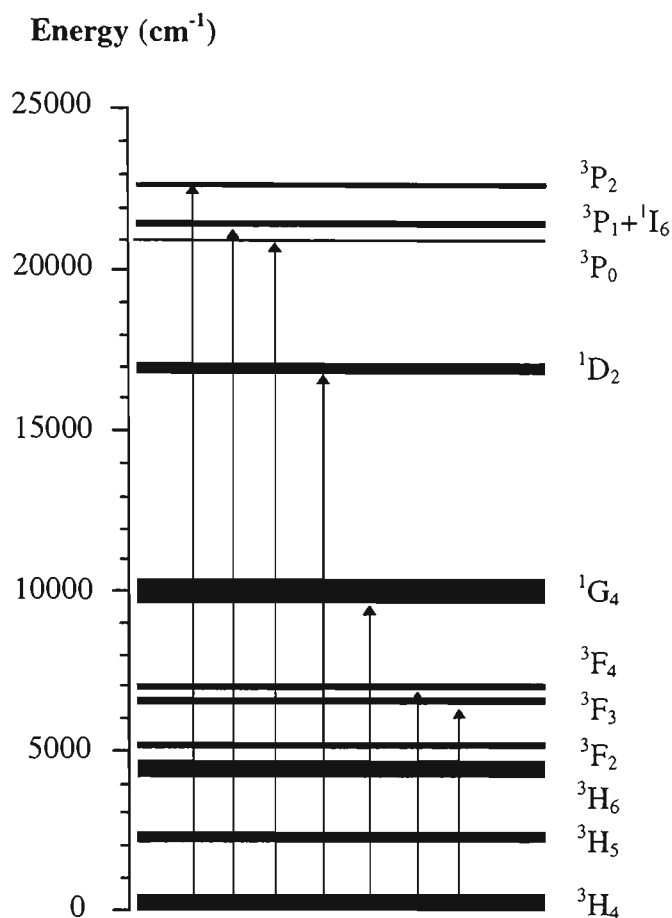


Figure 3.3.1 *Simplified energy level diagram of praseodymium. Arrows indicate the ground state absorption transition relevant to the peaks shown in the attenuation spectrum (Figure 3.3.3).*

The experimental arrangement used to measure the attenuation spectrum is shown in Figure 3.3.2. White light from a quartz-tungsten-halogen lamp, launched into the first microscope objective (O1), was collimated over a length suitable for interaction with the praseodymium-doped sample. The second objective (O2) coupled some of the remaining light into an optical fibre, of core diameter 100 μm , and subsequently into an ANDO AQ-6310B optical spectrum analyser. The data was stored on a personal computer, via a GPIB interface, for further processing.

Adjustments were made to the attenuation spectrum such that the DC offset, which arises as a result of the background loss of the fluoride glass, was subtracted.

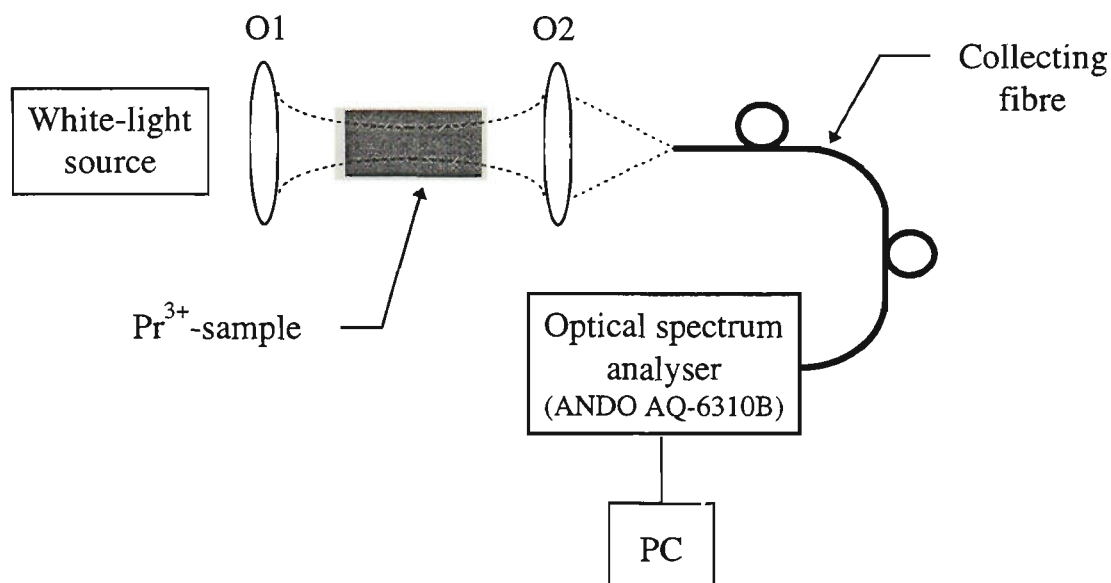


Figure 3.3.2 *Experimental arrangement used for attenuation measurements. The first microscope objective (O1) collimated the white light over a length suitable for interaction with the praseodymium-doped sample. Objective (O2) coupled some of the remaining light into an optical fibre (core diameter of 100 μm) and subsequently into an ANDO AQ-6310B optical spectrum analyser. The data was stored on a personal computer via a GPIB interface for further processing.*

The dimensions of the praseodymium doped samples are shown in Table 3.3.1 and, except for the 10000 ppm sample, the praseodymium-doped samples were approximately 40 mm in length and 8 mm in diameter. The concentration of each sample is given by the manufacturer in terms of parts per million (ppm). However, it is not completely clear whether the implied concentration is given by either the weight or the number of dopant ions relative to the other constituents making up the glass. In Section 3.7 the actual concentrations of the samples in (ions/m^3) have been determined so that in this Thesis the term *ppm* only serves as a guide to the relative dopant concentration of each glass sample.

The attenuation spectrum of praseodymium was recorded at room temperature between 400 nm and 1700 nm and is shown in Figure 3.3.3. The energy levels associated with the absorption peaks are also indicated. The absorption peaks agree well with earlier results for rare-earth-ions doped in fluorozirconate based glass [Davey S.T. and France P.W., 1989; France P.W., 1990; Ohishi Y. *et al.*, 1983]. Agreement between the energies of the absorption peaks also establishes that the rare-earth element was successfully incorporated into the fluorozirconate glass. Furthermore, for each sample there was no evidence of absorption due to the inadvertent incorporation of rare-earth ions other than the intended dopant.

Sample (ppm)	Concentration ($\times 10^{25}$) (ions/m ³)	length (mm)
500	2.8 ± 0.2	39.85 ± 0.05
1000	6.2 ± 0.3	40.70 ± 0.05
2000	12.5 ± 0.7	40.40 ± 0.05
4000	24.6 ± 1	40.65 ± 0.05
10000	67 ± 4	9.88 ± 0.05

Table 3.3.1 *The dimensions of praseodymium-doped samples. With the exception of the 10000 ppm sample, the praseodymium-doped samples were about 40 mm in length and 8 mm in diameter. The length of the 10000 ppm sample was 9.88 ± 0.05 mm and its diameter was 19.95 ± 0.05 mm. The concentration was calculated using Equation 3.3.2 and measurements of the attenuation coefficient (Section 3.3) and calculation of the absorption cross-section (Section 3.7).*

Attenuation
(dB/1000 ppm/m)

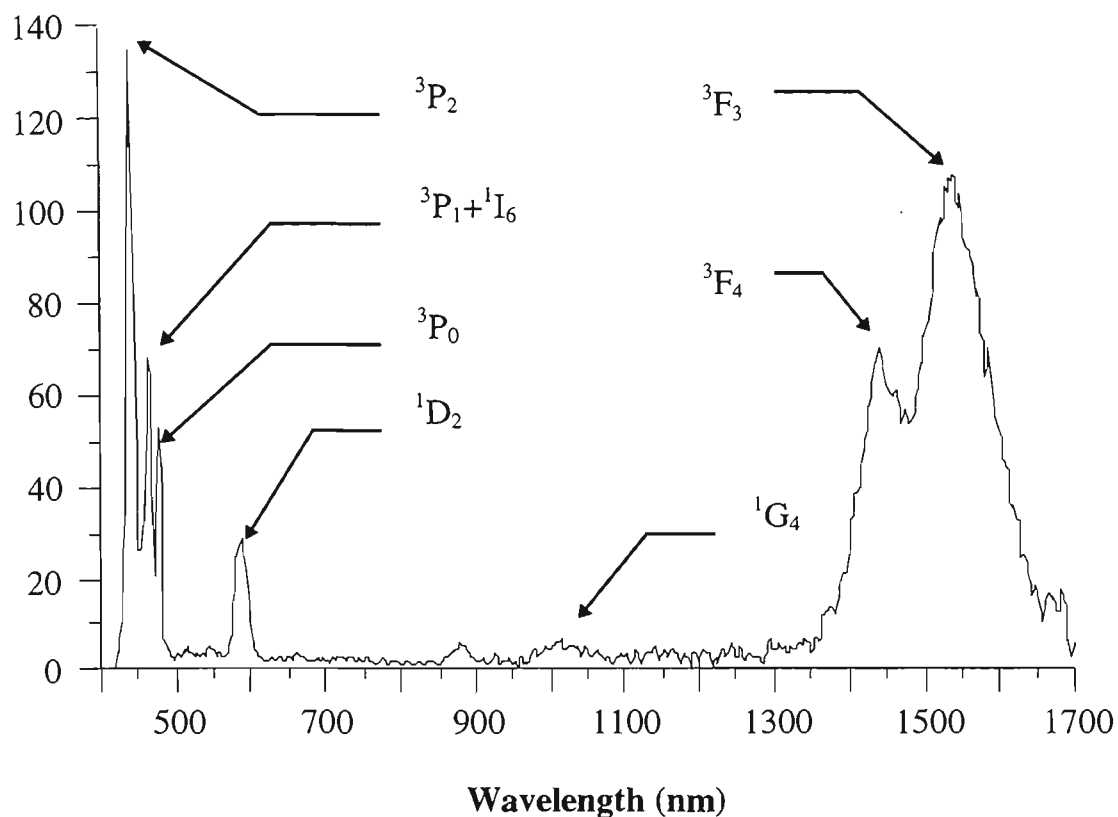


Figure 3.3.3 *The attenuation spectrum of praseodymium-doped fluorozirconate glass between 400 nm and 1700 nm recorded at room temperature.*

In the attenuation spectrum the group of three absorption peaks at around 450 nm (Figure 3.3.3) correspond to the 3P_2 , 3P_1 , 1I_6 and 3P_0 multiplets. However, the 3P_1 and 1I_6 Stark-split levels have considerable overlap and for the sake of simplicity are referred to as the 3P_1 state only. Transitions arising from these levels result in fluorescence bands in the visible region of the spectrum.

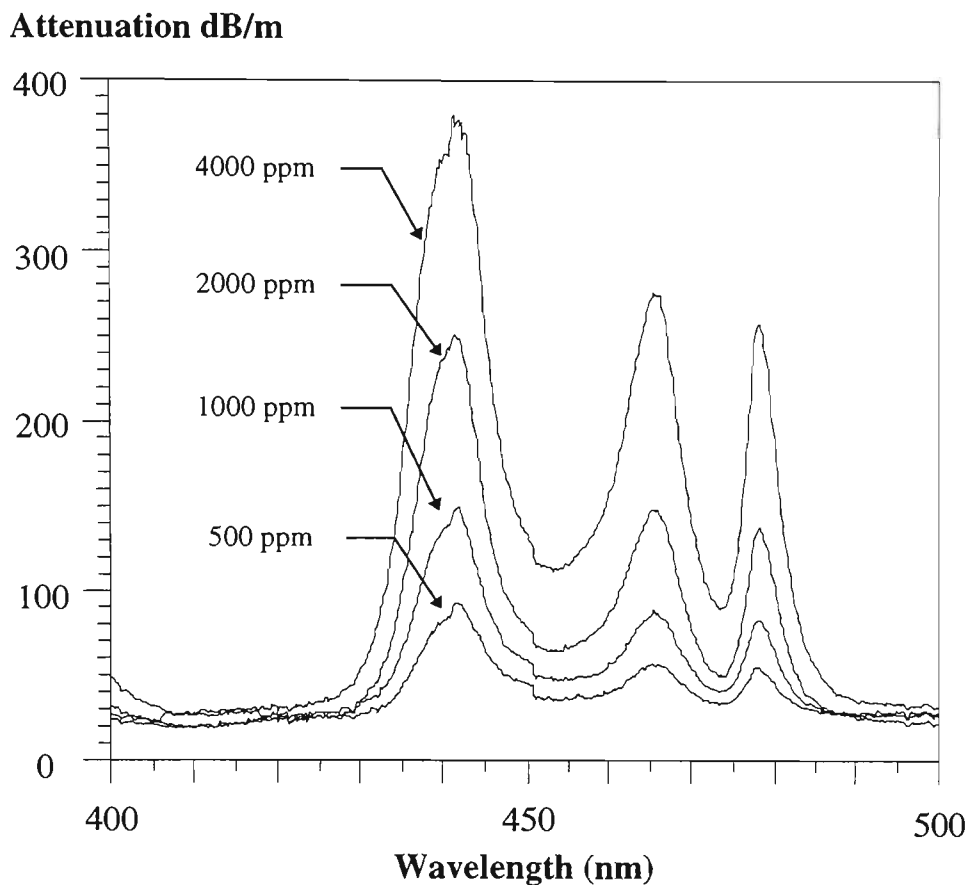


Figure 3.3.4. *The attenuation spectrum of praseodymium in a fluorozirconate glass host measured for 500 ppm, 1000 ppm, 2000 ppm and 4000 ppm samples between 400 nm and 500 nm.*

The attenuation was also measured between 400 nm and 500 nm for four of the samples to obtain a higher resolution spectra of the 3P multiplets and were normalised for length (Figure 3.3.4).

For each sample the attenuation coefficient was measured at 476.5 nm (Table 3.3.2). Using this data the attenuation coefficient at 476.5 nm for a 1000 ppm sample is $8.5 \pm 0.7 \text{ m}^{-1}$.

Sample (ppm)	Attenuation Coefficient (m^{-1}) $^3\text{P}_0$ (476.5 nm)
500	3.89
1000	8.54
2000	17.28
4000	33.96
10000	92.50

Table 3.3.2 *Attenuation coefficient at 476.5 nm measured for all four samples.*

3.4 MEASUREMENT OF RADIATIVE TRANSITIONS

The experimental arrangement used to measure radiative transitions (fluorescence) is shown in Figure 3.4.1. Components include an argon-ion laser pump source, a praseodymium-doped sample, a microscope objective ($\times 20$) to collect the spontaneous emission and an ANDO AQ-6310B optical spectrum analyser. The fluorescence was measured at side light so that a minimum amount of pump light

entered the collecting optics. The intensity of the pump was sufficiently low so no amplification distorted the emission spectrum.

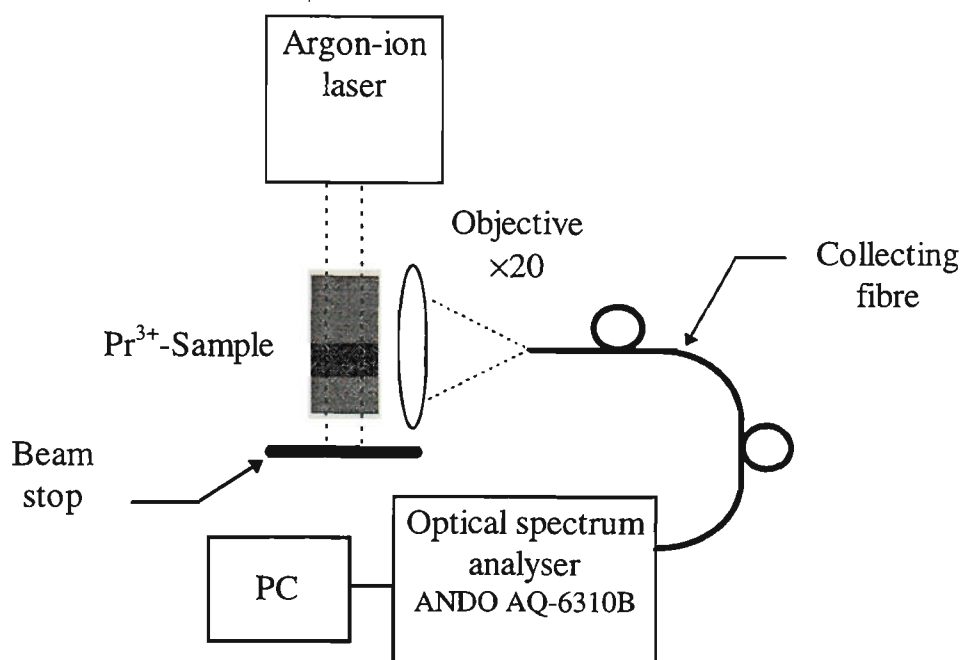


Figure 3.4.1 *Experimental arrangement for measuring the fluorescence spectrum.*

Ground state ions were excited into the 3P_1 state of praseodymium using 465.8 nm radiation from an argon-ion laser. The fluorescence spectrum was recorded between 450 nm and 950 nm and is shown in Figure 3.4.2. A partial energy level diagram is given in Figure 3.4.3 which indicates the possible transitions corresponding to the fluorescence peaks in Figure 3.4.2.

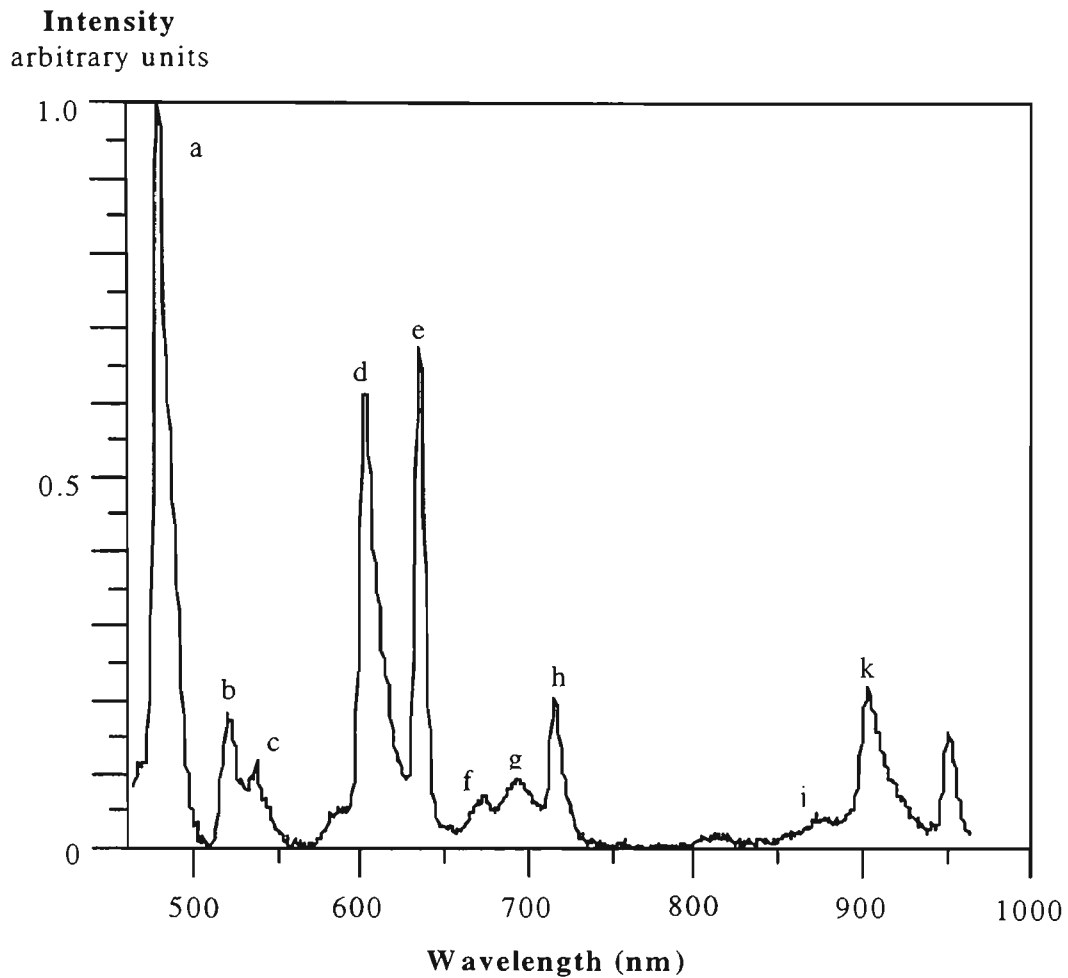


Figure 3.4.2 *Emission spectrum of praseodymium in a fluorozirconate glass host. A pump wavelength of 465.8 nm was used to raise ions into 3P_1 . The resultant spectrum is due mainly to transitions arising from 3P_0 . This is because of thermal coupling between the 3P_0 and 3P_1 levels.*

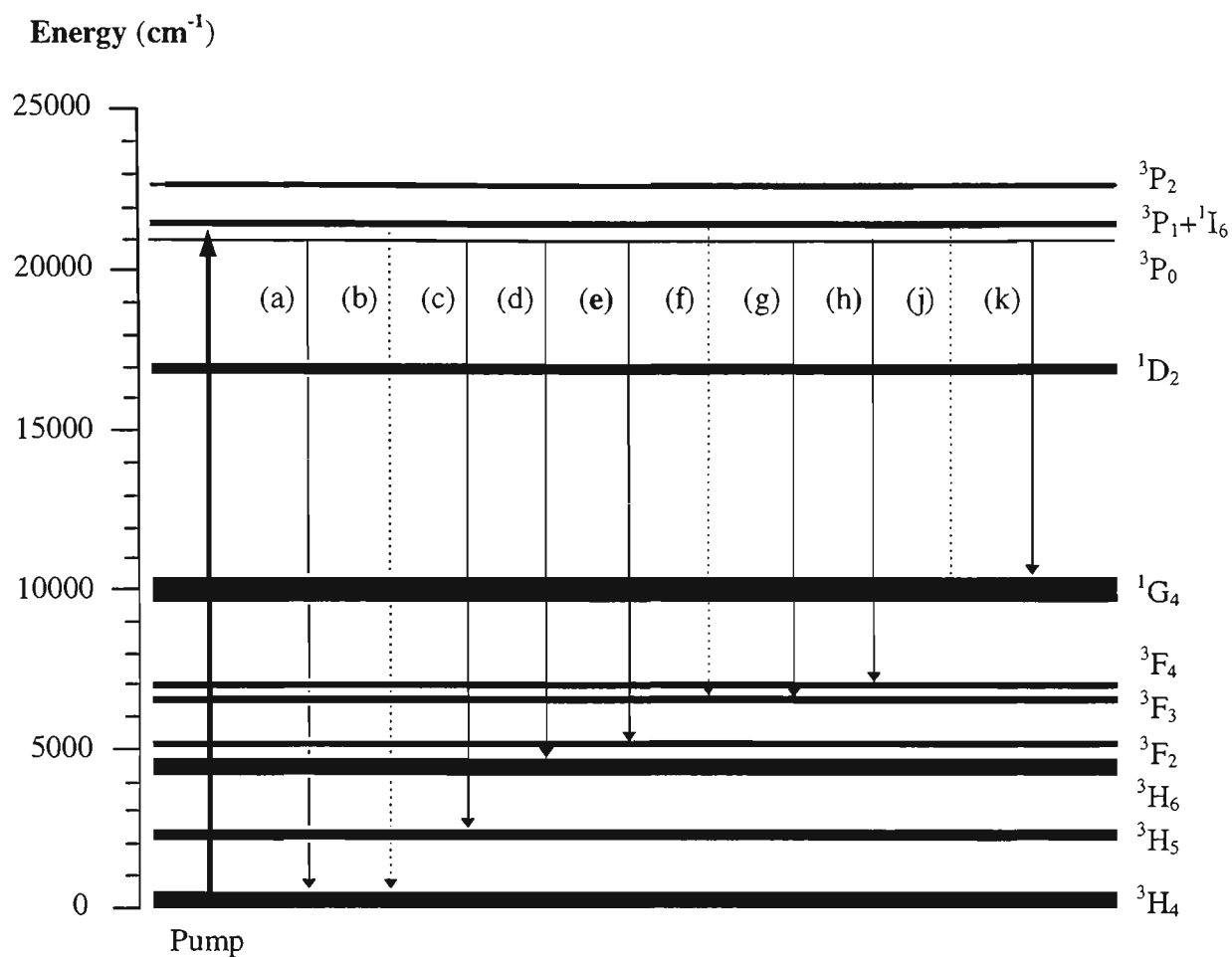


Figure 3.4.3 *Simplified energy level diagram for the praseodymium ion in fluorozirconate glass host. Arrows indicate the radiative transitions relevant to the peaks shown in the emission spectrum. Dashed lines indicate transitions arising from the 3P_1 state.*

Table 3.4.2 indicates the possible transitions arising from the 3P_0 and 3P_1 states corresponding to the fluorescence spectrum in Figure 3.4.2. For each transition the peak wavelength for each transition as measured from the fluorescence spectrum is also indicated in Table 3.4.1

Peak	Peak wavelength (λ)		Main Transition
	(nm)	(cm^{-1})	
a	480	20833	${}^3\text{P}_0 \rightarrow {}^3\text{H}_4$
b	521	19194	${}^3\text{P}_1 \rightarrow {}^3\text{H}_5$
c	537	18622	${}^3\text{P}_0 \rightarrow {}^3\text{H}_5$
d	603	16584	${}^3\text{P}_0 \rightarrow {}^3\text{H}_6$
e	635	15748	${}^3\text{P}_0 \rightarrow {}^3\text{F}_2$
f	672	14881	${}^3\text{P}_1 \rightarrow {}^3\text{F}_3$
g	694	14409	${}^3\text{P}_0 \rightarrow {}^3\text{F}_3$
h	716	13966	${}^3\text{P}_0 \rightarrow {}^3\text{F}_4$
j	873	11455	${}^3\text{P}_1 \rightarrow {}^1\text{G}_4$
k	904	11062	${}^3\text{P}_0 \rightarrow {}^1\text{G}_4$

Table 3.4.1. *Radiative transitions arising from the ${}^3\text{P}_0$ state and the ${}^3\text{P}_1$ state to lower-lying levels.*

The energy difference between the ${}^3\text{P}_0$ state and the ${}^3\text{P}_1$ state is approximately 600 cm^{-1} ($\sim 15 \text{ nm}$) measured from the absorption spectrum. These levels are said to be thermally coupled; ie. their relative populations follow a Maxwell-Boltzmann distribution given by

$$\frac{N_2}{N_1} = \frac{g_2}{g_1} \exp\left[-\frac{E_2 - E_1}{kT}\right] \quad (3.4.1)$$

where N_1 , N_2 are the populations of the levels with corresponding energies E_1 , E_2 . respectively, T is the temperature, k is Boltzmann's constant and g_1 and g_2 are the degeneracies ($g_i=2J_i+1$), or statistical weights of the levels. For the 3P_0 state $g_1=1$ and for the ${}^3P_1+{}^1I_6$ state $g_2=16$. Thus the population of 3P_1 is 5% of the population of 3P_0 at room temperature. The population distribution varies with temperature so that the magnitude of the fluorescence intensity for transitions arising from these two levels will be temperature-dependent.

Thermalisation is illustrated in Figure 3.4.4, showing the fluorescence spectra of the ${}^3P_0 \rightarrow {}^3H_5$ (537 nm) and the ${}^3P_1 \rightarrow {}^3H_5$ (521 nm) transitions recorded at 20°C (room temperature) and at 145°C.

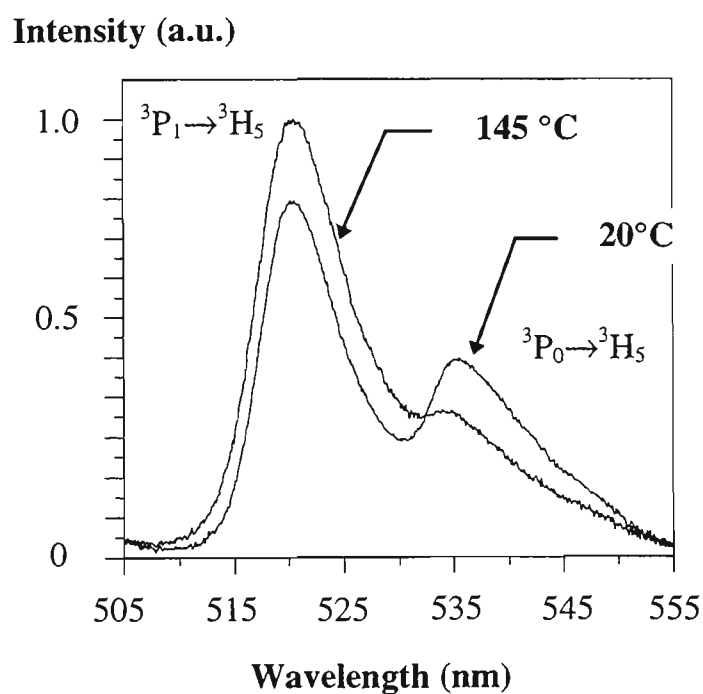


Figure 3.4.4 Fluorescence spectra indicating the ${}^3P_0 \rightarrow {}^3H_5$ and ${}^3P_1 \rightarrow {}^3H_5$ transitions recorded at 20°C and 145°C.

In Figure 3.4.5 the fluorescence spectra of the ${}^3P_0 \rightarrow {}^1G_4$ (900 nm) and the ${}^3P_1 \rightarrow {}^1G_4$ (884 nm) transitions were also recorded at 20°C and at 145°C. In both cases the population density of the 3P_1 state increased as a result of the temperature increase and is characterised by an increase in the fluorescence intensity of the ${}^3P_1 \rightarrow {}^3H_5$ and the ${}^3P_1 \rightarrow {}^1G_4$ transitions [Wade S.A. *et al.*, 1995; Maurice E. *et al.*, 1996].

Although these transitions are affected by temperature it is also important to note that no temperature variation in the fluorescence intensity for the ${}^3P_0 \rightarrow {}^3F_2$ transition was detected.

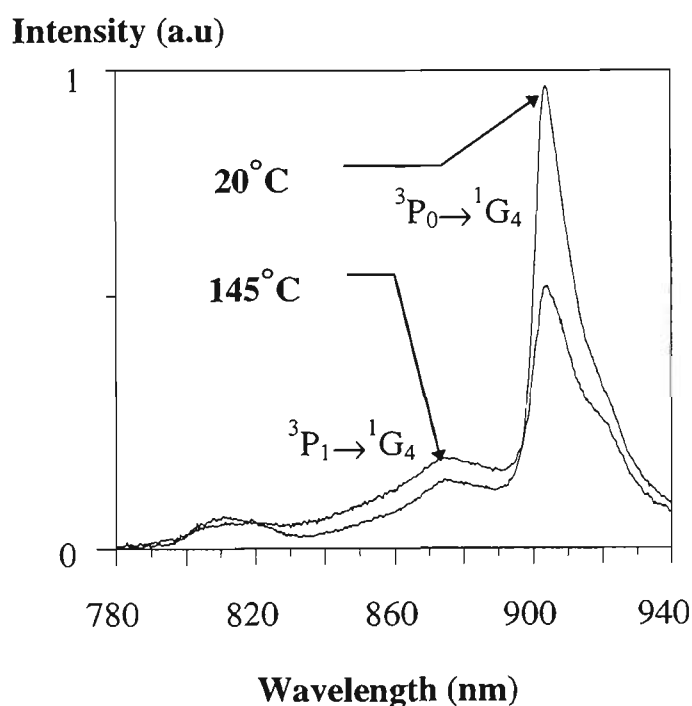


Figure 3.4.5 Fluorescence spectra indicating the ${}^3P_0 \rightarrow {}^1G_4$ and ${}^3P_1 \rightarrow {}^1G_4$ transitions recorded at 20°C and 145°C.

Transitions arising from 3P_0 to the lower lying levels result mainly in emission bands in the visible region of the electromagnetic spectrum. In particular, a transition to the 3F_2 state (indicated as peak *e* in Figure 3.4.2) results in a fluorescence band with a peak wavelength at approximately 635 nm (Figure 3.4.6). The width (FWHM) of this band was measured from the emission spectrum to be approximately 7.5 nm and is a consequence of the Stark splitting of the lower laser level [Kaminskii A.A., 1981]. It is also important to note that the 632.8 nm He-Ne wavelength is well within the gain profile of this transition (Figure 3.4.6).

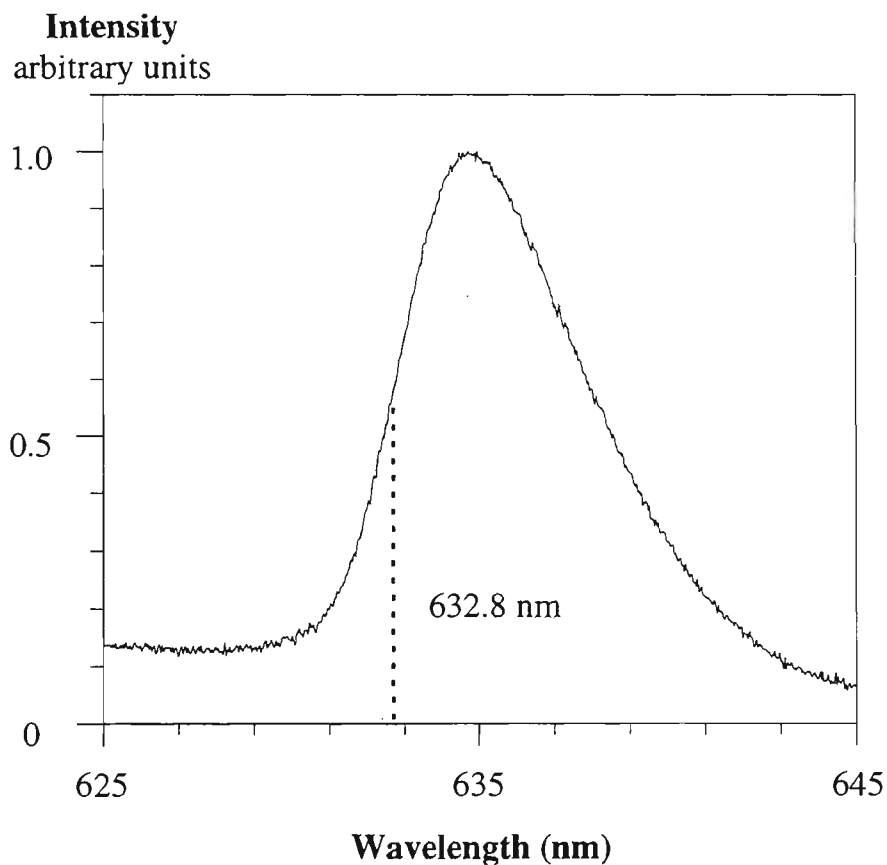


Figure 3.4.6 *The $^3P_0 \rightarrow ^3F_2$ radiative transition. The peak is centred on 635 nm and has a FWHM of about 7.5 nm.*

Log(Emission Intensity @635 nm)

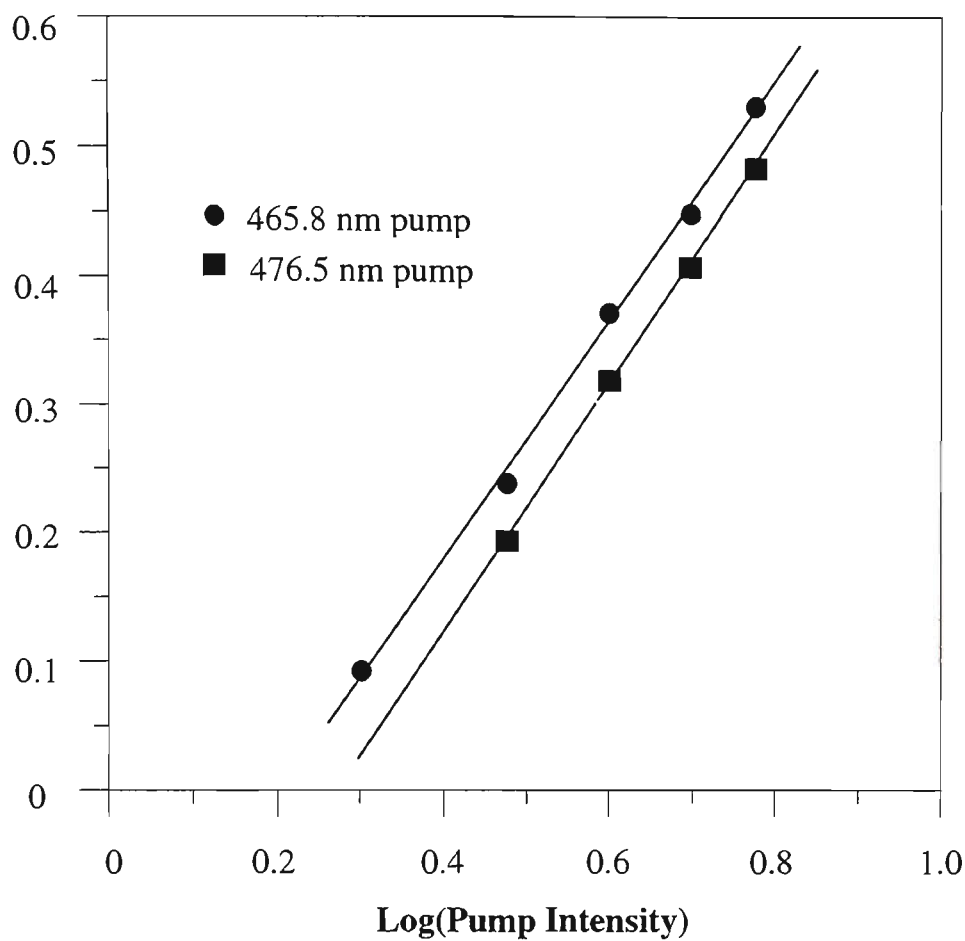


Figure 3.4.7 Fluorescence intensity of the ${}^3P_0 \rightarrow {}^3F_2$ (635 nm) radiative transition as a function of pump intensity using 476.5 nm and 465.8 nm pump wavelengths.

The peak intensity of the ${}^3P_0 \rightarrow {}^3F_2$ transition was recorded as a function of pump intensity. This was performed for direct pumping to the 3P_1 and 3P_0 states. The logarithm of the emission intensity as a function of the logarithm of the pump intensity is shown in Figure 3.4.7. The gradient for 476.5 nm pumping is 0.95 ± 0.09 while the gradient for 465.8 nm pumping is 0.92 ± 0.09 . These figures are very close to the expected gradient of 1, which indicates that for every pump photon there is

radiative emission of a photon. Furthermore, for the same pump power, the fluorescence intensity at 635 nm is greater for 465.8 nm pumping compared with 476.5 nm pumping. This is because the photon energy at 465.8 nm is greater than that at 476.5 nm.

Another important parameter that can be measured from the fluorescence spectrum is the branching ratio β_{ij} from an initial level i to some final level j . The branching ratio β_{32} , for the ${}^3P_0 \rightarrow {}^3F_2$ transition was calculated by integrating all the peaks which correspond to transitions arising from the 3P_0 state in the fluorescence spectrum (Figure 3.4.2). The 635 nm fluorescence band corresponds to about 15% of the total spectrum. This figure is an over-estimate since there are two factors which give rise to errors in calculating the branching ratio for the ${}^3P_0 \rightarrow {}^3F_2$ transition. Firstly, the ${}^3P_0 \rightarrow {}^3H_4$ transition is distorted by ground state absorption and secondly the fluorescence spectrum includes transitions from other levels. Other authors have also measured the branching ratio for the ${}^3P_0 \rightarrow {}^3F_2$ transition and other transitions arising from the 3P_0 state in praseodymium. These figures are given in Table 3.4.2 for a ZBLAN glass host and for comparison a ZBLA and InF_3 glass hosts also. The figure of 15% for the ${}^3P_0 \rightarrow {}^3F_2$ transition compares well with the most recent measurements (13%) [Remillieux A. *et al.*, 1996], but is appreciably higher than the earlier measurements [Eyal M. *et al.*, 1985; Arauzo A.B. *et al.*, 1994].

Main Transition	Branching ratio ZBLA host [Eyal M. <i>et al.</i> , 1985]	Branching ratio InF ₃ host [Arauzo A.B. <i>et al.</i> , 1994]	Branching ratio ZBLAN host [Remillieux A. <i>et al.</i> , 1996]
$^3P_0 \rightarrow ^3H_4$	0.56	0.49	0.23
$^3P_0 \rightarrow ^3H_5$	0.109	0.07	0.07
$^3P_0 \rightarrow ^3H_6$	0.157	0.3	0.27
$^3P_0 \rightarrow ^3F_2$	0.072	0.09	0.13
$^3P_0 \rightarrow ^3F_3$	-	0	0.14
$^3P_0 \rightarrow ^3F_4$	0.084	0.05	0.14
$^3P_0 \rightarrow ^1G_4$	0.018	-	-

Table 3.4.2. Branching ratios for the 3P_0 state are for (a) a ZBLA glass host, (b) a InF₃ glass host and (c) for a ZBLAN host.

3.5 CALCULATION OF NON-RADIATIVE TRANSITIONS

Once an ion has absorbed energy and is in some excited state, it may relax to lower lying intermediate levels by a variety of mechanisms. The most direct route is photon emission to an intermediate level or directly back to the ground state. However, a transition to a lower-lying level does not always result in radiative emission, as there is some probability for non-radiative decay, in which energy is

dissipated as heat. In non-radiative relaxation processes, an ion decays from an excited state to the next lowest state by emitting one or more vibrational quanta to the surrounding glass matrix. The probability for such a process decreases exponentially with increasing energy separation between levels (Equation 3.5.1).

Competing with the radiative transitions from the 3P_0 state is a non-radiative decay to the closest state 1D_2 . For a fluorozirconate glass host the multiphonon decay rate decreases as the energy gap between two states increases and becomes negligible beyond an energy gap of 4700 cm^{-1} [Eyal M. *et al.*, 1985]. The energy difference between the 3P_0 and the nearest state (1D_2) is approximately 3866 cm^{-1} [Eyal M. *et al.*, 1985].

The non-radiative decay rate W_{nr} depends on the number of phonons that have to be generated in order to lose energy to the next lowest level and is given by [Digonnet M.J.F., 1993]

$$W_{nr} = C(n(T) + 1)^p \exp(-\alpha\Delta E) \quad (3.5.1)$$

where C and α are host-dependent parameters, ΔE is the energy gap to the next lowest level, p is the number of phonons required to bridge the gap, and $n(T)$ is the Bose-Einstein occupation number for the effective phonon mode given by

$$n(T) = \frac{1}{\exp(\hbar\omega/kT) - 1} \quad (3.5.2)$$

where ω is the phonon angular frequency. In general the lower the fundamental phonon energies in the material the lower the non-radiative decay rates. In Table 3.5.1 the material parameters for the non-radiative relaxation of rare-earth-ions in glass are given for fluorozirconate and, for comparison, silicate glass and LaF_3 crystals.

Host	C (s ⁻¹)	α (10 ⁻³ cm)	ħω (cm ⁻¹)
Fluorozirconate	1.59×10 ¹⁰	5.19	500
Silica	1.4×10 ¹²	4.7	1100
LaF ₃ crystal	6.6×10 ⁸	5.6	350

Table 3.5.1 *Material parameters for fluorozirconate and silica glass and LaF₃ crystal [Digonnet M.J.F., 1993].*

Using the parameters given in Table 3.5.1, the calculated non-radiative rate W_{nr} , as a function of energy level separation ΔE , is given in Figure 3.5.1. The non-radiative rate between 3P_0 and the next lowest level, 1D_2 , is approximately 75 Hz for a fluorozirconate glass host. For comparison, the calculated non-radiative rate between 3P_0 and 1D_2 for silica glass is as high as 2×10^4 Hz and as low as 3 Hz for a LaF₃ crystal. In a silica glass host the non-radiative rate between 3P_0 and 1D_2 is greater than that for a fluorozirconate glass and would ultimately result in lower radiative rates for the 3P_0 state.

For the intermediate levels between and including 3F_4 and 3H_5 , the energy separation is no greater than 2000 cm^{-1} . From Figure 3.5.1 this would mean the non-radiative relaxation rate would be greater than 1×10^6 Hz. Clearly the main relaxation mechanism for ions in these levels is non-radiative decay. The importance of this observation is that for the $^3P_0 \rightarrow ^3F_2$ amplifier transition, the lower laser level depopulates rapidly through cascaded non-radiative processes back to the ground

state. This suggests that the populations of the intermediate levels between 3F_4 and 3H_5 can be neglected in the amplifier models.

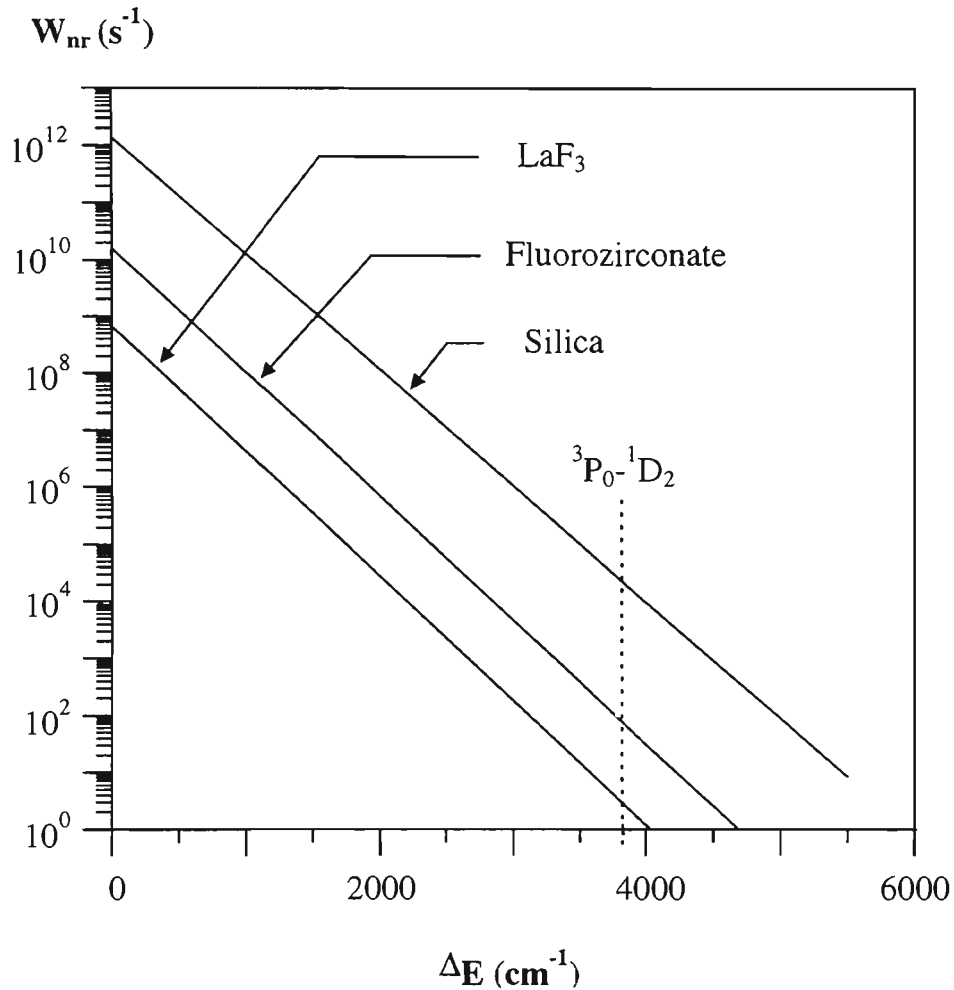


Figure 3.5.1 *Non-radiative decay rates as a function of energy separation for a fluoro-zirconate glass host, a silica glass host and a LaF₃ crystal host. The energy gap between 3P_0 and 1D_2 is also indicated.*

3.6 MEASUREMENT OF THE FLUORESCENCE LIFETIME OF THE 3P_0 STATE

3.6.1 INTRODUCTION

In Figure 3.6.1.1 a simplified energy level diagram of praseodymium indicates the relevant levels and transitions for lifetime measurements. The time behaviour of the population density of the 3P_0 state can be described using this simplified model and the appropriate rate equations for the levels. The model shown in Figure 3.6.1.1 is similar to an idealised four-level model (Section 2.2) except that the pump level and the metastable level are the same.

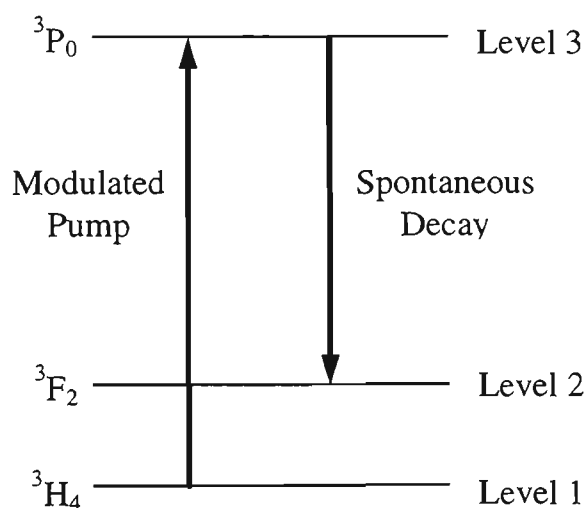


Figure 3.6.1.1 *Simplified energy level diagram for praseodymium indicating the levels and transitions for lifetime measurements.*

The time behaviour of the population density for the metastable level (level 3) at time t , is given by (Section 2.2)

$$\frac{dN_3}{dt} = R_{13}(1 - 2N_3) - \frac{N_3}{\tau_3} \quad (3.6.1.1)$$

where N_3 is the metastable level population, R_{13} is the pump rate and τ_3 is the lifetime of the level. The first term on the right hand side describes the time-dependent pumping of the 3P_0 state while the second term is the spontaneous decay. Using Equation 3.6.1.1 the time behaviour of the population density can be obtained immediately after pump turn-on and pump turn-off. The simplest solution is obtained immediately after turn-off, for which Equation 3.6.1.1 simplifies to

$$\frac{dN_3}{dt} = -\frac{N_3}{\tau_3} \quad (3.6.1.2)$$

This has a simple exponential decay solution given by

$$N_3(t) = N_3(0) \exp\left[-\frac{t}{\tau_3}\right] \quad (3.6.1.3)$$

where $N_3(0)$ is the steady-state population of the metastable level.

The rise of the fluorescence when the pump is switched on should approximate a single exponential with the characteristic time the same as when the pump is switched off. The time behaviour for the population density of the 3P_0 state immediately after pump turn-on can be obtained using $N_3(0)=0$ and $N_3(t \rightarrow \infty) = N_3^{ss}$ as the boundary conditions for Equation 3.6.1.1, and is given by

$$N_3(t) = N_3^{ss} \left[1 - \exp\left(-\frac{t}{\tau_3}(2R_{13}\tau_3 + 1)\right) \right] \quad (3.6.1.4)$$

where
$$N_3^{ss} = \frac{R_{13}\tau_3}{2R_{13}\tau_3 + 1}.$$

Two important properties not included in Equation 3.6.1.3 and Equation 3.6.1.4 are the pump modulation effects and intrinsic processes such as energy transfer. The pump modulation effects are discussed in Section 3.6.2 for when a mechanical chopper is used to modulate the pump beam. Intrinsic processes relevant to praseodymium are further discussed in Section 3.8.

3.6.2 LASER BEAM MODULATION

When a mechanical chopper is used to modulate a laser beam, in order to measure the fluorescence lifetime, the rise and fall time of the modulation should, ideally, be very much faster than the fluorescence lifetime. However, the fall time of the modulation obtained in this work was about 6 μ s, which is significant compared to the lifetimes measured here (between 30 μ s and 50 μ s). As the blade of the mechanical chopper covers a Gaussian spot (Figure 3.6.2.1) the leading and falling edge produce a time-dependent pump intensity and consequently a time-dependent population density in the 3P_0 state, distorting the fluorescence decay. This is normally dealt with by discarding fluorescence decay data that occurs too soon after the pump turn-off.

The total intensity of the Gaussian beam (Figure 3.6.2.1) can be described by

$$Total\ Intensity = \frac{1}{\pi r_0^2} \int_0^{\infty} \exp\left(\frac{-x^2}{r_0^2}\right) \cdot dr = 1 \quad (3.6.2.1)$$

The edge of the blade is assumed to be moving at constant velocity in only the x-direction. Thus the intensity of the Gaussian spot when the blade is at position x_0 is

$$I(x_0) = I_0 \frac{I}{r_0 \sqrt{\pi}} \int_x^{\infty} \exp\left(\frac{-x^2}{r_0^2}\right) \cdot dx \quad (3.6.2.2)$$

and hence

$$I(x_0) = I_0 \frac{I}{2} \operatorname{erfc}\left(\frac{x_0}{r_0}\right) \quad (3.6.2.3)$$

If r_l is the blade radius at where the laser spot hits the chopper edge and the blade angular velocity is $\omega = 2\pi f$ then the speed of the blade edge at r_l is $v_l = \omega r_l$ so that $x_0(t) = \omega r_l t$. It may be shown that the intensity of the pump as a function of time follows

$$I(t) = I_0 \left[\frac{1}{2} \operatorname{erfc}\left(\frac{t}{t_0}\right) \right] \quad (3.6.2.4)$$

Where I_0 is the initial intensity and t_0 is the turn-off time of the chopper given by $\frac{\omega r_l}{r_0}$. This was used to describe the rise and fall of the pump in accordance with the experimental conditions.

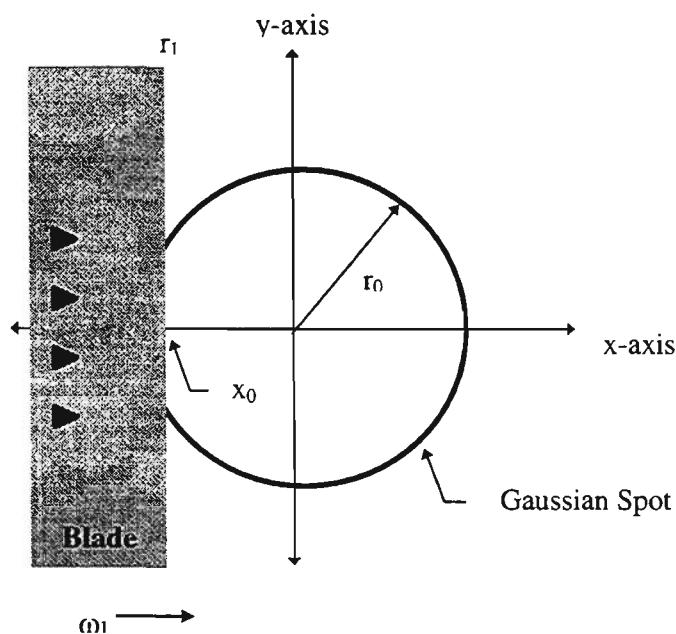


Figure 3.6.2.1 Diagram of a blade cutting across a Gaussian spot

For an idealised four-level system, the distortion of the fluorescence decay time is obtained from the solution of the following rate equation (Equation 3.6.1.1 modified) at steady-state

$$\frac{dN_3}{dt} = \frac{\sigma_p^a}{h\nu_p} I(t)(1 - 2N_3) - \frac{N_3}{\tau_3} \quad (3.6.2.5)$$

$$N_3 = \frac{\frac{\sigma_p^a}{h\nu_p} I(t)}{2I(t) \frac{\sigma_p^a}{h\nu_p} - \frac{1}{\tau_3}} \quad (3.6.2.6)$$

Numerical modelling of Equation 3.6.2.6 allows the calculation of the time at which pump modulation ceases to affect the fluorescence decay. This was determined for each decay curve. A simulated plot, using Equation 3.6.2.4 and Equation 3.6.2.6 of

the relationship between the relative population in the metastable level with time dependant pump intensity is shown in Figure 3.6.2.2.

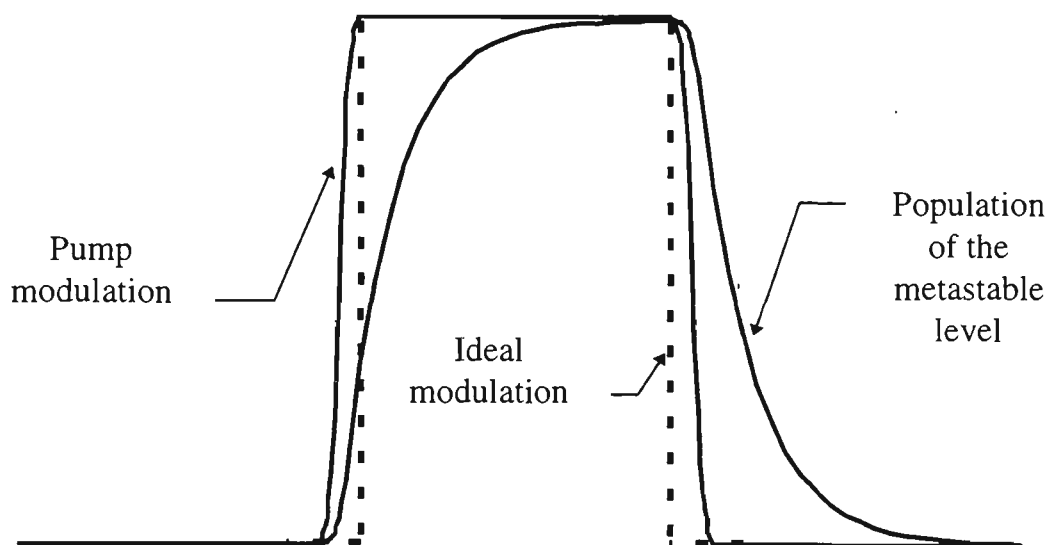


Figure 3.6.2.2 *Relative population density of the metastable level, due to pump modulation, as a function of time using Equation 3.6.2.6.*

3.6.3 EXPERIMENTAL MEASUREMENTS AND RESULTS

The fluorescence decay of 3P_0 state was observed using the experimental arrangement shown in Figure 3.6.3.1. An argon ion laser emitting at 476.5 nm, modulated by a mechanical chopper, was used to pump ground state ions into the 3P_0 state of praseodymium. The samples used in all experiments were 40 mm in length and 8 mm in diameter (Table 3.3.1). The fluorescence intensity decay was monitored with a PIN photodiode (OPF-480) coupled to a Tektronix TDS-320 oscilloscope. Data was stored on a personal computer (PC) for further processing.

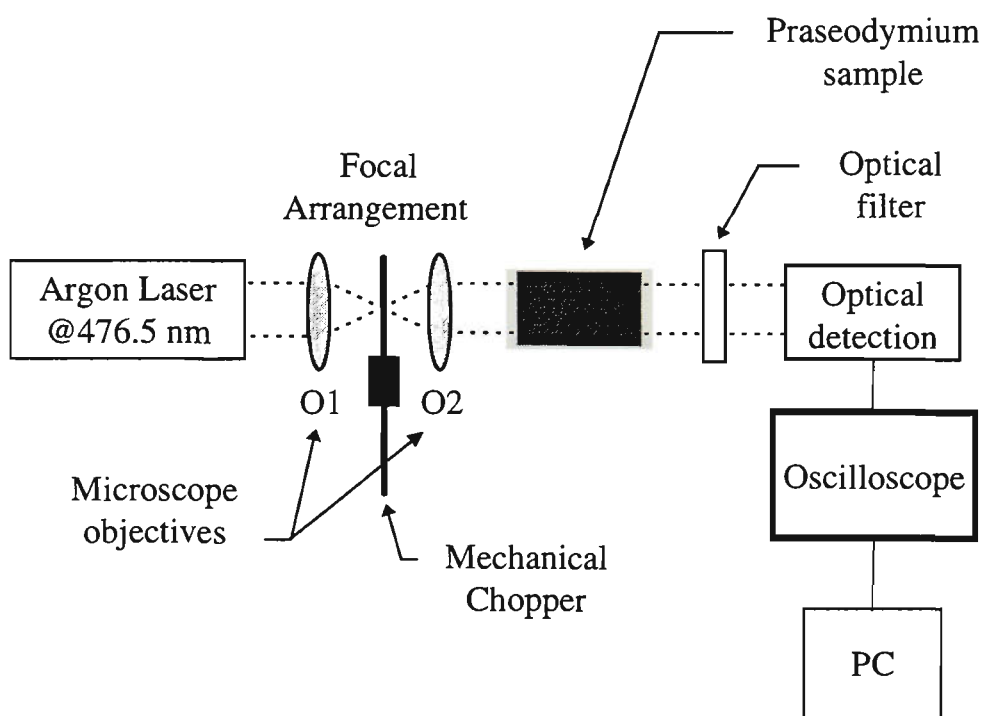


Figure 3.6.3.1 *Experimental arrangement for lifetime measurements.*

The laser beam was focused to a spot and then, after the second objective, re-established at close to the original beam diameter (Figure 3.6.3.1). By placing the mechanical chopper at the focal point the effect of the system response was minimised. The response time of the detection circuitry was of the order of 10 ns and was considered to not affect the measurement significantly.

The OPF-480 is a low noise silicon PIN photodiode mounted in a low cost package for fibre-optic applications. It has fast response at low bias and low capacitance (< 2 pf) and yields good signal to noise performance. The peak response is at 820 nm with good response between 500 nm to 1000 nm. The response in the

red region of the spectrum is about 75% of the peak. The rise time of the detector is typically between 0.5 ns and 2 ns.

Data on the fluorescence decay was obtained for five different samples having dopant concentrations of 500 ppm, 1000 ppm, 2000 ppm, 4000 ppm and 10000 ppm. The logarithm of the fluorescence intensity as a function of time, as obtained with the oscilloscope, for these concentrations is shown in Figure 3.6.3.2.

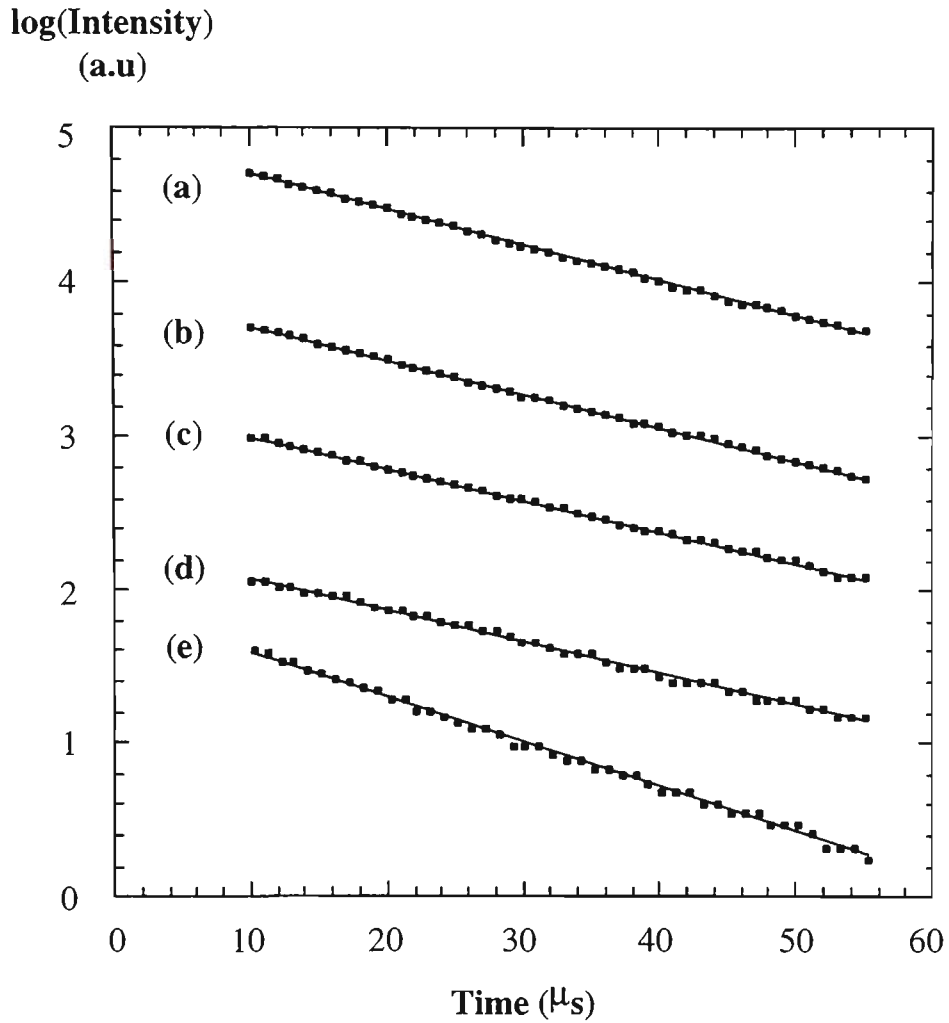


Figure 3.6.3.2 Fluorescence decay curves for (a) 500 ppm, (b) 1000 ppm, (c) 2000 ppm, (d) 4000 ppm and (e) 10000 ppm praseodymium-doped samples.

For each decay curve a least squares fit was performed with

$$y = a \exp[-xb] + c \quad (3.6.3.1)$$

as the fitting function, where the parameter b is the decay rate and the decay time is $1/b$. For a particular decay curve, data after some time interval (τ) was discarded immediately after pump turn-off. This was performed for various values of τ and for

each value a separate curve fit and fitting parameters were obtained, which enabled the uncertainty in b to be minimised. This process is depicted in Figure 3.6.3.3 which shows the parameter b , obtained from fitting the various data sets. It can be seen that the value for b (the decay rate) plateaus and indicates that the decay rate of the 3P_0 state is no longer affected by the pump turn-off modulation. The decay rate is given by the value in this plateau region.

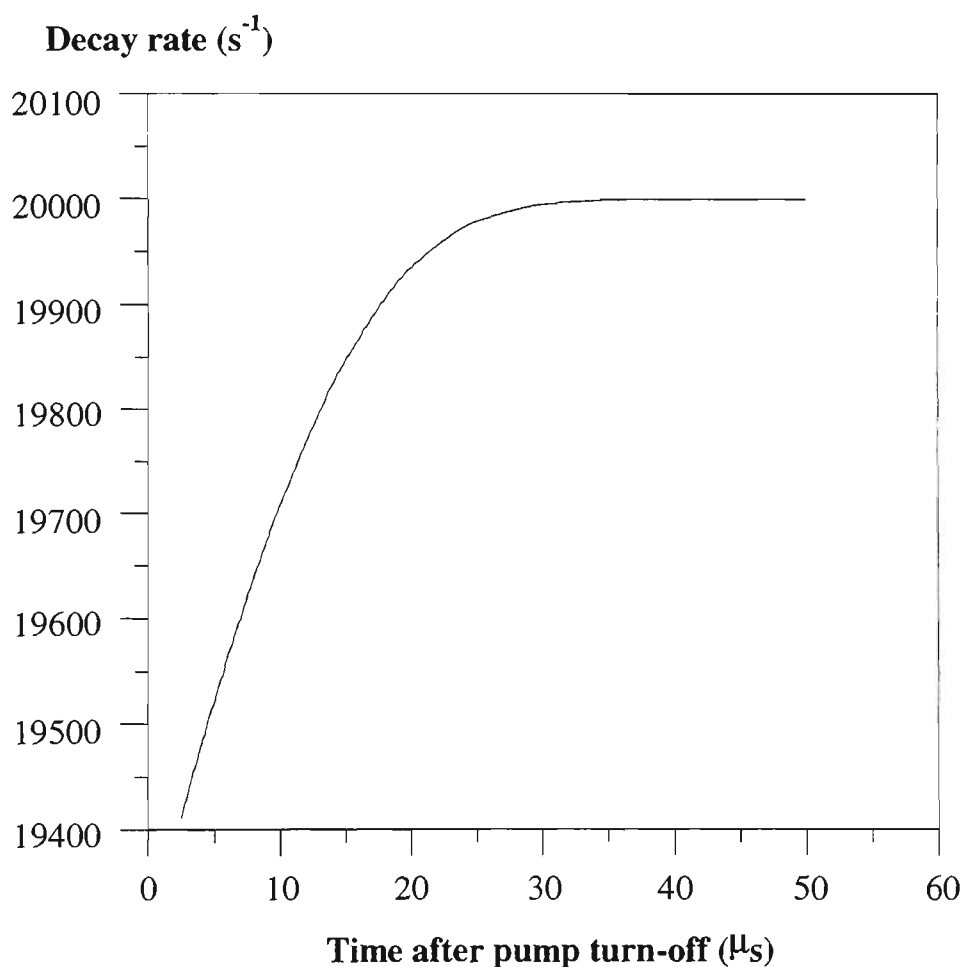


Figure 3.6.3.3 *An example of the decay rates obtained from a decay curve and by discarding data multiple times some time interval after pump turn-off.*

Sample	Concentration ($\times 10^{25}$) (ion/m ³)	Measured decay rate (Hz)
500 ppm	2.8 ± 0.2	20644 ± 85
1000 ppm	6.2 ± 0.3	20894 ± 56
2000 ppm	12.5 ± 0.7	21386 ± 32
4000 ppm	24.6 ± 1	23234 ± 187
10000 ppm	67 ± 4	28645 ± 212

Table 3.6.3.1 *Summary of the measured decay rate of the 3P_0 state with varying praseodymium concentration.*

The resultant decay rates (Γ_3) as a function of concentration are given in Table 3.6.3.1 and plotted in Figure 3.6.3.4. Calculations of the concentration are given in Section 3.7.

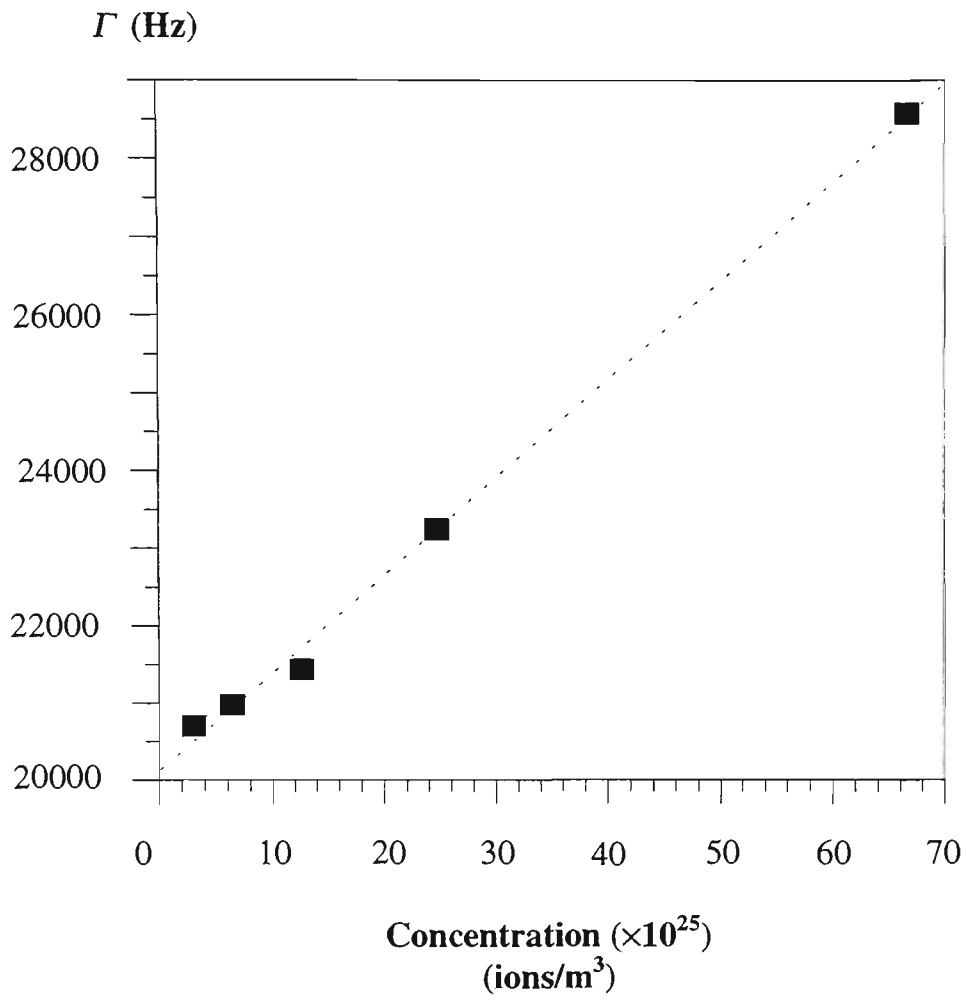


Figure 3.6.3.4 *Measured decay constants as a function of praseodymium concentration. The dashed line was obtained using Equation 3.8.3.7 as the fitting function.*

3.7 CALCULATION OF ABSORPTION AND EMISSION CROSS-SECTIONS

The stimulated emission cross-section of the ${}^3P_0 \rightarrow {}^3F_2$ transition can be estimated from the fluorescence lifetime, τ , fluorescence linewidth, $\Delta\nu$, and the branching ratio, β , using Fuchtbauer-Ladenburg analysis for a transition with a depleted lower state [Barnes W.L. *et al.*, 1991]. The Fuchtbauer-Ladenburg analysis relates the normalised absorption spectrum to the peak absorption cross-section and the normalised fluorescence spectrum to the peak emission cross-section. The equations are derived from the Einstein relation for the A and B coefficients of a two-level system [Barnes W.L. *et al.*, 1991; Edwards J.G., 1966]. The emission cross-section may be written as

$$\sigma_{32}(\nu) = \frac{\lambda_{peak}^2 A_{32}}{8\pi n^2} \frac{I(\nu)}{\int I d\nu} \quad (3.7.1)$$

and the absorption cross-section as

$$\sigma_{13}(\nu) = \frac{g_3}{g_1} \frac{\lambda_{peak}^2 A_{31}}{8\pi n^2} \frac{I(\nu)}{\int I d\nu} \quad (3.7.2)$$

where n is the refractive index of the core, $A_{31} = \beta_{31} A_3$ is the spontaneous transition probability, g_1 and g_3 are the level degeneracies, and $I(\nu)$ is the intensity at frequency ν [Barnes W.L. *et al.*, 1991; Pedersen B. *et al.*, 1991a]. $I(\nu)/\int I d\nu$ is the lineshape function and may be given by a Gaussian or Lorentzian distribution. For the absorption cross-section a Lorentzian distribution was chosen as it better describes the broadening of a level with no Stark splitting. For the emission lineshape

a Gaussian distribution was assumed. Table 3.7.1 indicates the values for the parameters used, with reference to Equation 3.7.1, to calculate the emission cross-section.

Parameter	
λ_{peak}	635.5 nm
A_{32}	2610 Hz
$\Delta\nu$	7.5 nm
n_{core}	1.514
β_{32}	13%
$\tau_3(\rho \rightarrow 0)$	49.8 μs^*

Table 3.7.1 *Values for the parameters in Equation 3.7.1 used to calculate the emission cross-section. (* this is extrapolated from Figure 3.6.3.4) which is the lifetime in the limit of zero concentration)*

Figure 3.7.1 shows the calculated emission cross-section for the ${}^3\text{P}_0 \rightarrow {}^3\text{F}_2$ transition. The emission cross-section at 632.8 nm was calculated to be $2.1 \times 10^{-24} \text{ m}^2$ ($3.4 \times 10^{-24} \text{ m}^2$ at the peak).

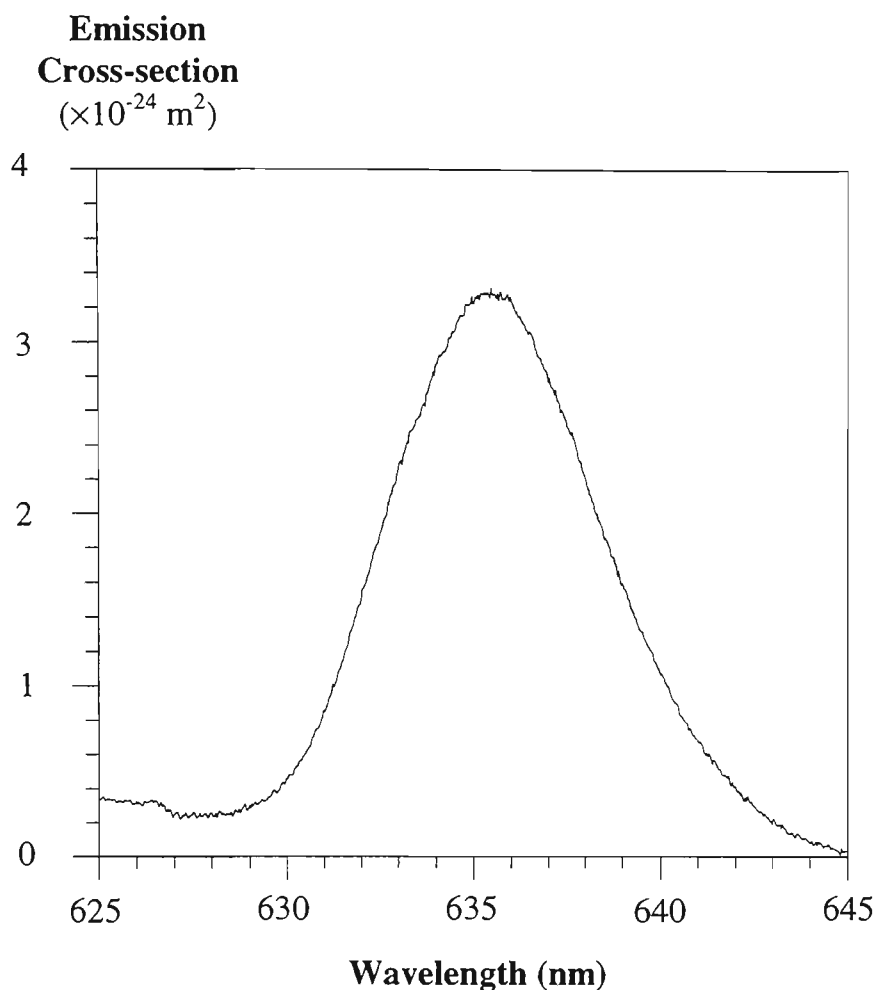


Figure 3.7.1 *Calculated emission cross-section, using Fuchtbauer-Ladenburg analysis, for the $^3P_0 \rightarrow ^3F_2$ transition.*

Table 3.7.2 indicates the values for the parameters used, with reference to Equation 3.7.2, to calculate the emission cross-section. Figure 3.7.2 shows the calculated absorption cross-section for the 3P_0 absorption band. For the pump wavelength (476.5 nm) the absorption cross-section was calculated as $0.14 \times 10^{-24} \text{ m}^2$ ($0.2 \times 10^{-24} \text{ m}^2$ at the peak).

Parameter	
λ_{peak}	478 nm
A_{31}	4619 Hz
Δv	5 nm
n_{core}	1.514
g_1	9
g_3	1
β_{31}	23%
$\tau_3(\rho \rightarrow 0)$	49.8 μs^*

Table 3.7.2 Values for the parameters in Equation 3.7.2 used to calculate the absorption cross-section. (* this is extrapolated from Figure 3.6.3.4 which is the lifetime in the limit of zero concentration)

The validity of the Fuchtbauer-Ladenburg equations has been questioned by others who have shown that in erbium the cross-sections may be up to 20% too low [Dybdal K. *et al.*, 1989; Pedersen B. *et al.*, 1991b]. However, there is currently no evidence that there are similar problems associated with praseodymium. Finally, the values for the absorption and emission cross-sections will be used to calculate the expected gain, with reference to Equation 2.4.2.7, in Chapter 5.4.

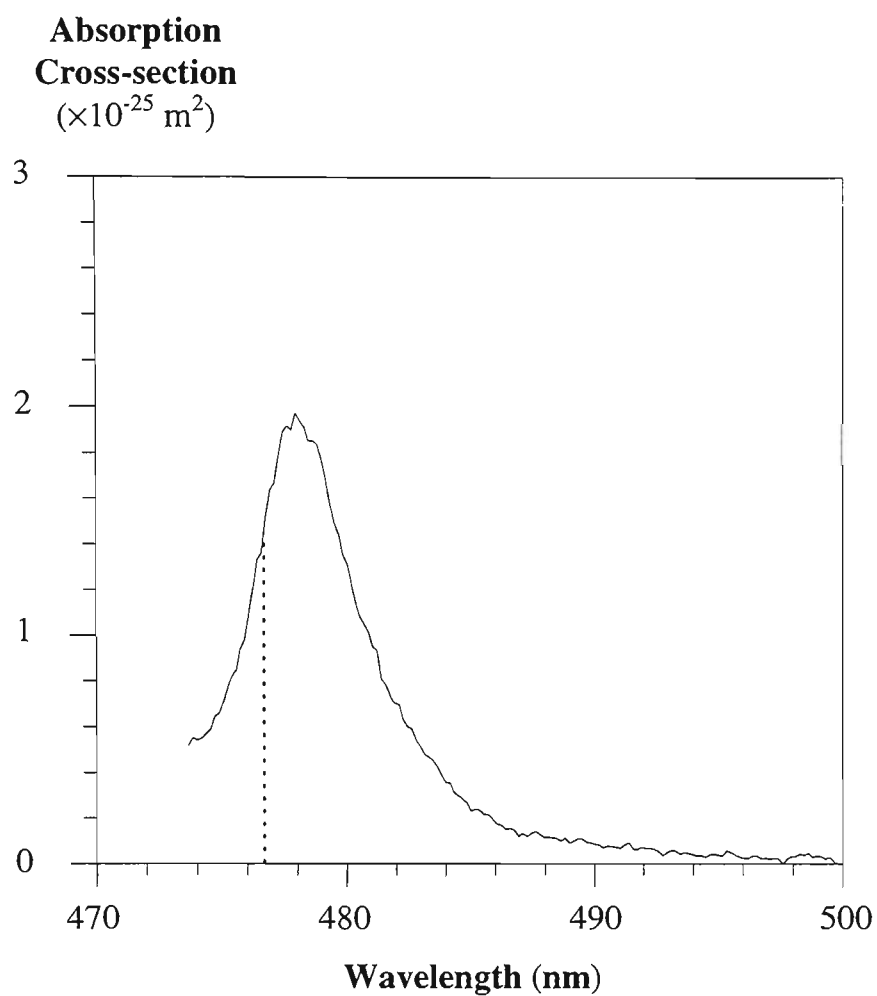


Figure 3.7.2 Calculated absorption cross-section, using Fuchtbauer-Ladenburg analysis, for the $^3H_4 \rightarrow ^3P_0$ transition. Dashed line indicates 476.5 nm.

3.8 ION-ION INTERACTIONS IN PRASEODYMIUM

3.8.1 INTRODUCTION

An ion in any level may decay at a rate determined by the sum of the radiative, non-radiative and energy transfer rates

$$A_{total} = A_{radiative} + A_{nonradiative} + A_{energy\ transfer} \quad (3.8.1.1)$$

The radiative relaxation rate and the non-radiative relaxation rate are measures of the photon and phonon emission rates respectively, neither of which are concentration dependent. Energy transfer is a cooperative effect where one ion will change state by donating energy to a nearby acceptor ion at a rate which will depend on the separation of the interacting ions, and thus the process is concentration dependent. Two examples of energy transfer processes are cross-relaxation and cooperative upconversion.

Cross-relaxation and cooperative upconversion generally involve an exchange of energy between ions. This exchange of energy may occur among rare-earth ions of the same or different species. When energy transfer takes place between two different ions, the ion that is optically excited is referred to as the donor and the one that receives the excitation is called the acceptor ion.

According to the theory of Dexter D.L., 1953, the transition probability for an electric dipole process in which a donor ion transfers energy to an acceptor is proportional to the overlap integral between the emission band corresponding to the donor transitions and the absorption band of the acceptor ion and may be written in terms of the product of the fluorescence line-shape or emission cross-section of the

donor transition and the absorption line-shape or the absorption cross-section of the acceptor.

Cross-relaxation is a process in which one ion in an excited state transfers part of its energy to a neighbouring ion. An example of cross relaxation is shown in Figure 3.8.1.1. Here, an ion initially in an excited state (level 3) may interact with a nearby ion in level 1 (this level can either be the ground or an intermediate state) and the donor ion may subsequently transfer part or all of its energy to the acceptor ion, promoting both into an intermediate level 2.

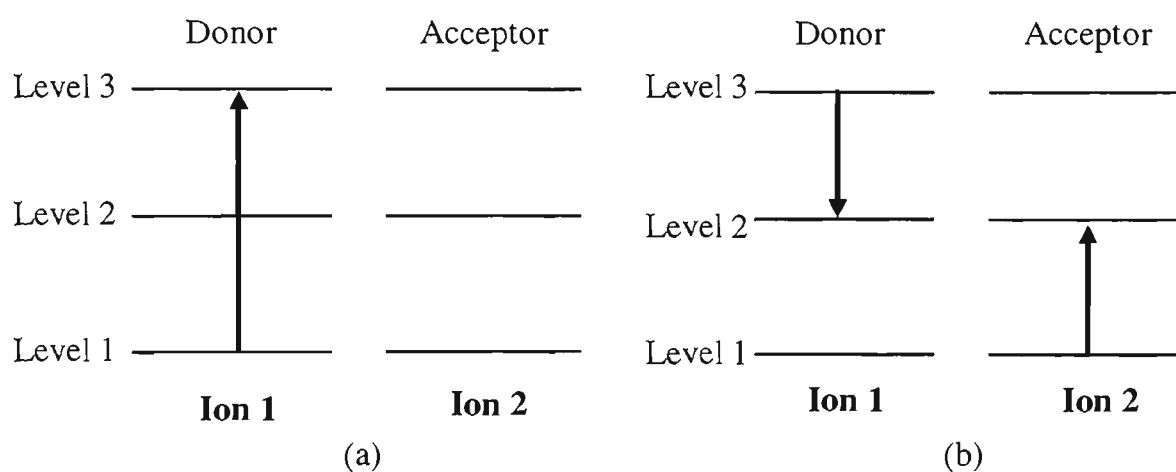


Figure 3.8.1.1. *An example of cross relaxation where (a) an ion is excited into level 3, (b) an ion in level 3 decays to level 2 and transfers its energy to an ion in a lower lying state (level 1) thereby raising it to level 2.*

Cooperative up-conversion is a special case of cross-relaxation in that the acceptor ion is already in an excited state. Similarly the donor ion transfers part or all of its energy to the acceptor ion. Again the donor and acceptor may be of the same or different species of ion. This is depicted in Figure 3.8.1.2.

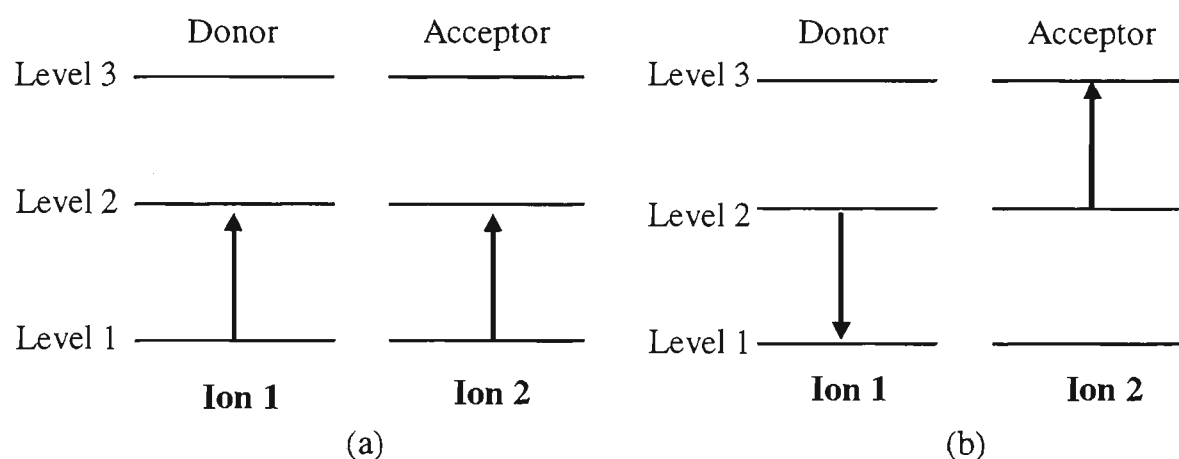


Figure 3.8.1.2. *An example of energy transfer between two ions. In this case (a) an ion is excited into level 2 of both the donor and the acceptor, (b) the donor ion in level 2 decays to level 1 and transfers its energy to the nearby acceptor ion thereby raising it to level 3.*

3.8.2 CROSS RELAXATION AND ENERGY TRANSFER IN PRASEODYMIUM

There are two main channels for cross-relaxation of the 3P_0 state [Eyal M. *et al.*, 1985]. A partial energy level diagram of praseodymium is shown in Figure 3.8.2.1(a). Included in this figure are three possible cross-relaxation paths. One possible path for cross-relaxation is depicted in Figure 3.8.2.1(b) and is assigned the parameter α_{cr1} . In this case a donor ion in an excited state (3P_0) may de-excite to 1G_4 by transferring its energy to an ion in the ground state, with the acceptor ion being raised to 1G_4 . Another channel for cross-relaxation, assigned the parameter α_{cr2} , is shown in Figure 3.8.2.1(c). For this energy transfer process, a donor ion in the 3P_0 state may de-excite to 1D_2 by transferring its energy to another ion in the ground state. The ground state acceptor ion is thus raised into the 3H_6 state. Cross-relaxation is possible since the energy differences between the 3P_0 - 1D_2 transition and the 3H_4 - 3H_6 transition and the 3P_0 - 1G_4 transition and the 3H_4 - 1G_4 transition are nearly equal.

There is, however, a third cross-relaxation channel which is depicted in Figure 3.8.2.1(d). It involves the 3P_0 state relaxing to the 3H_6 state and transferring energy to a ground state ion which is raised to the 1D_2 state. Cross-relaxation is possible since the energy differences between the 3P_0 - 3H_6 transition and the 3H_4 - 1D_2 transition are nearly equal. This process has not been identified previously by other authors including [Petreski B.P. *et al.*, 1996], but it has been included in this chapter.

Another mechanism which has been observed and which may also deplete the 3P_0 state is an upconversion process attributed to a cooperative energy transfer from a pair of praseodymium ions in the 3P_0 state to a nearby ion in the same state [Lee L.S.

et al., 1984]. The energy transfer process is a three ion interaction in which the two donor ions and the participating acceptor ion are all praseodymium in the same excited state (3P_0). Through this interaction process the two donor ions can de-excite to the 1G_4 and 3F_2 states while releasing sufficient energy to up-convert the acceptor ion to the 1S_0 state at about 47000 cm^{-1} . This is depicted in Figure 3.8.2.2.

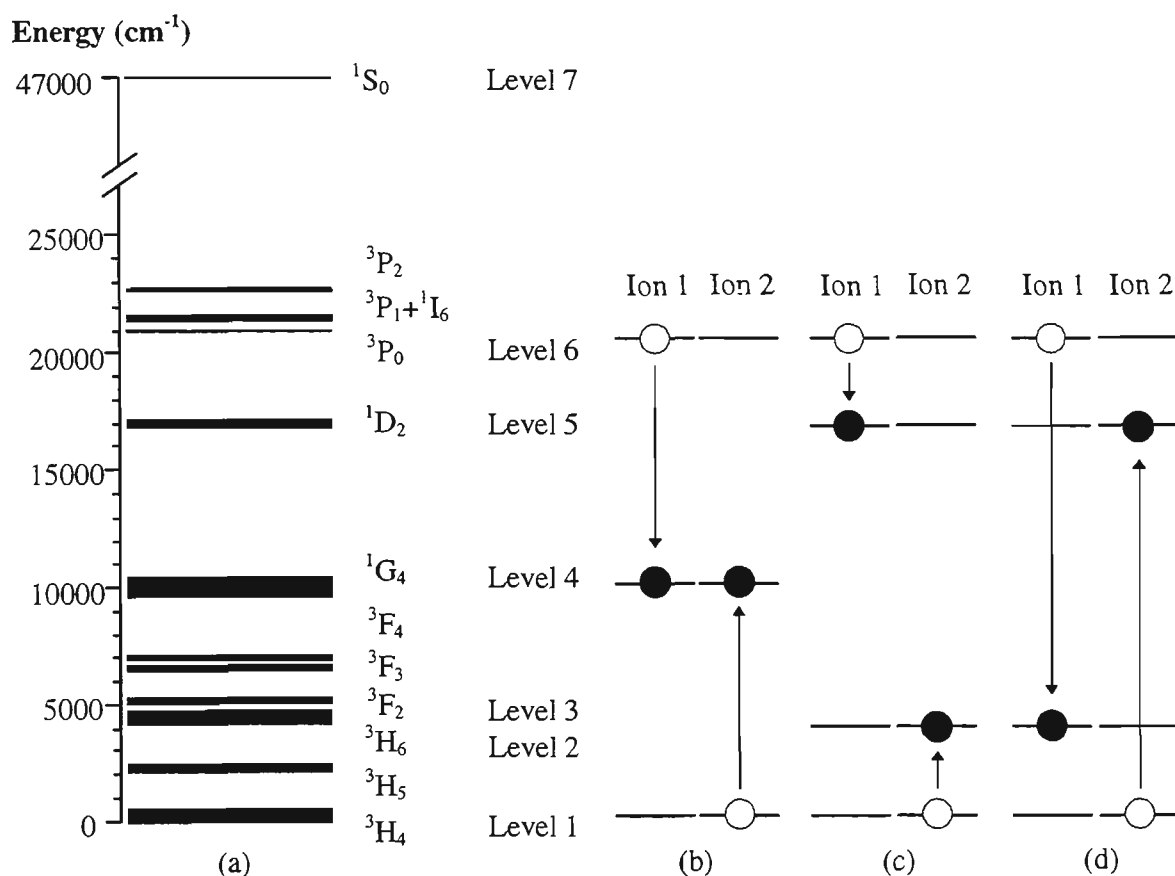


Figure 3.8.2.1 (a) Partial energy level diagram for praseodymium in a fluorozirconate glass host, cross-relaxation process
 (b) $(^3P_0 \rightarrow ^1G_4)$ and $(^3H_4 \rightarrow ^1G_4)$, (c) $(^3P_0 \rightarrow ^1D_2)$ and $(^3H_4 \rightarrow ^3H_6)$
 and (d) $(^3P_0 \rightarrow ^3H_6)$ and $(^3H_4 \rightarrow ^1D_2)$.

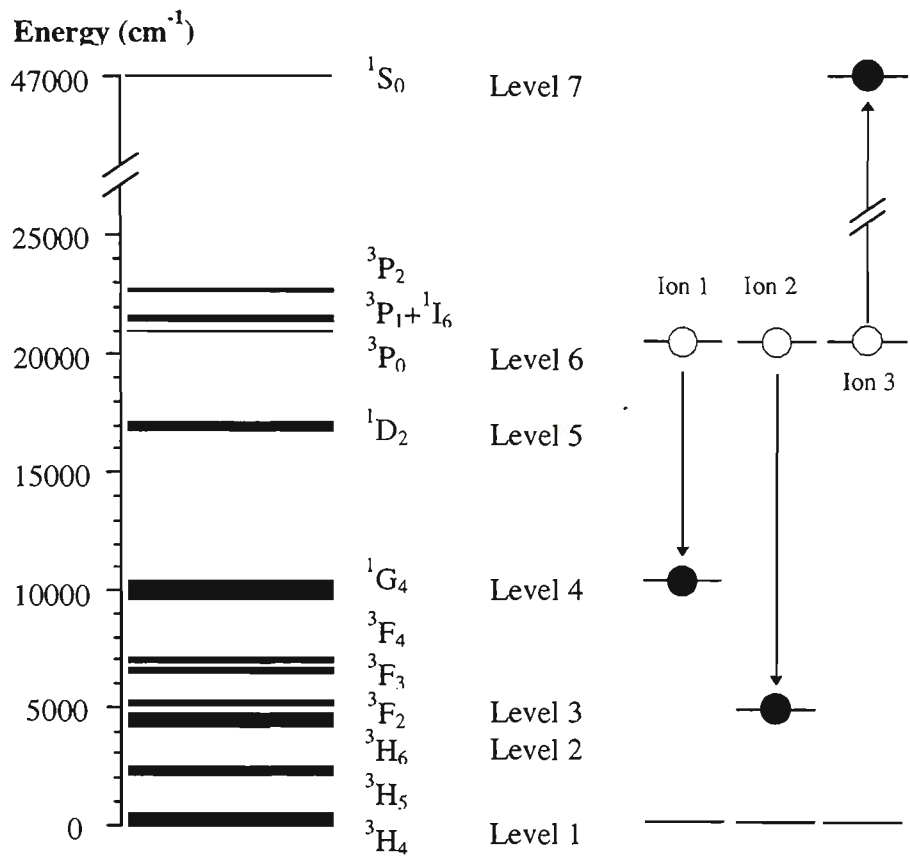


Figure 3.8.2.2. Cooperative energy transfer process for praseodymium in a fluorozirconate glass host.

3.8.3 RATE EQUATION MODEL

The cross-relaxation and cooperative upconversion processes are described by the following rate equation for the ${}^3\text{P}_0$ state

$$\begin{aligned} \frac{dN_6}{dt} = & R_{16}(N_1 - N_6) \\ & - \frac{N_6}{\tau_6} - \frac{1}{2}\alpha_{cr1}N_1N_6 - \frac{1}{2}\alpha_{cr2}N_1N_6 - \frac{1}{2}\alpha_{cr3}N_1N_6 \\ & - \beta_{et}N_6^3 \end{aligned} \quad (3.8.3.1)$$

where N_i is the population density of state i as labelled in Figure 3.8.2.1, τ_6 is the lifetime of state 6 in the limit of zero concentration. The first term describes the pumping while the second term is the spontaneous decay of the ${}^3\text{P}_0$ state, the third, fourth and fifth terms are the cross-relaxation rates and the last term is the energy transfer rate characterised by the parameter β_{et} . For simplicity, it is assumed that the pump absorption and emission cross-sections are equal and all other intermediate levels decay quickly back to the ground level.

To make the concentration dependence explicit in the rate equation we can normalise the population densities of the levels by writing $N_i = \rho n_i$, where ρ is the concentration of the dopant ions (ion/m^3) and n_i is the normalised population density of level i . The consequent decay of the ${}^3\text{P}_0$ state in the absence of pumping (pumping term in Equation 3.8.3.1 is neglected because $R_{16}=0$) is then given by

$$\frac{dn_6}{dt} = -\frac{n_6}{\tau_6} - \frac{1}{2}(\alpha_{cr1} + \alpha_{cr2} + \alpha_{cr3})\rho n_1 n_6 - \beta_{et}\rho^2 n_6^3. \quad (3.8.3.2)$$

In the experiments described here, relatively low powers of the exciting laser were used so that the fraction of ions in the 3P_0 state was always small. Under these conditions the final term in equation 2 may be neglected since it depends on the cube of a small quantity and thus equation 2 simplifies to

$$\frac{dn_6}{dt} = -\frac{n_6}{\tau_6} - \frac{1}{2}(\alpha_{cr1} + \alpha_{cr2} + \alpha_{cr3})\rho n_1 n_6. \quad (3.8.3.3)$$

Fluorescence decay measurements of level 3 require that it has an initial population, so that when the pump source is removed (*ie.* $R_{13} \rightarrow 0$) Equation 3.8.3.1 will only contain losses from that level. The consequent decay is then given by:

$$\frac{dn_6}{dt} = -\frac{n_6}{\tau_6} - \frac{1}{2}\alpha_{cr}\rho n_1 n_6. \quad (3.8.3.4)$$

where $\alpha_{cr} = \alpha_{cr1} + \alpha_{cr2} + \alpha_{cr3}$.

As the pump rate to the 3P_0 state is dependent on pump intensity, the diameter of the pump beam was kept relatively large at the sample, ensuring minimal depletion of the ground level population density. As is evident in Figure 3.6.3.2, no deviation from exponential decay, for all data, was observed which justifies the validity of the previous statement. This also indicates that the energy upconversion process (term 5 in Equation 3.8.3.1) is relatively small. Since the ground state is depleted minimally, the normalised population density of the ground level can be approximated to unity and Equation 3.8.3.4 no longer depends on n_1 . This allows Equation 3.8.3.4 to be written as

$$\frac{dn_6}{dt} = -n_6 \left[\frac{1}{\tau_6} + \frac{1}{2}\alpha_{cr}\rho \right]. \quad (3.8.3.5)$$

This has a solution of the form

$$n_6(t) = n_6(0) \exp\left(-t/\tau\right) \quad (3.8.3.6)$$

where

$$\frac{1}{\tau} = \frac{1}{\tau_6} + \frac{1}{2} \alpha_{cr} \rho \quad (3.8.3.7)$$

From Equation 3.8.3.7, τ is the measured lifetime, $1/\tau_6$ is the sum of the radiative and non-radiative rates, $\frac{1}{2} \alpha_{cr} \rho$ is the energy transfer rate, and $n_6(0)$ is the population density in level 6 at the end of the pump pulse. Equation 3.8.3.7 indicates the relationship between the lifetime of level 6 and the dopant concentration.

Using this relationship we applied a least squares fit to the data in Figure 3.6.3.4 to relate the measured lifetime of level 6 with dopant concentration. The sum of the cross-relaxation parameters (α_{cr}) was determined to be $2.8 \pm 0.1 \times 10^{-23} \text{ m}^3/\text{s}$. The lifetime of the $^3\text{P}_0$ state was determined to be $\tau_6(\rho \rightarrow 0) = 49.8 \pm 0.3 \text{ } \mu\text{s}$ in the limit of zero concentration. Furthermore, the value for the cross-relaxation parameter is different from that given by Petreski B.P. *et al.*, 1996. The main reason is that the concentration of each sample was calculated (Equation 3.3.2) using a different absorption cross-section value. The absorption cross-section is different because it was calculated using a different value for the branching ratio between the $^3\text{P}_0$ state and the ground state. The branching ratio (56%) [Eyal M. *et al.*, 1985] was used even though the material properties were different to the glass host used in these experiments. However, the new value of 23% [Remillieux A. *et al.*, 1996], is adopted and used throughout this Thesis since the glass host it was measured in is similar to that used here.

All three cross-relaxation processes involve an ion in the 3P_0 excited state interacting with a ground state ion. From our experiments and rate equation models we are unable to distinguish between the three cross-relaxation processes as we have quantified only their sum, $\alpha_{cr} = \alpha_{cr1} + \alpha_{cr2} + \alpha_{cr3}$. For the purposes of modelling the system in a laser or amplifier configuration this sum of cross-relaxation parameters is all that is required. However, the relative contributions of the respective cross-relaxation processes depend on the radiative transition rates and branching ratios for the respective transitions. The radiative transition rates for the $^3P_0 \rightarrow ^1G_4$, $^3P_0 \rightarrow ^1D_2$ and $^3P_0 \rightarrow ^3H_6$ are approximately 55.8 Hz, 0.352 Hz and 3830 Hz respectively [Eyal M. *et al.*, 1985]. The calculated branching ratio for the $^3P_0 \rightarrow ^1D_2$ transition is negligible and about 2% for the $^3P_0 \rightarrow ^1G_4$ transition and 12% for the $^3P_0 \rightarrow ^3H_6$ transition [Remillieux A. *et al.*, 1996]. As a consequence we may conclude that the ($^3P_0 \rightarrow ^3H_6$) and ($^3H_4 \rightarrow ^1D_2$) cross-relaxation process is significantly greater than the ($^3P_0 \rightarrow ^1D_2$) and ($^3H_4 \rightarrow ^3H_6$) process and the ($^3P_0 \rightarrow ^1G_4$) and ($^3H_4 \rightarrow ^1G_4$) process. Thus the cross-relaxation parameter is mainly attributed to α_{cr3} .

At this point it is important to note that there is an apparent circular argument concerning the calculation of the absorption cross-section, the lifetime in the limit of zero concentration, the cross-relaxation parameter and the concentrations. The difficulty is that the radiative lifetime is required for the determination of the absorption cross-section (Equation 3.7.2) which is in turn used to calculate the concentrations of the various samples (Equation 3.3.2). Following this, the lifetime in the limit of zero concentration and the cross-relaxation parameter are obtained from a least squares fit of Equation 3.8.3.7 to the radiative relaxation rate as a function of

concentration data. This value for the lifetime in the limit of zero concentration can then be used to recalculate the absorption cross-section and hence the concentration. This apparent circularity is resolved by using a self consistent iterative technique illustrated in Figure 3.8.3.1 which rapidly converges to the values quoted above for the radiative lifetime in the limit of zero concentration ($\tau_6(\rho \rightarrow 0)$), the absorption cross-section (σ_a), the concentration (ρ) and the cross-relaxation parameter (α_{cr}) regardless of the initial guess for the radiative lifetime. The final values for the absorption and emission cross-sections are $\sigma_a = 0.14 \pm 0.02 \times 10^{-24} \text{ m}^2$ and $\sigma_e = 2.1 \pm 0.2 \times 10^{-24} \text{ m}^2$ respectively. It is this value for the absorption cross-section that was used to calculate the concentration.

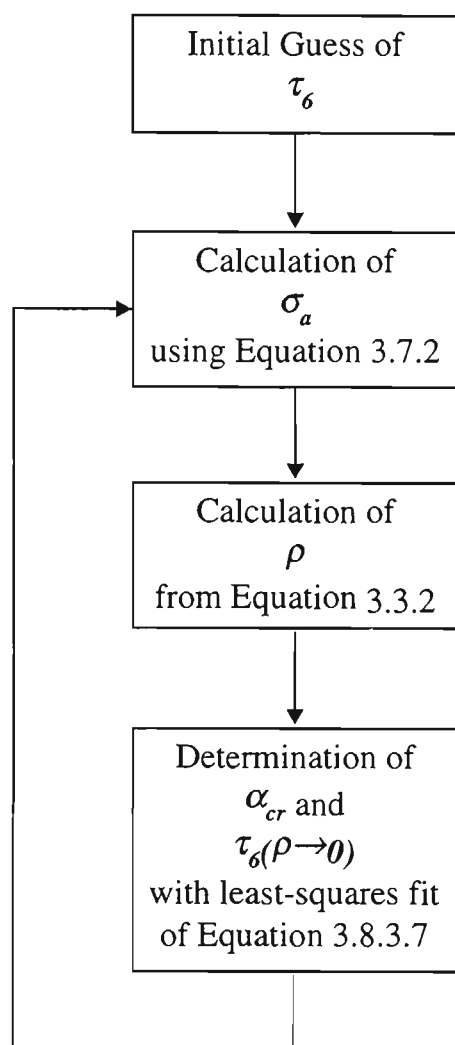


Figure 3.8.3.1 *Apparent circularity of the calculation of the absorption cross-section, calculation of the concentration determination of the lifetime in the limit of zero concentration and the cross-relaxation parameter.*

3.8.4 EFFECTS ON GAIN

By neglecting the overlap between the pump and signal beams and the ion distribution, with respect to the model described in Chapter 2.4, the gain for transitions arising from the 3P_0 state is given by

$$G = 4.343 \frac{\sigma_s^e \tau_6^{total}}{h\nu_p} \cdot \frac{P_{abs}}{A} \quad (dB). \quad (3.8.4.1)$$

This equation clearly indicates that the gain coefficient is proportional to the radiative lifetime of the 3P_0 state. However, the total lifetime of the 3P_0 state, as shown in Section 3.8.3, is given by

$$\frac{1}{\tau_6^{total}} = \frac{1}{\tau_6^{radiative+NR}} + \frac{1}{2} \alpha_{cr} \rho \quad (3.8.4.2)$$

By substituting Equation 3.8.4.2 into Equation 3.8.4.1 the gain coefficient is given by

$$G = 4.343 \frac{\sigma_s^e}{h\nu_p} \cdot \frac{P_{abs}}{A} \cdot \left[\frac{1}{\tau_6^{radiative+NR}} + \frac{1}{2} \alpha_{cr} \rho \right]^{-1} \quad (dB). \quad (3.8.4.3)$$

Using Equation 3.8.4.3, the gain can be estimated as a function of praseodymium concentration. For a constant pump power of 100 mW, the calculated gain as a function of concentration is shown in Figure 3.8.4.1 (the values for the parameters in Equation 3.8.4.3 were taken from Chapter 5). Figure 3.8.4.3 indicates that lower gain would be expected with higher dopant levels. The dotted line in Figure 3.8.4.1 indicates the concentration of the praseodymium-doped fibre used in the experimental investigations of gain in Chapter 5.

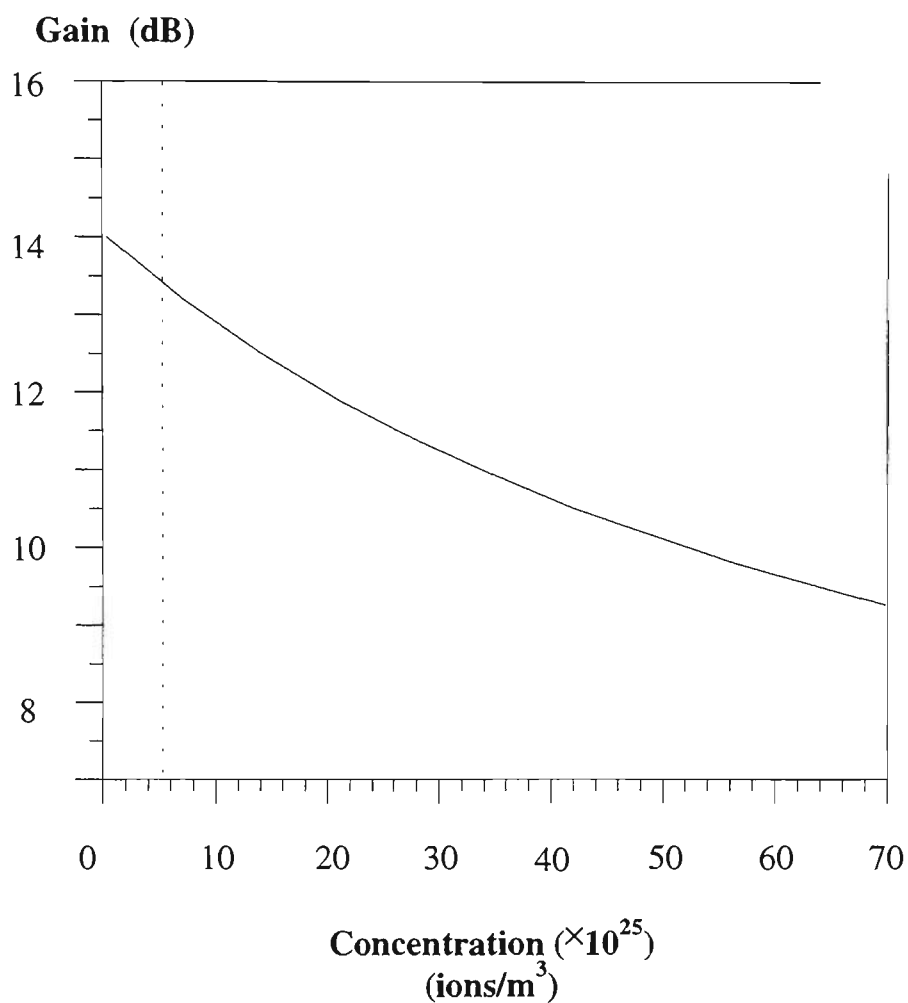


Figure 3.8.4.1 Gain as a function of concentration as calculated using Equation 3.8.4.3. The values for the parameters are the same as that used in Chapter 5. The dotted line indicates the concentration and expected gain for the amplifier used in this work.

3.9 CONCLUSION

In this chapter experimental investigations of the spectroscopic parameters that influence the optical gain on the ${}^3\text{P}_0 \rightarrow {}^3\text{F}_2$ transition in praseodymium-doped fluorozirconate glass have been given. These parameters include the branching ratio of ${}^3\text{P}_0 \rightarrow {}^3\text{F}_2$ transition (β_{32}), the fluorescence lifetime of the ${}^3\text{P}_0$ state (τ_3), the absorption cross-section at the pump wavelength and the emission cross-section at 632.8 nm on the ${}^3\text{P}_0 \rightarrow {}^3\text{F}_2$ transition. Furthermore, parasitic processes, including cross-relaxation and energy transfer, that may de-populate the ${}^3\text{P}_0$ state, were also investigated.

The branching ratio, β_{32} , was measured to be approximately 15% and was calculated by integrating over the emission spectrum. It is also important to note that the measured branching ratio compares well with the most recent measurements as summarised in Table 3.4.2

The fluorescence lifetime of the ${}^3\text{P}_0$ state was measured for varying dopant concentrations ranging from 2.8×10^{25} ions/m³ to 67×10^{25} ions/m³. For these concentrations, the fluorescence lifetime was found to vary between 49 μs and 33 μs respectively. As the concentration increases the radiative lifetime of the ${}^3\text{P}_0$ state decreases due to increasing cross-relaxation rates. From fluorescence lifetime measurements and a rate equation analysis of the level dynamics, values for the cross-relaxation parameter and the lifetime of the ${}^3\text{P}_0$ state in the limit of zero concentration were also obtained. The cross-relaxation parameter was measured for the first time and was calculated to be $2.6 \pm 0.1 \times 10^{-23}$ m³/s which was obtained from

a least squares fit of Equation 3.8.3.7 to the lifetime measurements as a function of concentration. From the same least squares fit, the lifetime in the limit of zero concentration was determined to be $\tau_6(\rho \rightarrow 0) = 49.8 \pm 0.3 \mu\text{s}$. Furthermore, the cross-relaxation parameter was used to calculate the extent to which the gain at 632.8 nm would be affected.

From the fluorescence lifetime measurements and measurement of the branching ratio of the ${}^3\text{P}_0 \rightarrow {}^3\text{F}_2$ transition, the absorption and emission cross-sections were calculated using Fuchtbauer-Ladenburg analysis. The emission cross-section at 632.8 nm was calculated to be $\sigma_e = 2.1 \pm 0.2 \times 10^{-24} \text{ m}^2$ and the absorption cross-section at the pump wavelength (476.5 nm) was calculated to be $\sigma_a = 0.14 \pm 0.02 \times 10^{-24} \text{ m}^2$.

The branching ratio, the fluorescence lifetime, the cross-relaxation parameter, and the absorption and emission cross-sections of the ${}^3\text{P}_0 \rightarrow {}^3\text{F}_2$ transitions are all key parameters required for accurate modelling and qualitative understanding of the optical properties of the amplifier material. The values obtained for these parameters will be used to calculate the expected gain in Chapter 5.4 for comparison with experimental measurements.

Chapter 4

CHARACTERISATION OF PRASEODYMIUM DOPED FIBRE PARAMETERS

- 4.1 Introduction
- 4.2 Measurement of the mode profile and determination of the intensity spot-size
 - 4.2.1 Introduction
 - 4.2.2 Confocal scanning images of the mode profile
 - 4.2.3 Determination of intensity spot-size from the mode profile
- 4.3 Measurement of the concentration profile
 - 4.3.1 Introduction
 - 4.3.2 Experimental measurements and results
- 4.4 Conclusion

4.1 INTRODUCTION

The small signal gain coefficient for a four-level atomic system in the limit of low pump power, as described in Chapter 2 (Equation 2.4.2.7), is given by

$$g_{coeff}^{low} \cdot L = \frac{\tau_3 \sigma_s^e P_{ubs}(L)}{h\nu_p} \cdot \frac{\Gamma_{p,s}}{\Gamma_s} \quad (4.1.1)$$

where

$$\frac{\Gamma_{p,s}}{\Gamma_s} = \frac{2}{\pi(\omega_s^2 + \omega_p^2)} \frac{\left(1 - \exp\left[-2a^2 \left(\frac{\omega_s^2 + \omega_p^2}{\omega_s^2 \omega_p^2} \right) \right] \right)}{\left(1 - \exp\left[-\frac{2a^2}{\omega_p^2} \right] \right)}. \quad (4.1.2)$$

The first group of terms on the right hand side of Equation 4.1.1 are described by the spectroscopic properties discussed in Chapter 3. Other than the spectroscopic properties of praseodymium the gain coefficient is also dependant on the physical characteristics of the optical fibre waveguide. In particular the overlap function given in Equation 4.1.2 is dependant upon the core radius (a) and the intensity spot-size of the pump (ω_p) and signal modes (ω_s). Mode profile measurements of the 632.8 nm beam propagating in the praseodymium-doped fluorozirconate optical fibre, given in Section 4.2.2, are used in Section 4.2.3 to determine the intensity spot-size of the fundamental mode. The experimentally determined spot-size is compared to that obtained from Gaussian approximations and Bessel function solutions.

Optimisation and modelling of rare-earth-doped fibre amplifiers and lasers also requires a knowledge of the absolute concentration and the profile of the rare-earth dopant in the fibre core [Ankiewicz A. *et al.*, 1994]. In much of the published modelling it is assumed that the concentration of the rare-earth dopant is uniform over the fibre

core, as has been the assumption in this Thesis thus far. While this assumption slightly simplifies the calculation, the main reason for the assumption is that the information about the spatial variation of the concentration is often unavailable. In Section 4.3 measurements of the concentration profile of praseodymium-doped fluorozirconate fibre by confocal microscopy are reported. These measurements are novel in that they rely directly on concentration dependent processes in the material, and as a result do not require calibration of experimental equipment.

4.2 MEASUREMENT OF THE MODE PROFILE AND DETERMINATION OF THE INTENSITY SPOT-SIZE

4.2.1 INTRODUCTION

The parameters that determine the waveguiding properties of an optical fibre are the core radius a and the refractive indices of the core (n_{core}) and the cladding (n_{clad}). From these the numerical aperture NA , the normalised frequency V and the cut-off wavelength λ_c can be determined. The fibre parameters as provided by the manufacturer are summarised in Table 4.2.1.1. It should be noted that the figures for the refractive index of the core and the cladding are given at 1300 nm. Here, it is assumed that the refractive index of the core and the cladding will be the same around 632.8 nm since there is evidence that the NA and V are reasonably constant over the range of wavelengths in this work [Sanghera J.S. and Aggarwal I.D., 1993].

Parameter	Value
a	$\sim 2 \mu\text{m}$
$n_{\text{core}}(1300 \text{ nm})$	1.514
$n_{\text{cladding}}(1300 \text{ nm})$	1.499
NA	0.21
λ_c	1150 nm

Table 4.2.1.1 *Summary of praseodymium-doped fibre parameters as provided by the manufacturer. The NA and λ_c have been evaluated using these values.*

The normalised frequency calculated for the signal and pump beams are $V_s = 4.17$ and $V_p = 5.54$ respectively indicating that the praseodymium amplifying fibre was multimoded at both. The degenerate modes are listed in Table 4.2.1.2 for the first six LP modes in the praseodymium-doped step-index fibre. The first four modes are allowed for the signal beam while all six modes are allowed for the pump beam.

V_c	Degenerate modes	LP Designations
0	HE ₁₁	LP ₀₁
2.405	TE ₀₁ , TM ₀₁ , HE ₂₁	LP ₁₁
3.832	EH ₁₁ , HE ₃₁	LP ₂₁
3.832	HE ₁₂	LP ₀₂
5.136	EH ₂₁ , HE ₄₁	LP ₃₁
5.520	TE ₀₂ , TM ₀₂ , HE ₂₂	LP ₁₂

Table 4.2.1.2 *Cutoff conditions and designation of the first six LP modes in a step-index fibre [Buck J.A., 1995].*

Using Bessel functions the intensity distribution in the core and the cladding for any LP mode can be expressed as [Snyder A.W. and Love J.D., 1983]

$$I_{lm}(r, \phi) = \begin{cases} I_0 J_l^2 \left(U \frac{r}{a} \right) \sin^2(l\phi) & r \leq a \\ I_0 \left(\frac{J_l(U)}{K_l(W)} \right)^2 K_l^2 \left(W \frac{r}{a} \right) \sin^2(l\phi) & r > a \end{cases} \quad (4.2.1.1)$$

respectively, where J_l is the Bessel function of order l and K_l is a modified Bessel function of order l . The fibre parameters U and W are the eigenvalue parameters and are related to V through $W^2 = V^2 - U^2$, where U can be approximated by [Gloge D., 1971]

$$U = \frac{(1 + \sqrt{2})V}{1 + (4 + V^4)^{1/4}} \quad (4.2.1.2)$$

for the LP₀₁ mode only. For the other modes values for U and W were taken from Snyder A.W. and Love J.D., 1983. The mode distribution for the signal beam is given in

Figure 4.2.1.1, for the first three modes, propagating in the core and the cladding regions. The mode profile is an important characteristic of a fibre waveguide from which the intensity spot-size (ω_s) can be determined for the signal beam.

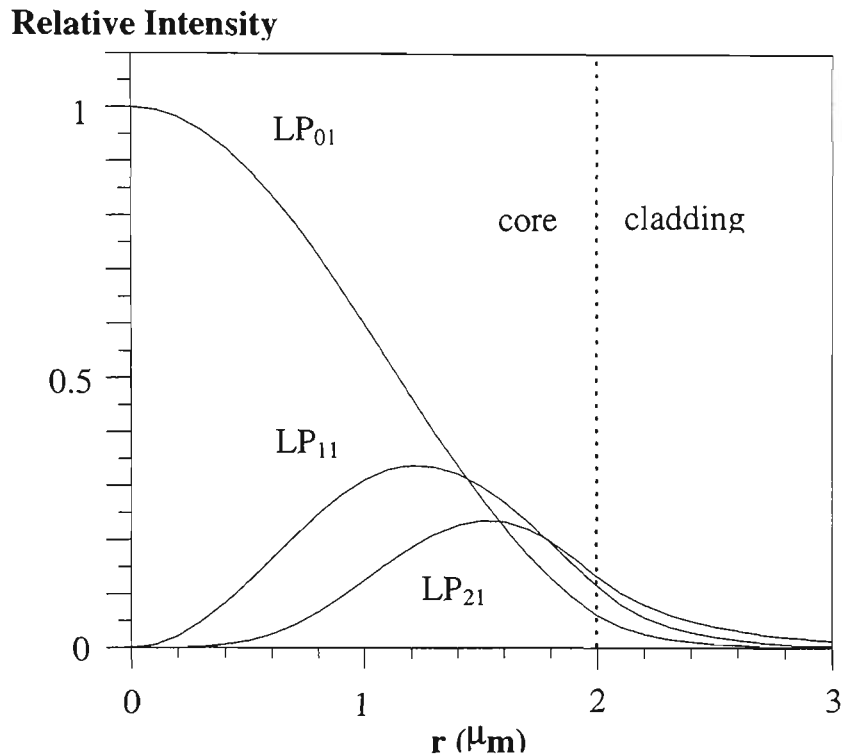


Figure 4.2.1.1 *The first three modes propagating inside the core and in the cladding at 632.8 nm.*

4.2.2 CONFOCAL SCANNING IMAGES OF THE MODE PROFILE

The mode profile at the signal wavelength was measured using the experimental arrangement given in Figure 4.2.2.1. Light from a He-Ne laser was launched into the praseodymium-doped fibre using a microscope objective (O3). The other end of the fibre was clamped to a mount on the piezo-electric positioner. The positioner could be programmed to raster scan the fibre through a maximum region of $20 \mu\text{m}^2$. This allowed the collecting optics to remain stationary. The collecting optics consisted of a $\times 40$

microscope objective (O2) (ZEISS 0.75 NA). The collimated light was focused using objective O3, and spatially filtered using a pinhole with a circular aperture of diameter 10 μm . All light was spectrally filtered using a standard 632.8 nm He-Ne band-pass filter before the silicon detector. Spatially resolved intensity measurements were recorded on a PC.

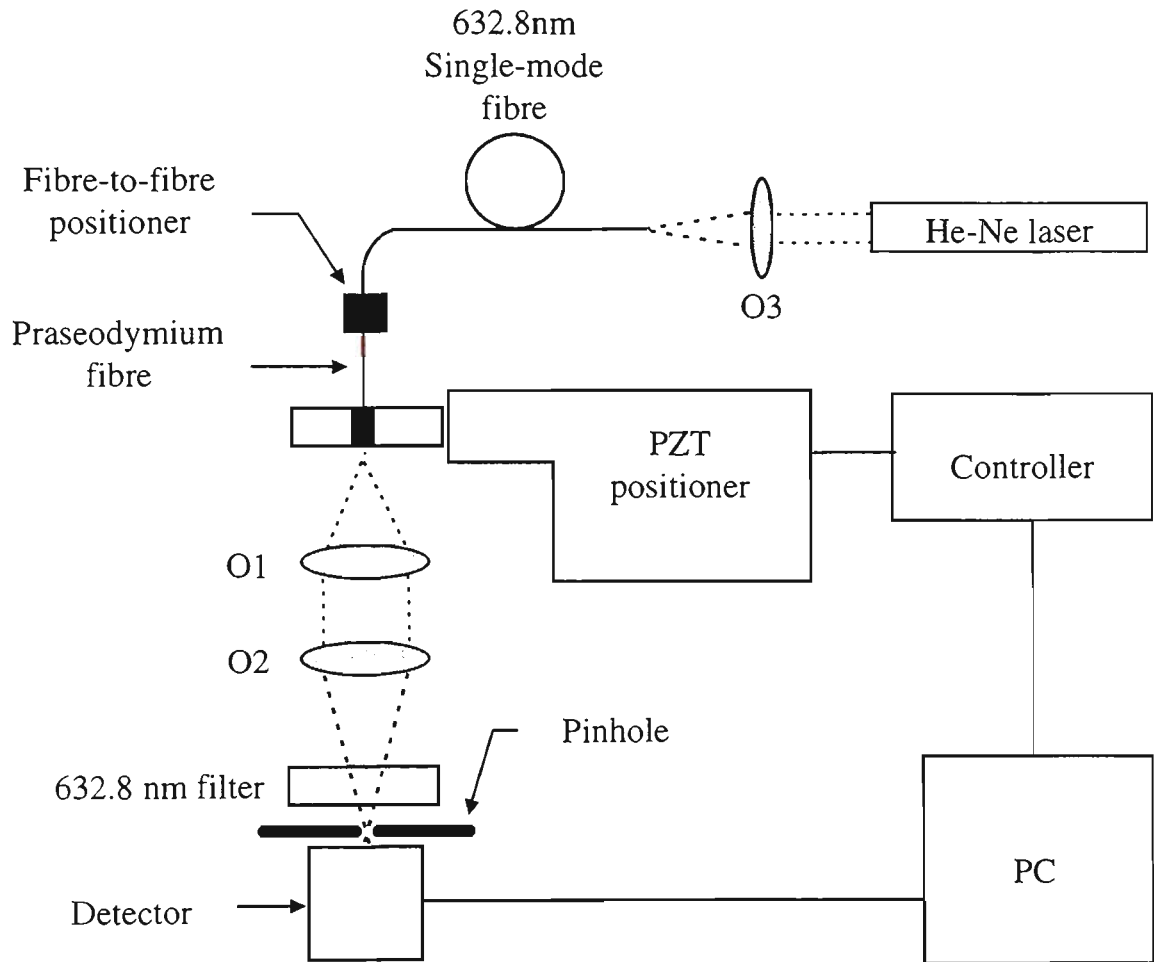
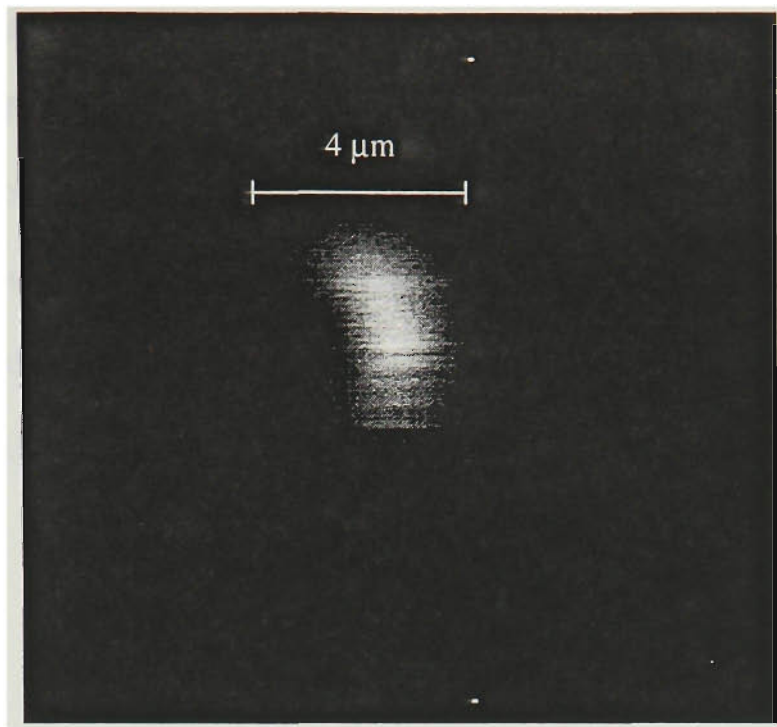
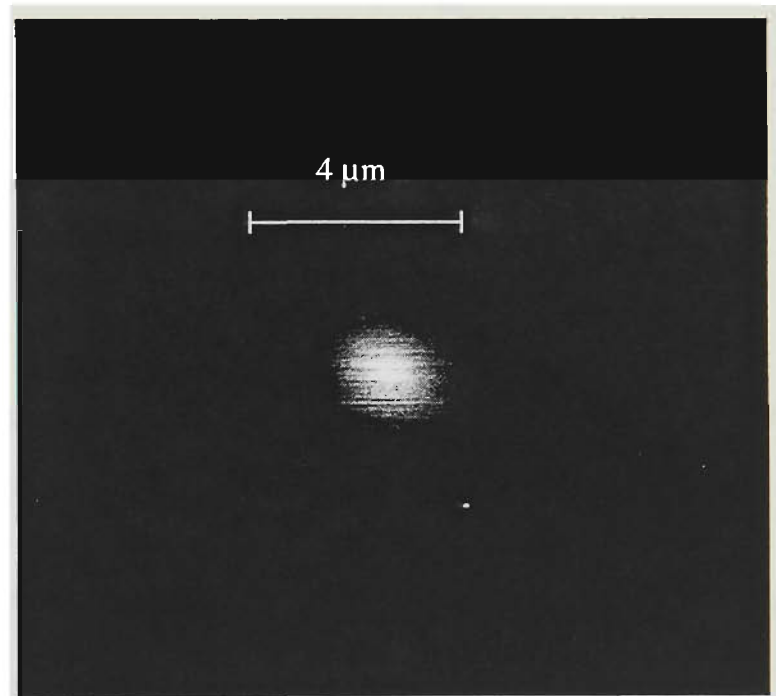


Figure 4.2.2.1 *Experimental arrangement used to measure the mode profile of the 632.8 nm He-Ne wavelength in the praseodymium-doped fluorozirconate optical fibre.*

Images of typical mode profiles of 632.8 nm light propagating through the praseodymium-doped fibre are shown in Figure 4.2.2.2. Any movement or macrobending of the launch fibre resulted in significant modal variations. From the near field measurements of the fundamental mode, the intensity spot-size can be determined (Section 4.2.3).



(a)



(b)

Figure 4.2.2.2 *Examples of typical images of mode profiles of 632.8 nm light propagating in the praseodymium-doped optical fibre.*

4.2.3 DETERMINATION OF INTENSITY SPOT-SIZE FROM THE MODE

PROFILE

In common with many fibre amplifier models, the radial distribution of the pump and signal beams within the fibre is assumed to follow a Gaussian distribution. In the Gaussian approximation the mode envelopes for the pump and signal beams in an optical fibre are (from Equation 2.3.11 and Equation 2.3.12)

$$I_p(r) = I_p(0) \exp\left[-2 \frac{r^2}{\omega_p^2}\right] \quad (4.2.3.1)$$

and

$$I_s(r) = I_s(0) \exp\left[-2 \frac{r^2}{\omega_s^2}\right] \quad (4.2.3.2)$$

respectively, where ω_s and ω_p are the $1/e^2$ intensity spot-sizes given by the Marcuse polynomial [Marcuse D., 1977]

$$\omega_i^{Marcuse} = a \left(0.65 + \frac{1.619}{V_i^{3/2}} + \frac{2.879}{V_i^6} \right) \quad (4.2.3.3)$$

Using the Gaussian approximation, the intensity spot-size for the signal and pump beams are $\omega_s^{Gaussian} = 1.67 \mu\text{m}$ and $\omega_p^{Gaussian} = 1.54 \mu\text{m}$ respectively.

The mode-field-radius, ω_0 , for the fundamental mode can be given exactly, in terms of Bessel functions, by [Desurvire E., 1994a & b]

$$\omega_0 = a \frac{VK_1(W)}{UK_0(W)} J_0(U) \quad (4.2.3.4)$$

where the intensity spot size is related to the mode-field-radius by $\omega_0 = \frac{\omega}{\sqrt{2}}$.

Figure 4.2.3.1 shows a comparison of the mode intensity distribution between the Gaussian approximation and the exact distribution using Bessel functions. For the

praseodymium-doped fibre, the mode radius of the fundamental mode, for each of the signal and pump beams were calculated to be $\omega_s^{Bessel}=1.75 \mu\text{m}$ and $\omega_p^{Bessel}=1.65 \mu\text{m}$ respectively.

It is important to note here that there are errors involved in calculating the intensity spot-size for both the Gaussian approximation and Bessel function solution. The error margins are associated with the error in the core radius and the refractive indices of the core and the cladding of the amplifier. However, the error margins in these parameters are unavailable thus the error margin in the intensity spot-size has not been determined.

Strictly speaking the intensity spot size calculations discussed in this section are applicable to single mode operation. However, they are commonly applied to amplifiers operating in a few modes.

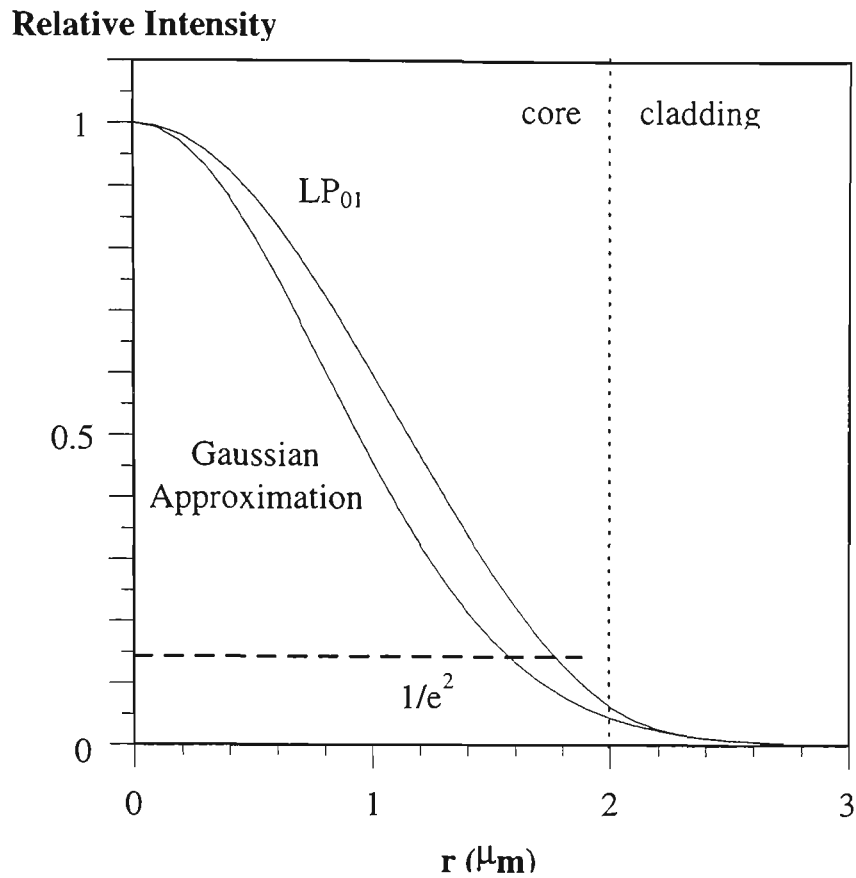


Figure 4.2.3.1 Comparison of the intensity distribution corresponding to the Bessel function solution for the LP_{01} mode and the Gaussian mode approximation of the signal beam.

With the experimental arrangement described in Section 4.2.2 it was also possible to excite only the LP_{01} mode of the praseodymium-doped fibre, by varying the coupling conditions between the single mode silica fibre and the praseodymium fibre. In Figure 4.2.3.2 the data indicate the radial distribution of the LP_{01} mode in the praseodymium-doped fibre. Also shown in Figure 4.2.3.1 is the result of a Gaussian curve fit to the data points. From the curve-fit the intensity spot-size was determined to be $\omega_s^{exp} = 1.6 \pm 0.1 \mu\text{m}$.

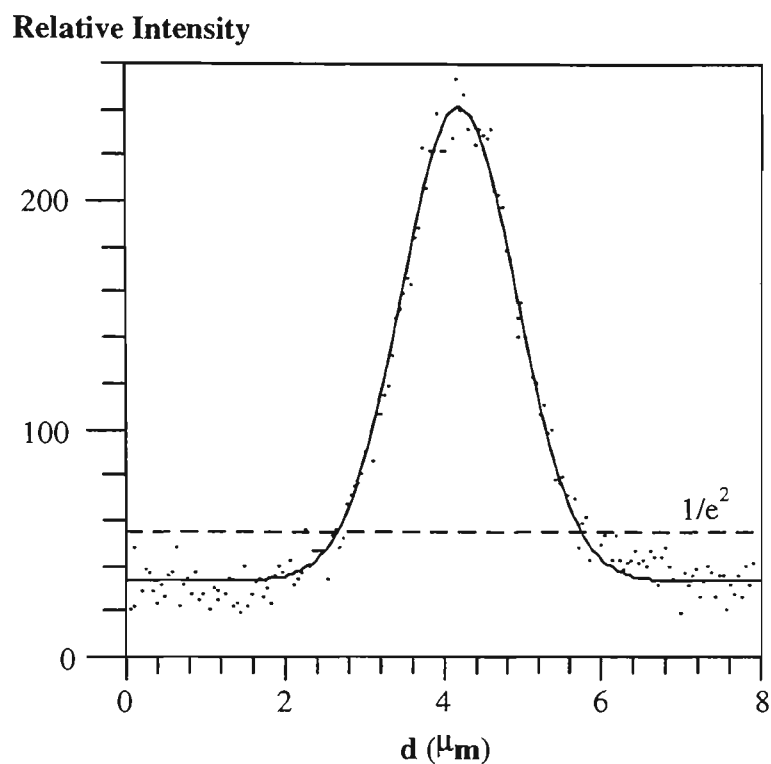


Figure 4.2.3.2 *Measurement of single-mode propagation of 632.8 nm light in the praseodymium-doped fibre in the transverse direction. The full line indicates the resultant curve-fit of a Gaussian distribution including the background for which the intensity spot-size $\omega_s = 1.6 \pm 0.1 \mu\text{m}$ was obtained.*

4.3 MEASUREMENT OF THE CONCENTRATION PROFILE

4.3.1 INTRODUCTION

Two optical scanning techniques have been previously used to determine the ion distribution in optical fibres namely, confocal optical microscopy and near field scanning optical microscopy.

In 1994, Uttamchandani D. *et al.*, used a confocal optical microscope to determine the concentration profile of an erbium-doped fibre. Spatially resolved fluorescence at 565 nm, generated under 488 nm excitation, was used to contrast the distribution of the erbium ions. Following this, in 1995 Othonos A. *et al.*, extended this technique by using a phase sensitive detection technique that enabled better detector sensitivity and an improved signal-to-noise ratio.

In 1992, Trautman *et al.*, investigated the potential of near field optical microscopy for fluorescence image contrast of dye samples. In this paper, 488 nm pump light was launched into a near field probe that was positioned close to the surface of a microscope cover slip, coated with a dye solution, and enabled spatially resolved images of the fluorescence.

In previous attempts to determine, optically, the concentration profile of rare-earth dopants in optical fibre cores it has been assumed that the observed fluorescence intensity is proportional to the local concentration of the rare-earth dopant. For example, the fluorescence intensity resulting from transitions arising from the 3P_0 state follows the relationship given by

$$I_{\text{fluorescence}} = Kn_3\rho\gamma_{\text{radiative}} \quad (4.3.1.1)$$

where n_3 is the population probability density of the 3P_0 state, ρ is the concentration and $\gamma_{radiative}$ includes radiative terms related to the 3P_0 state. The constant K , is a factor that is usually dependant on the spatial resolution, the solid angle of detection and the efficiency of the instrument used to measure the fluorescence intensity. Consider the rate equation for the 3P_0 state in the absence of cross-relaxation given by

$$\frac{dn_3}{dt} = R_{13}n_1 - \frac{n_3}{\tau_3} \quad (4.3.1.2)$$

and the rate equation for the 3P_0 state with the cross-relaxation the rate included given by

$$\frac{dn_3}{dt} = R_{13}n_1 - \frac{n_3}{\tau_3} - \frac{1}{2}\alpha_{cr}\rho n_1 n_3. \quad (4.3.1.3)$$

Here we assume that $n_1 + n_3 = 1$. It is important to note that the approximation $n_1 + n_3 = 1$ is only reasonable at low pump powers. Analytic solutions for Equation 4.3.1.2 and Equation 4.3.1.3 can be obtained for steady-state conditions so that the population probability density of the 3P_0 state, in the absence of cross-relaxation, is given by

$$n_3 = \frac{R_{13}}{R_{13} + A_3} \quad (4.3.1.4)$$

while ($A_3 = 1/\tau_3$), with cross-relaxation included, the population probability density of the 3P_0 state is given by

$$n_3^{x-relax} = \frac{2R_{13} + 2A_3 + \alpha\rho}{2\alpha\rho} - \frac{\sqrt{4R_{13}^2 + 8R_{13}A_3 - 4\alpha\rho R_{13} + 4A_3^2 + 4A_3\alpha\rho + \alpha^2\rho^2}}{2\alpha\rho} \quad (4.3.1.5)$$

The ratio $\frac{n_3^{x-relax}}{n_3}$ as a function of pump rate (R_{13}) and concentration (ρ) is shown

in Figure 4.3.1.1. The ratio indicates that the cross-relaxation process significantly affects the population probability density of the 3P_0 state in the case of increasing

concentration and low pump rates. It is expected that in this regime concentration quenching will prevail. For all other cases the following approximation can be made

$$n_3^{x-relax} \approx \frac{R_{13}}{R_{13} + A_3} . \quad (4.3.1.6)$$

Thus, the assumption that the fluorescence is linearly related to the concentration is often unwarranted, in particular for high concentrations, since concentration-dependent cooperative processes can alter the relaxation processes in the dopant and hence the fluorescence intensity. Consequently, fluorescence intensity is not a reliable method for determining the relative concentration profile of a doped optical fibre, nor is it a means for measuring the absolute concentration. However, praseodymium offers a particularly simple solution to the problem of obtaining absolute concentration and concentration profile measurements since it has been shown in Section 3.8 that the relaxation rate of the 3P_0 state of praseodymium varies linearly with concentration according to (Equation 3.8.3.7)

$$\frac{1}{\tau} = \frac{1}{\tau_0} + \frac{1}{2} \alpha_{cr} \rho . \quad (4.3.1.7)$$

This relation was determined by calibrating the fluorescence lifetime of the 3P_0 state as a function of concentration and is used subsequently to determine the concentration profile and the absolute concentration of a praseodymium optical fibre by confocal microscopy.

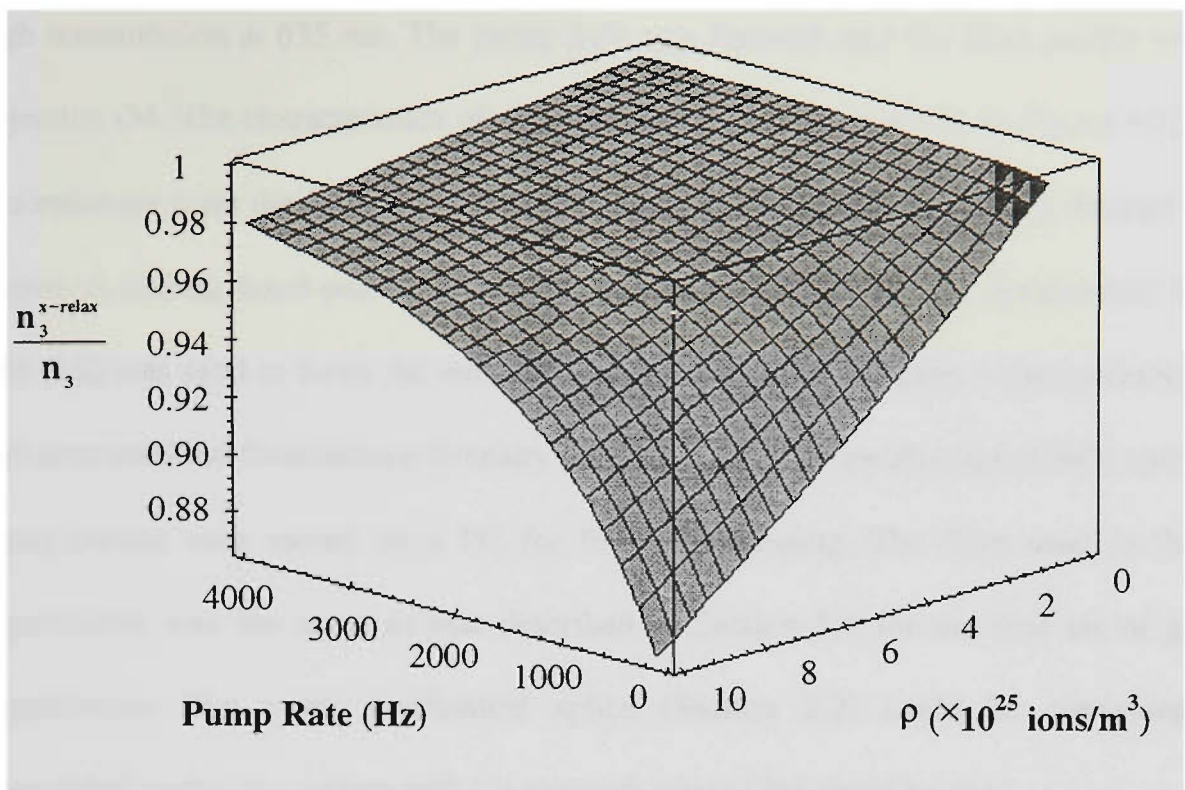


Figure 4.3.1.1 *The ratio of the population probability density of the 3P_0 state (with and without cross-relaxation) as a function of pump rate (R_{13}) and concentration (ρ).*

4.3.2 EXPERIMENTAL MEASUREMENTS AND RESULTS

The confocal microscope used to measure the intensity and time resolved fluorescence is given schematically in Figure 4.3.2.1. Light from an argon-ion laser at 476.5 nm was launched into an optical fibre of 4 μm diameter using a microscope objective (O3). Prior to this, the beam was modulated using a mechanical chopper at the focal points of O1 and O2. The beam modulation is the same as that in Section 3.4. The fibre was required because the confocal microscope was in a different laboratory to the laser source. A lens (L1), with the same numerical aperture as the fibre, collimated light from the output end of the fibre. The beam size was adjusted by a circular aperture. The pump light was reflected using a mirror which had a high reflectance at 476.5 nm and

high transmission at 635 nm. The pump light was focused onto the fibre sample using objective O4. The characteristics of objective O4 are the same as O1 in Figure 4.2.2.1. Fluorescence from the fibre was also collected by O4 and transmitted back through the mirror. A 635 nm band-pass filter ensured that no pump light entered the detector. The lens (L2) was used to focus the red light through a pinhole and onto a silicon detector. The time resolved fluorescence intensity was recorded on an oscilloscope (CRO) and the decay curves were stored on a PC for further processing. The fibre used in these experiments was the same as that described in Section 5.3 for the first set of gain experiments. The rotary mechanical splice (Section 5.2) could be conveniently dismantled so that the section with the praseodymium fibre could be used.

In the confocal experiments there was some difficulty encountered locating the core of the praseodymium-doped fibre which is only a few micrometers in diameter. The PZT positioner was manually adjusted while observing the image of the fibre prior to the 635 nm band-pass filter on white cardboard. In these images the cladding interface with the glass ferrule was distinguished easily and was used as a reference point to find the core. In particular the outermost horizontal point of this interface was located first. Once this point was established then by adjusting the horizontal position the core could be located relatively easily.

The time resolved fluorescence was recorded at many different positions on the fibre core. The lifetime for each decay curve was obtained using the same method described in Section 3.6. The lifetime data were related to the local concentration using the linear relationship between concentration and relaxation rate shown in Equation 4.3.1.6. The concentration profile of the fibre core thus obtained is shown in Figure 4.3.2.2. The data are noisy but are consistent with lifetime measurements in Chapter 3.6.

The fluorescence intensity profile shown in Figure 4.3.2.3 was obtained from the same data and is slightly different to that obtained for the concentration profile. The fluorescence intensity as a function of position measurement were performed in many different fibre depths (up to 20 μm and steps of 1 μm). These planes were reconstructed to form the three dimensional fluorescence intensity image shown in Figure 4.3.2.4. It is important to note that in this experiment the pump was increased so that the fluorescence was able to saturate the detector thereby making the core and cladding interface more apparent. Furthermore in Figure 4.3.2.4 the core region seems to be larger at the polished end of the fibre compared to the core diameter at some depth along the fibre. The effect may be the result of preparation of the fibre end for imaging. This needs further investigation.

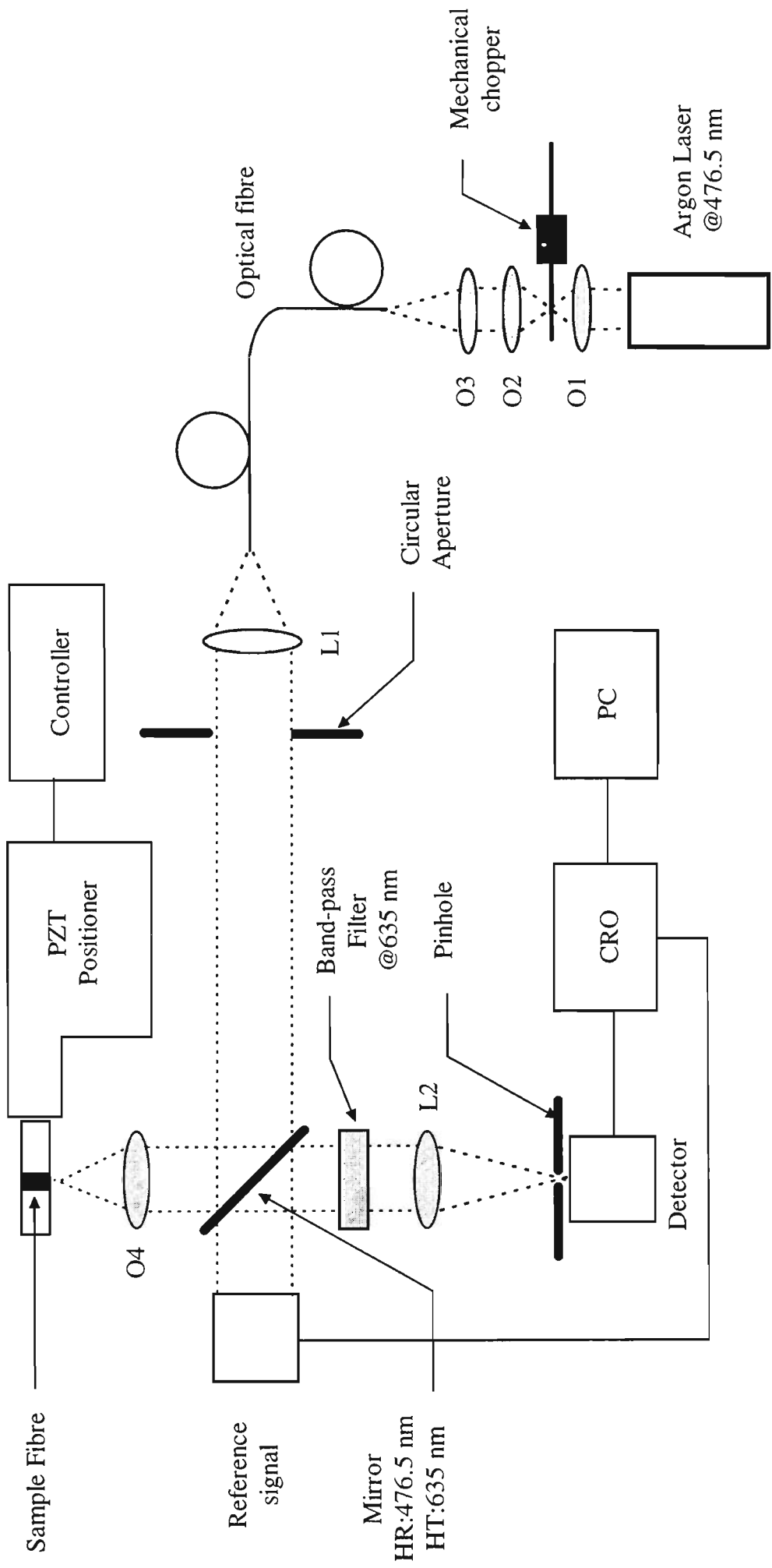


Figure 4.3.2.1 Experimental arrangement of confocal system

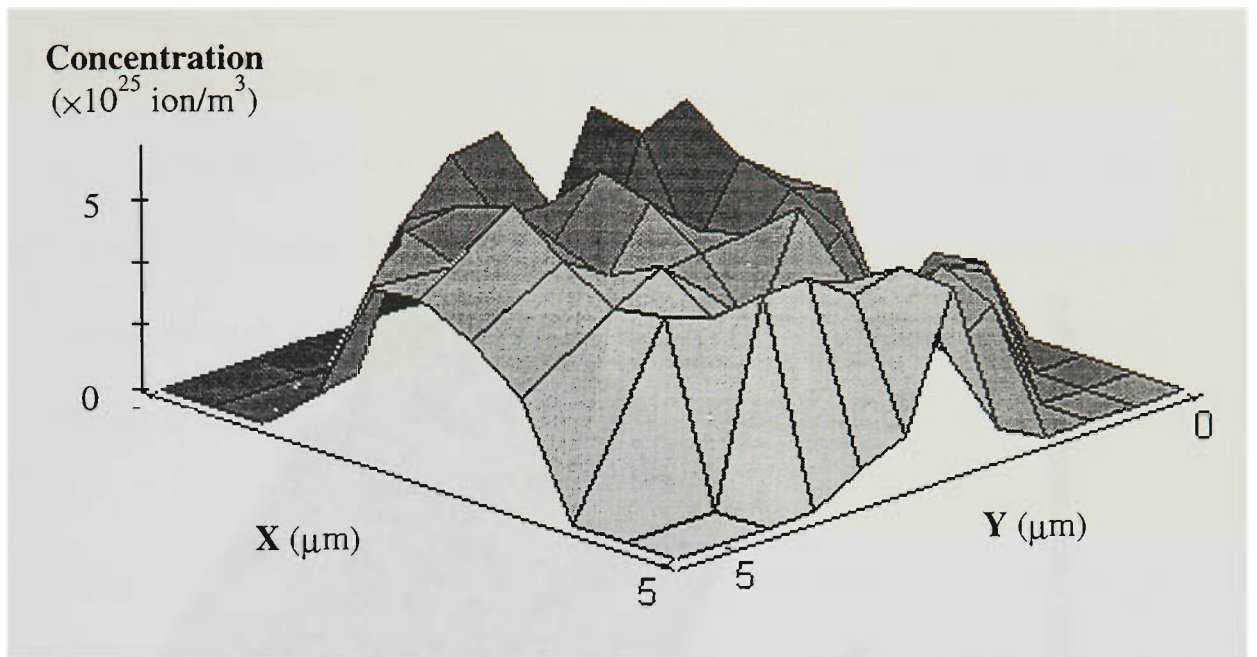


Figure 4.3.2.2 *Praseodymium concentration profile obtained by near field measurements of lifetime of the 3P_0 state related Equation 4.3.1.7*

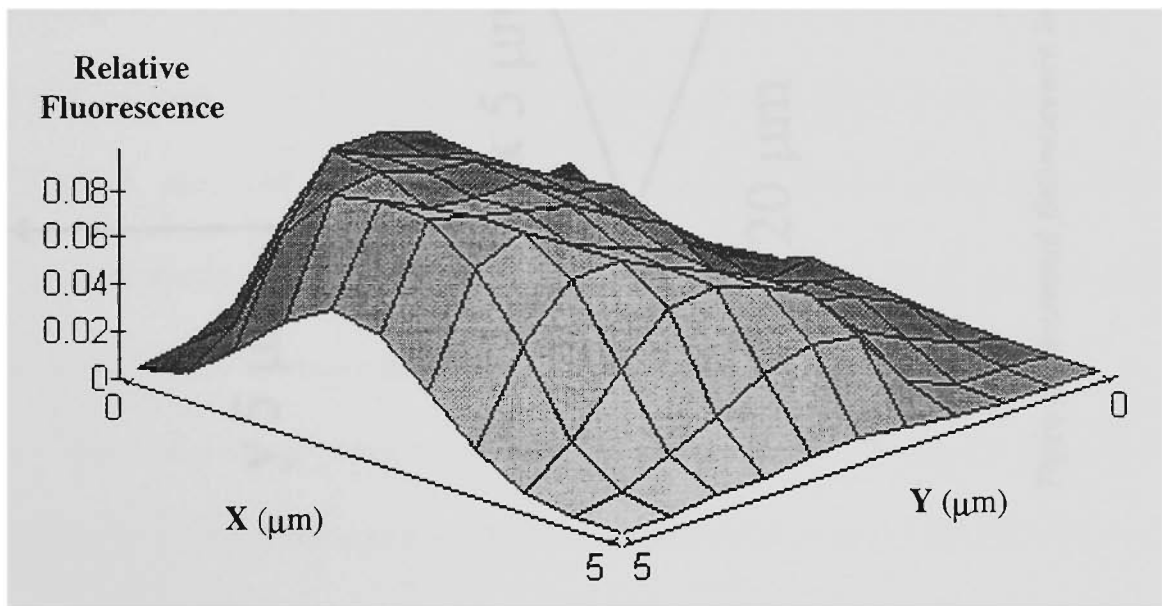
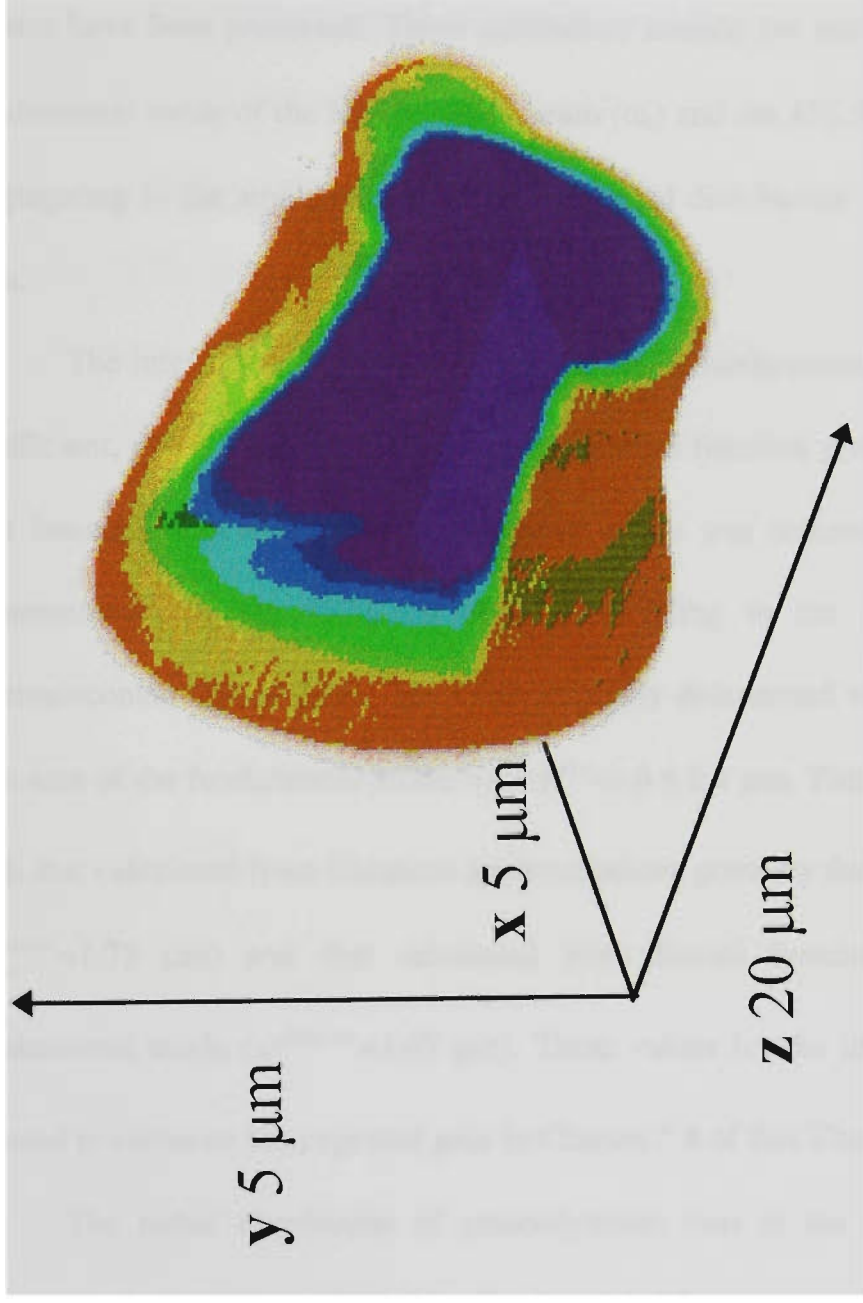


Figure 4.3.2.3 *Praseodymium fluorescence profile.*



Three dimensional fluorescence intensity profile reconstructed from multiple images.

Figure 4.3.2.4

4.4 CONCLUSION

In this chapter experimental investigations of the optical fibre parameters that influence the overall performance of the 632.8 nm praseodymium-doped amplifier system have been presented. These parameters include the intensity spot-size of the fundamental mode of the He-Ne signal beam (ω_s) and the 476.5 nm pump beam (ω_p) propagating in the amplifying fibre and the radial distribution of the praseodymium ions.

The intensity spot-size is a parameter that is fundamentally related to the gain coefficient, given by Equation 4.1.1, in the overlap function given by Equation 4.1.2. The intensity spot-size of the fundamental mode was determined from near field measurements of the 632.8 nm beam propagating in the praseodymium-doped fluorozirconate optical fibre. The experimentally determined value for the intensity spot-size of the fundamental mode was $\omega_s^{exp} = 1.6 \pm 0.1 \mu\text{m}$. This value compares well with that calculated from Gaussian approximations given by the Marcuse polynomial ($\omega_s^{Bessel} = 1.75 \mu\text{m}$) and that calculated from Bessel function solutions for the fundamental mode ($\omega_s^{Gaussian} = 1.67 \mu\text{m}$). These values for the intensity spot-size will be used to calculate the expected gain in Chapter 5.4 of this Thesis.

The radial distribution of praseodymium ions in the fibre core is another parameter that was investigated in Section 4.3. Measurements of the concentration dependant relaxation rates of the 3P_0 state of praseodymium, spatially resolved by confocal microscopy, were analysed to give an absolute measure of the concentration profile in praseodymium-doped fluorozirconate optical fibre. The results obtained in

Section 4.3 are consistent with experimental measurements recorded in Chapter 3.7 and indicate, to some extent, that the dopant ion distribution is radially constant. The measurements are novel in that they rely directly on concentration-dependent processes in the material and as a result do not require calibration.

The intensity spot-size of the fundamental mode of the He-Ne signal beam (ω_s), the 476.5 nm pump beam (ω_p) propagating in the amplifying fibre and the radial distribution of the praseodymium ions are key parameters required for accurate modelling of the praseodymium-doped fibre amplifier. The values for the optical fibre parameters obtained in this chapter, along with the spectroscopic parameters obtained in Chapter 3, will be used in Chapter 5.4 to calculate the expected gain.

Chapter 5

AMPLIFICATION AT THE 632.8 nm He-Ne WAVELENGTH IN PRASEODYMIUM-DOPED FLUOROZIRCONATE OPTICAL FIBRE.

- 5.1 Introduction
- 5.2 General experimental arrangement
- 5.3 Measurement of small signal gain
- 5.4 Rate equation model and calculation of gain
- 5.5 Conclusion

5.1 INTRODUCTION

To determine experimentally the gain of an optical fibre amplifier, a signal of known power (P_{in}) is launched into the amplifying fibre and then measured again once it has propagated through the fibre (P_{out}). The multiplicative gain is then given by

$$G_{net} = \frac{P_{out}}{P_{in}} \quad (5.1.1)$$

This method requires that the signal power be known accurately. However, as this is not often the case, large errors may be introduced in the gain measurements.

Conversely, the gross gain may be determined by measuring the ratio of the detected output signal when the fibre is optically pumped $P_{out}(Pumped)$, to that when it is not pumped $P_{out}(Unpumped)$ and is given by

$$G_{gross} = \frac{P_{out}(Pumped)}{P_{out}(Unpumped)}. \quad (5.1.2)$$

For this method there is no need to measure the signal power launched into the fibre. Another advantage is that all the measurements are taken at one end of the fibre. This second method is only good for measuring the gain in a four-level system since the fibre, in its un-pumped state, ought to be transparent to the signal. The latter method does not take into account the background losses and is termed gross gain. To determine the net gain, background losses and connector losses can be included in the calculation.

The experimental arrangement for gain measurements is described in Section 5.2. The components integral to the praseodymium-doped fibre amplifier system including the pump laser, the probe or signal laser, the directional coupler and its characteristics and the praseodymium-doped fibre are described. Some methods used to connect fluorozirconate optical fibre with silica fibres are also discussed. Results for gain as a function of injected pump power, amplifier length and input signal power are also presented.

Furthermore, in this chapter the gain is calculated by using Equation 5.4.6 and Equation 5.4.7 together with the measured spectroscopic parameters given in Chapter 3 and the praseodymium-doped fibre parameters given in Chapter 4. Finally, the measured gain and the calculated gain are compared.

5.2 GENERAL EXPERIMENTAL ARRANGEMENT

The small signal gross gain was investigated using the general experimental arrangement shown in Figure 5.2.1. The optical pump source used was an argon-ion laser since its output wavelength matches that required for the 3P multiplets of praseodymium. The laser output at 476.5 nm was selected since it matches the ground state absorption transition to the 3P_0 state. The range of single line wavelengths of the argon-ion laser is given in Table 5.2.1 which also indicates the typical output powers at particular wavelengths.

The pump light was launched into the amplifying fibre through a four-port coupler. The fibre in the coupler had a core diameter of about 4 μm and a numerical aperture of 0.12, and was single mode at 633 nm while there were two LP modes at

476.5 nm. The coupling ratio at 633 nm was about 50:50 while the coupling ratio at 476.5 nm was about 97:3. The excess loss of the coupler was 0.41 dB at 633 nm. This was determined experimentally, for a range of input 476.5 nm pump powers launched through port #4 by measuring the output power for port #1 and port #2, and is given in Figure 5.2.2.

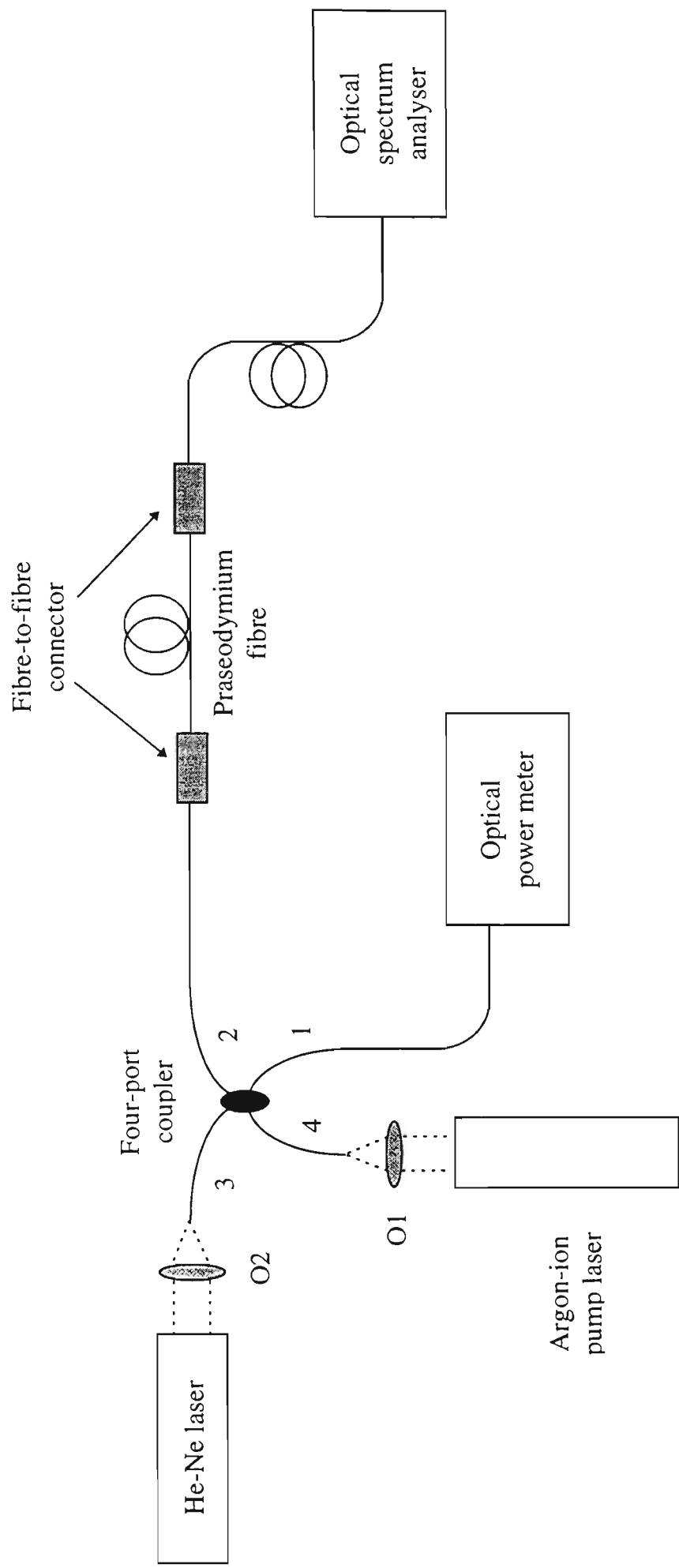


Figure 5.2.1 Experimental arrangement used to measure the small signal gain in praseodymium-doped fluorozirconate fibre.

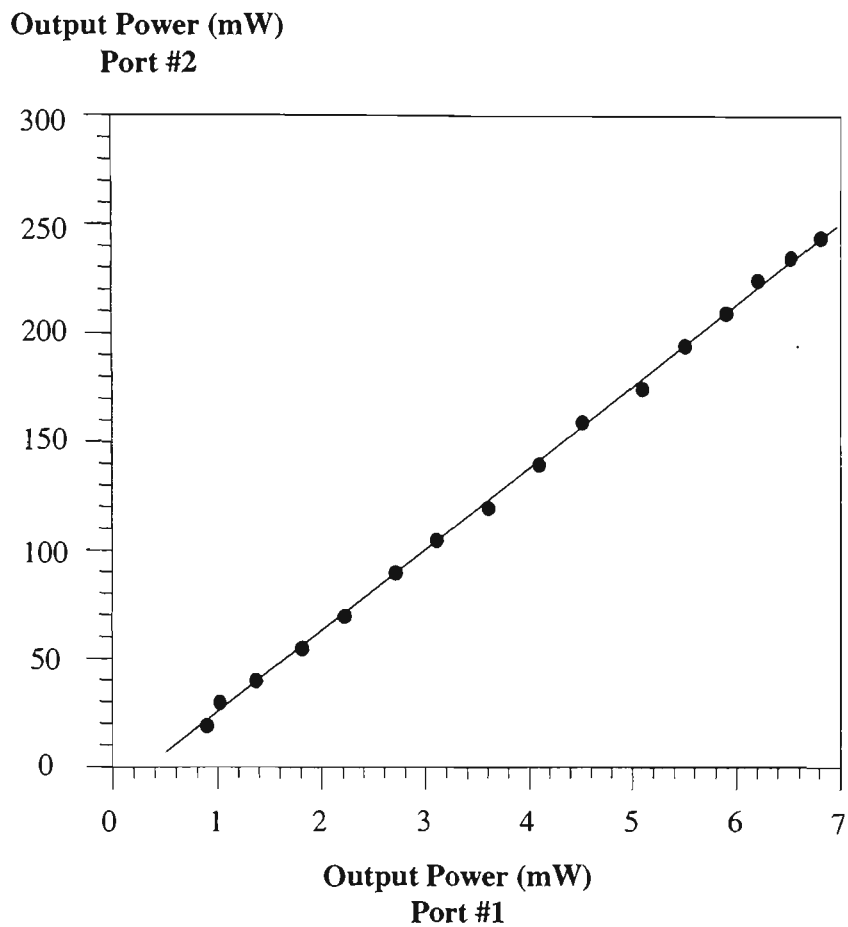


Figure 5.2.2 *Output power through port #1 and port #2 when the power of 476.5 nm laser light is launched through port #4, is varied.*

The He-Ne probe beam was also coupled into the praseodymium fibre through the four-port coupler (port #3). The spare port of this coupler was used to monitor either the probe or pump power injected into the praseodymium-doped fibre. An optical power meter or spectrum analyser was used at the output end of the amplifier to measure the exit power and spectrum, respectively.

Single-line output wavelength (nm)	Typical output power (W)
514.5	2.000
501.7	0.400
496.5	0.700
488.0	1.500
476.5	0.750
472.7	0.300
465.8	0.200
457.9	0.350
454.5	0.120

Table 5.2.1 *Selected wavelengths of the argon-ion pump laser and typical single-line powers of the argon-ion laser when there is 5 W of output power in multiline operation [Spectra Physics specifications].*

Connecting a fluorozirconate optical fibre to a silica optical fibre was a difficult task mainly because the fluorozirconate fibre is extremely weak and has different material properties from silica. Three different methods were used to connect the praseodymium-doped fluorozirconate optical fibre to standard silica fibre. These were a v-groove connector, an AT&T rotary mechanical splice (RMS), and a mechanical stage.

A v-groove connector is used by placing two fibres, which are to be connected, in grooves cut into an object. The grooves act as guides for the fibres so that the cores match up when they are brought together and clamped in position. The drawback of using a v-groove connector is that the core of the fluorozirconate fibre is known often not to be central to the cladding region resulting in alignment mismatch. Another problem is that it requires a clamp to hold the two fibres together usually resulting in destruction of the fluorozirconate fibre. With high pump powers (up to 300 mW) the index matching gel between the fibres can heat up considerably. Often the fluorozirconate fibre would need re-cleaving which was indicative of the damage that had occurred to the fibre end face.

A rotary mechanical splice (RMS) was also used to connect the fluorozirconate fibre with the silica fibre. It consisted of two glass ferrules placed at the end of each fibre. The fibres were inserted and glued in these ferrules. Once the glue set, the ends of the ferrules were polished. Using a sleeve as a guide, the ferrules were brought together and rotated to maximise the coupling. An index matching gel was also used between the fibres. This method of connecting was very tedious as it required a considerable amount of preparation.

Another method used was a simple butt joint. Two mechanical stages with movement in the x , y , and z planes were used to bring the fibre ends together. A microscope was used in tandem to view the fibre ends while they were positioned. This was considered to be the best method since the fluorozirconate fibre was not stressed in any way.

For all three methods it was difficult to avoid misalignment, such as longitudinal separation, lateral misalignment and finite angular displacement because

of the small size of the fluorozirconate fibre core diameter (4 μm). Furthermore, the fluorozirconate optical fibre was multimoded at both the pump and signal wavelengths while the fibre of the coupler was single-mode at the signal wavelength. A single-mode fibre connected to a multimode fibre ultimately results in an amplitude distribution mismatch between the respective LP_{01} modes because of the different mode-field-radii, causing further extrinsic losses. Using the Gaussian approximation for the radial field distribution, the coupling efficiency is given by [Marcuse D., 1977]

$$\eta = \left(\frac{2\omega_1\omega_2}{\omega_1^2 + \omega_2^2} \right)^2 \quad (5.2.1)$$

where ω_1 and ω_2 are the mode-field-radii of the two fibres at the signal wavelength. The coupling efficiency between the fibre from the four-port coupler and the praseodymium-doped fluorozirconate amplifying fibre is about 99.6% which corresponds to a minimum coupling loss of 0.02 dB for the fundamental mode.

5.3 MEASUREMENT OF SMALL SIGNAL GAIN

A range of praseodymium-doped fluorozirconate optical fibres with different dopant concentrations and core diameters were investigated with specific results reported here for 1000 ppm dopant concentration and 4 μm core diameter. In particular the manufacturer supplied two very different samples of fibre. In the first case (denoted Type A) the material properties of the fibre were extremely poor, mainly due to high scattering losses resulting in relatively low gain, but nevertheless the gain measurements and results are discussed in this section. The material

properties of the second fibre (Type B) had been improved considerably by the manufacturer, resulting in much lower scattering losses and consequently a higher gain coefficient. The results of these experiments are also given in this section.

The experimental arrangement was based on the general arrangement described in Section 5.2. In the first set of experiments an AT&T rotary mechanical splice enabled low loss injection from the directional coupler into the Type A praseodymium fibre core. The length of amplifying fibre used was about 1.4 metres.

Figure 5.3.1 shows gross gain as a function of launched pump powers and indicates an amplifier efficiency of 3.3 dB/mW for the 632.8 nm probe. The highest gain achieved at 315 mW was 11 dB, but as this was not easily reproduced the highest repeatable gain of 9.8 dB is indicated in Figure 5.3.1.

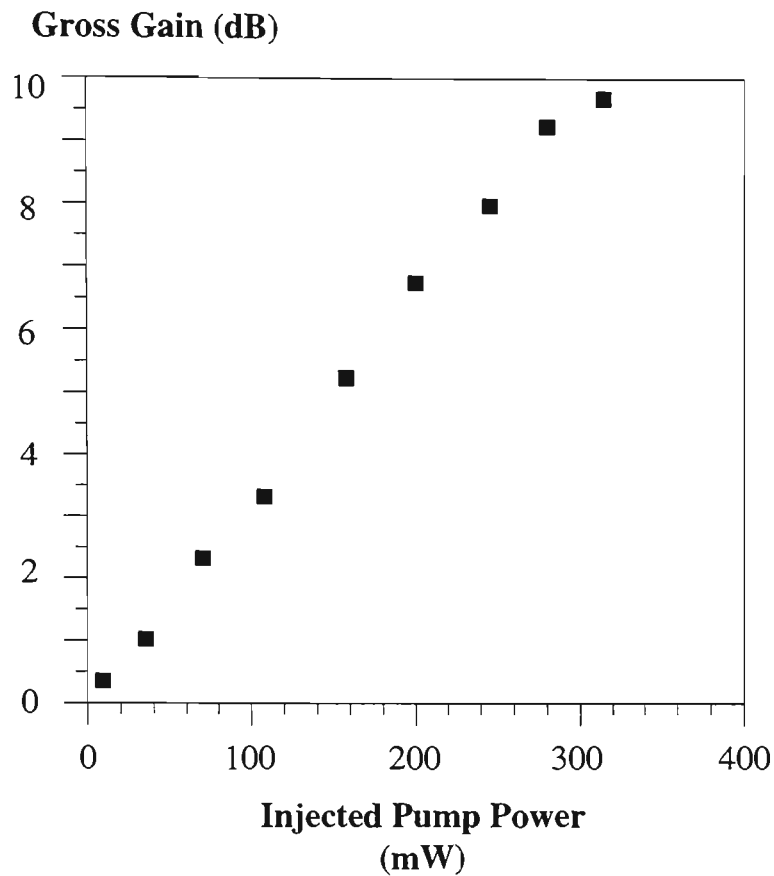


Figure 5.3.1 Gross gain as a function of injected pump power for Type A fibre of length 1.4 m.

The data in Figure 5.3.1 correspond to small signal gain because it was found that the gain remained constant for input signal powers between $0.3 \mu\text{W}$ and $300 \mu\text{W}$. The measurements for this required an adjustable attenuator to be placed in the signal port #3 of the directional coupler. Figure 5.3.2 shows the measured gross gain as a function of launched probe/signal powers. This also indicates the extent to which the gain measurements varied.

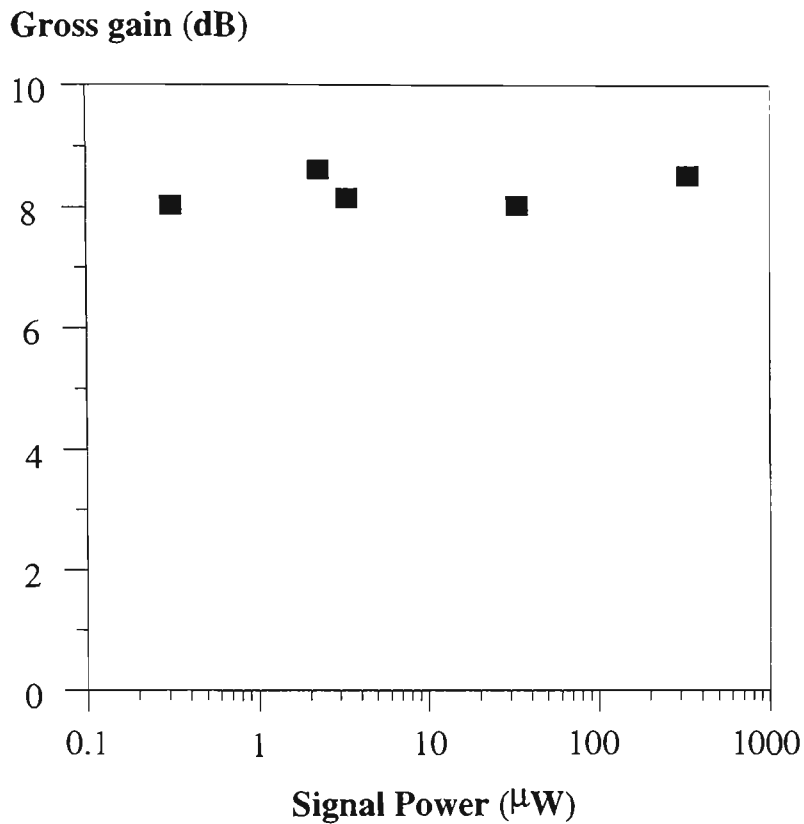


Figure 5.3.2 *Gain as a function of injected probe power with a constant pump power of 250 mW.*

The absorption coefficient at the signal wavelength was measured on a number of fibre samples (Type A) to be between 15 dB/m and 20 dB/m. The total attenuation of the pump radiation in the 1.4 m length of fibre was measured to be 63 dB (ie. 45 dB/m). With 25 μW input signal power, the signal level at the output end of the amplifying fibre was measured to be 35 nW without pumping and 334 nW with 315 mW of injected pump power (9.8 dB gross gain). In this case the gain experienced by the signal was insufficient to overcome the high background losses of the fibre. Obtaining representative data for extinction and absorption per metre of the praseodymium fibre proved difficult due to the variable quality of its core. This was

evident from observations of non-uniform fluorescence and scattering along the length of the fibre.

In any fibre amplifier the gain efficiency is dependent on the overlap of the pump and signal modes and is optimised by ensuring single-mode operation for both. The praseodymium amplifying fibre was multimoded at the pump and probe wavelengths having normalised frequencies of 5.54 and 4.17 respectively. For a multimode fibre a coherent source appears as a complicated modal pattern. The modal pattern may fluctuate in time due to changes in the relative phases of the different modes and the power coupled into the LP_{01} mode will also fluctuate. It is believed that this modal mismatch contributed to instability in the gain measurements (referred to as modal noise), because it was noted that the gain varied with mechanically induced modal changes in the pump arm of the 3 dB coupler. However, one can assume that there was effective coupling between the fundamental mode of the single mode fibre to the fundamental mode of the multimode fibre.

It is important to note that only gross gains were achieved in this fibre rather than net gains because the fibre was considerably longer than required for this application. The measured absorption coefficient at the pump wavelength of 45 dB/m indicates that the pump radiation was reduced to ~5% of its input value after only ~0.3 m of the fibre. This is consistent with the observation of negligible fluorescence beyond the first 0.4 m of fibre. Thus the final 1 m of amplifying fibre contributed little to the pumping and merely attenuated the signal by ~ 20 dB. If allowances were made for this attenuation then it would appear that a net gain would be achieved in a fibre length between 0.3 m and 0.4 m.

This was investigated by determining the relationship between gross gain and injected pump power for different fibre lengths is illustrated in Figure 5.3.3. Measurements started with a 260 mm length and then the fibre was progressively shortened. The maximum gross gain measured was 4.8 dB, which was obtained for a 210 mm length of amplifying fibre and for a 72 mW injected pump.

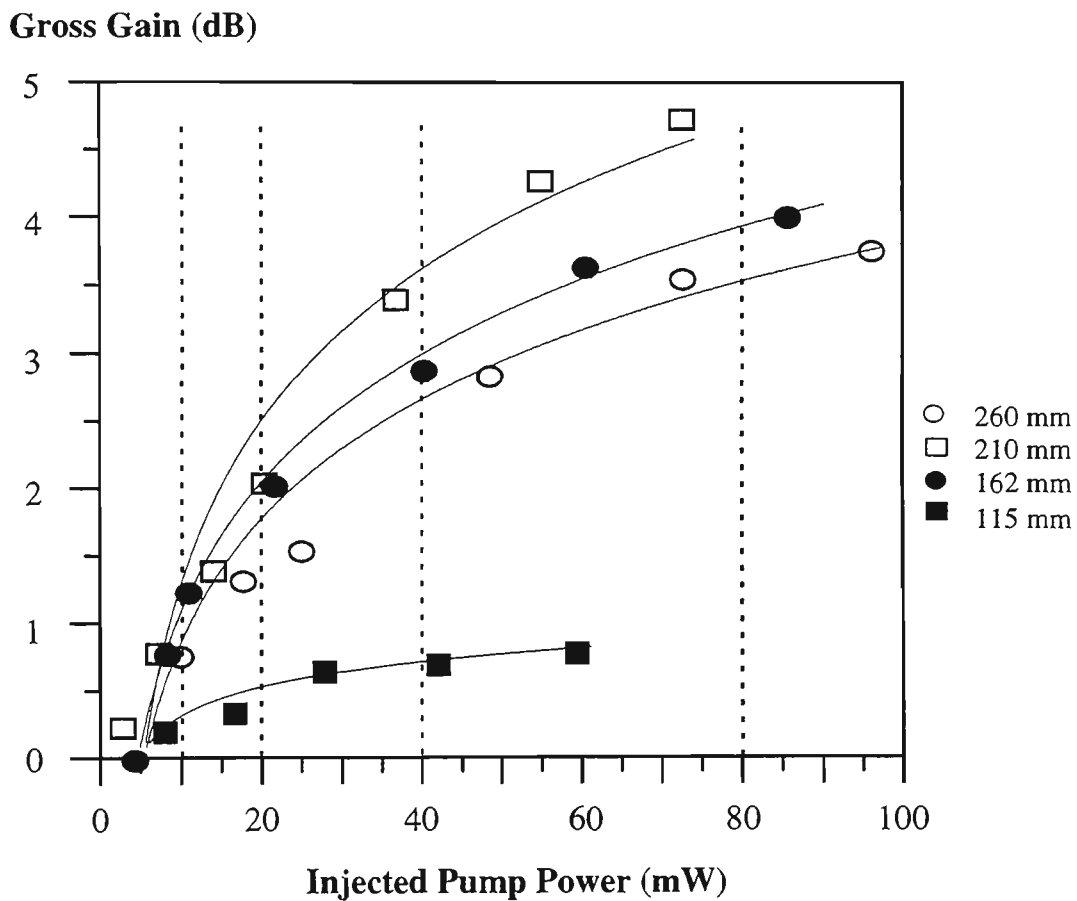


Figure 5.3.3 Gross gain as a function of injected pump power for 260 mm, 210 mm, 162 mm and 115 mm lengths of fibre. The full lines are meant as a guide to the eye.

To determine the dependence of gross gain on fibre length for a fixed pump power, values were interpolated from Figure 5.3.3 for 10 mW, 20 mW, 40 mW and 80 mW injected pump powers, and these are shown in Figure 5.3.4. For each of the curves the gain reaches a peak and then diminishes at a rate comparable to the background attenuation.

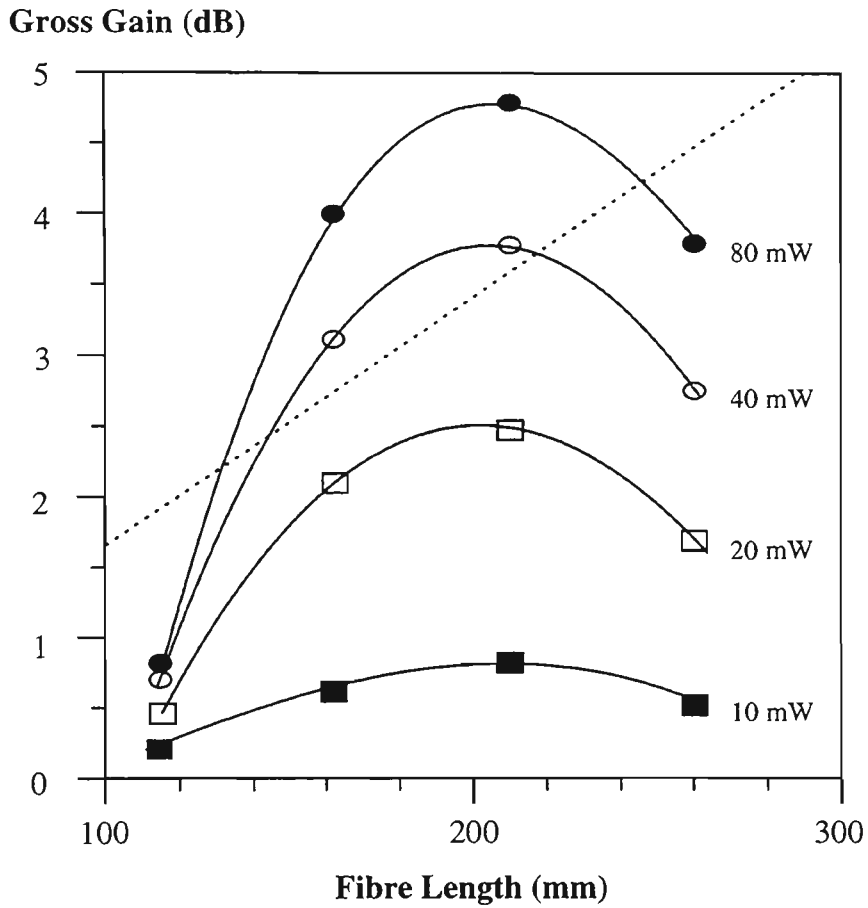


Figure 5.3.4 Gross gain as a function of fibre length for fixed pump powers of 10 mW, 20 mW, 40 mW and 80 mW interpolated from Figure 5.3.3. The dotted line indicates the background loss of the fibre. The full lines are meant as a guide to the eye. The maximum actual measured gain is also indicated.

The fibre background loss at the signal wavelength was measured after each cutback. The attenuation at 632.8 nm was measured to be 0.17 dB/cm and varied significantly by up to ± 0.03 dB/cm. To allow an estimation of the net gain the background loss of the fibre is also shown in Figure 5.3.4. This indicates that the maximum gross gain (4.8 dB) corresponds to net gain of about 1.4 dB.

The high background loss can be attributed mainly to stress fractures in the praseodymium-doped fibre (Type A). At a particular fracture a large amount of scattered pump light was observed. A number of fractures were apparent along the length of the amplifying fibre and clearly limited the overall system gain in this particular experiment.

For the next set of experiments the material properties of the praseodymium-doped fluorozirconate fibre had been improved considerably. Type B fibre had identical properties to Type A fibre except that the background attenuation was measured to be less than 1 dB/m and no scattering points were apparent. Using the general experimental arrangement described in Section 5.2 the gross gain (Equation 5.1.2) as a function of injected pump power was investigated and the results are shown in Figure 5.3.5. For this experiment a mechanical stage (Photon Control) was used to connect the doped fibre to the output port #2 of the directional coupler as discussed in Section 5.2.

The absorption coefficient at the pump wavelength was measured to be about 40 dB/m which is consistent with that obtained for the glass samples in Chapter 3.3. The length of amplifying fibre used in this experiment was approximately 3 m, and since the background attenuation was low there was no need to cut-back the fibre.

The 635 nm transition was found to have such a high gain that lasing was easily achieved due to the 4% Fresnel reflections at the bare cleaved ends. The single pass gain at threshold in such a resonator requires 14 dB of gain to compensate the 96% loss out of the fibre end [Smart R.G. *et al.*, 1991]. Thus for the onset of lasing the single pass gain needs to be at least 14 dB with a net round trip gain of 28 dB. At the threshold of lasing the absorbed pump power was measured to be about 95 mW.

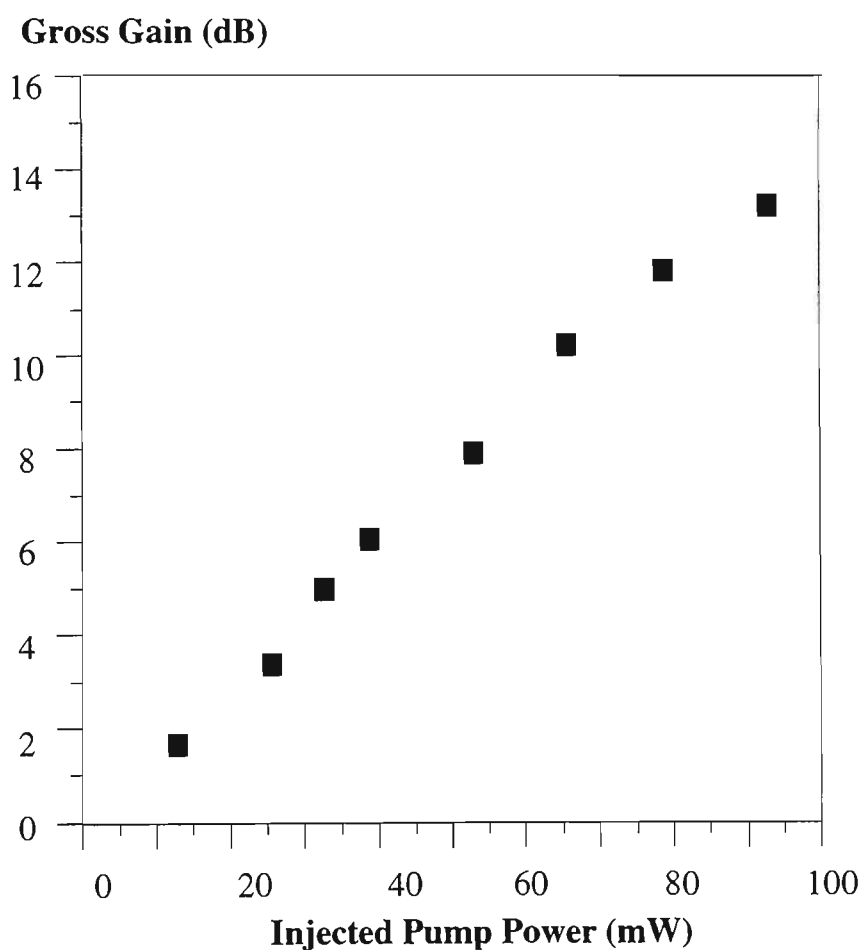


Figure 5.3.5 *Gain as a function of injected pump power for 3 m of Type B fibre.*

5.4 RATE EQUATION MODEL AND CALCULATION OF GAIN

The gain is governed by the propagation of the pump and signal beams in the optical fibre, the population dynamics of the levels and competition between transitions. The processes involved in amplification may be understood by reference to the partial energy level diagram of the praseodymium ion in Figure 5.4.1. The relevant levels and transitions are also shown in Figure 5.4.1, namely the ground state (3H_4) multiplet (level 1), the metastable state (3P_0) (level 3), and the 3F_2 multiplet (level 2), which is the terminating level for the 635 nm transition. The full lines represent stimulated transitions while the dotted lines represent spontaneous emission.

The population of the metastable level is governed by an increase of population due to the pumping process (given by the rate $N_1 R_{13}$ where $R_{13} = \frac{\sigma_p^a I_p}{h\nu_p}$, σ_p^a is the signal emission cross-section, I_p is the signal intensity and $h\nu_p$ is the pump photon energy) using the 476.5 nm pump wavelength. A decrease in population occurs due to spontaneous emission, related to the emission probability, A_3 , for level 3 (where $A_3 = 1/\tau_3$ and τ_3 is the lifetime of level 3), and stimulated emission due to the interaction of the He-Ne probe beam with the atomic system (given by the rate $N_3 W_{32}$ where $W_{32} = \frac{\sigma_s^e I_s}{h\nu_s}$, σ_s^e is the signal emission cross-section, I_s is the signal

intensity and $h\nu_s$ is the signal photon energy). The time behaviour of the metastable level population (N_3) can be described using the following rate equation

$$\frac{dN_3}{dt} = N_1 \frac{\sigma_p^a I_p}{h\nu_p} - N_3 \frac{\sigma_p^e I_p}{h\nu_p} - N_3 \frac{\sigma_s^e I_s}{h\nu_s} + N_2 \frac{\sigma_s^a I_s}{h\nu_s} - N_3 A_3 \quad (5.4.1)$$

where σ_p^e is the emission cross-section at the pump wavelength and σ_s^a is the absorption cross-section at the signal wavelength. For simplicity the stimulated emission at the pump wavelength can be neglected.

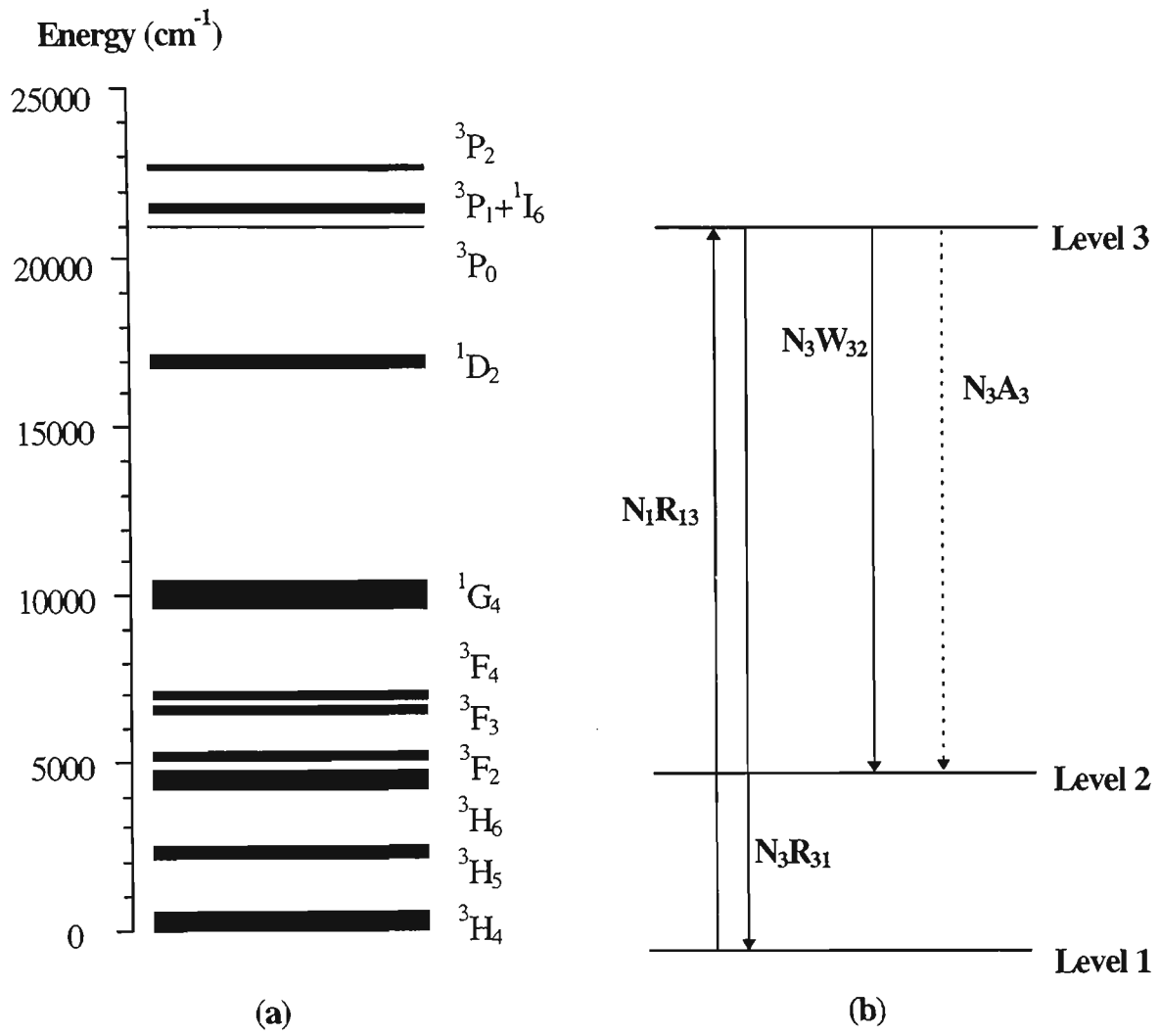


Figure 5.4.1 (a) Simplified energy level diagram for the praseodymium ion in ZBLAN and (b) Transitions central to the amplification process and the labelling scheme used for the rate equation model.

Parasitic effects such as cross-relaxation and cooperative upconversion have been neglected. Although spontaneous emission is accounted for, amplified spontaneous emission (ASE) is also neglected. This is valid for input signal powers that are significantly above the equivalent ASE noise input power as was the case here. Small signal gain was investigated since in most situations it is more useful to evaluate the gain in the limit of negligible signal saturation (as in the case of a low gain amplifier with a small input signal). The consequence of a small signal is that the metastable population is not significantly depleted by the interaction of the signal wave with the metastable level such that $W_s=0$. With this simplification the time-dependent population of level 3 is given by

$$\frac{dN_3}{dt} = N_1 \frac{\sigma_p^a I_p}{h\nu_p} - N_3 \frac{1}{\tau_3} \quad (5.4.2)$$

where τ_3 is the measured lifetime of level 3. The lifetime of level 2 is considered to be very fast and ions may decay rapidly via multiphonon relaxation back to the ground level either directly or through multiple cascaded transitions. This assumes that at any instant there is no significant accumulation of population in any level other than levels 1 and 3, such that

$$N_1 + N_3 = \rho. \quad (5.4.3)$$

To obtain the steady-state solutions, the rate is set to zero ($dN_3/dt = 0$) and so the population of the metastable level (N_3) is given by

$$N_3 = \rho \cdot \frac{\frac{\tau_3 \sigma_p^a}{h\nu_p} I_p}{1 + \frac{\tau_3 \sigma_p^a}{h\nu_p} I_p}, \quad (5.4.4)$$

and the population of the ground level (N_1) is given by

$$N_1 = \rho \cdot \frac{I}{I + \frac{\tau_3 \sigma_p^a}{h\nu_p} I_p} \quad (5.4.5)$$

These steady-state solutions are the same as those obtained for an idealised four-level system discussed in Chapter 2 even though for the praseodymium transitions considered here only 3 levels are considered.

The small signal gain coefficient for a four-level atomic system in the limit of low pump power, as described in Chapter 2 (Equation 2.4.2.7), is given by

$$g_{coeff}^{low} \cdot L = \frac{\tau_3 \sigma_s^e P_{abs}(L)}{h\nu_p} \cdot \frac{\Gamma_{p,s}}{\Gamma_s} \quad (5.4.6)$$

where

$$\frac{\Gamma_{p,s}}{\Gamma_s} = \frac{2}{\pi(\omega_s^2 + \omega_p^2)} \frac{\left(1 - \exp\left[-2a^2 \left(\frac{\omega_s^2 + \omega_p^2}{\omega_s^2 \omega_p^2} \right) \right] \right)}{\left(1 - \exp\left[-\frac{2a^2}{\omega_p^2} \right] \right)} \quad (5.4.7)$$

The first group of terms on the right hand side of Equation 5.4.6 are described by the spectroscopic properties discussed in Chapter 3. The overlap function given in Equation 5.4.7 is a function of the mode-field-radius of the pump and signal beams and the core radius. Calculated and measured values of the mode-field-radii are given in Chapter 4. A summary of these parameters is given in Table 5.4.1. These parameters were incorporated into Equation 5.4.6 and Equation 5.4.7, the result of which is depicted in Figure 5.4.2. The gain was calculated for different values of the mode-field-radius, namely for that calculated using the Bessel function solution (full line), the Gaussian approximation or the Marcuse polynomial (dashed-dotted)

and the measured mode-field-radius (dotted). It is important to note that the mode-field-radius of the pump beam was not actually measured but rather it was calculated as a ratio of the mode-field-radius for the pump and signal beams obtained from the Gaussian approximation and the measured mode-field-radius of the signal beam. As a comparison the measured gain is also shown in Figure 5.4.2. The calculated and measured gains compare well with the best fit provided by the Gaussian approximation.

Parameters	
a	$2 \mu\text{m}$
$h\nu_p$	$4.2 \times 10^{-18} \text{ J}$
$\tau_3(\rho \rightarrow 0)$	$49.8 \pm 0.3 \mu\text{s}$
σ'_s	$2.1 \pm 0.2 \times 10^{-24} \text{ m}^2$
P_{abs}	0 to 100 mW
ω_s, ω_p	$\omega_s = 1.67 \mu\text{m}$
(Gaussian)	$\omega_p = 1.54 \mu\text{m}$
ω_s, ω_p	$\omega_s = 1.75 \mu\text{m}$
(Bessel)	$\omega_p = 1.65 \mu\text{m}$
ω_s, ω_p	$\omega_s = 1.6 \pm 0.1 \mu\text{m}$
(Measured)	* $\omega_p = 1.47 \mu\text{m}$

Table 5.4.1

*Summary of parameters relevant to the gain coefficient (Equation 5.4.6). (*Note that the measured intensity spot-size of the pump beam was calculated as a ratio of the intensity spot-size for the pump and signal beams obtained from the Gaussian approximation and the measured intensity spot-size*

of the signal beam, ie. $\omega_p^{measured} = \omega_s^{measured} \times \frac{\omega_p^{Gaussian}}{\omega_s^{Gaussian}}$).

Gross Gain (dB)

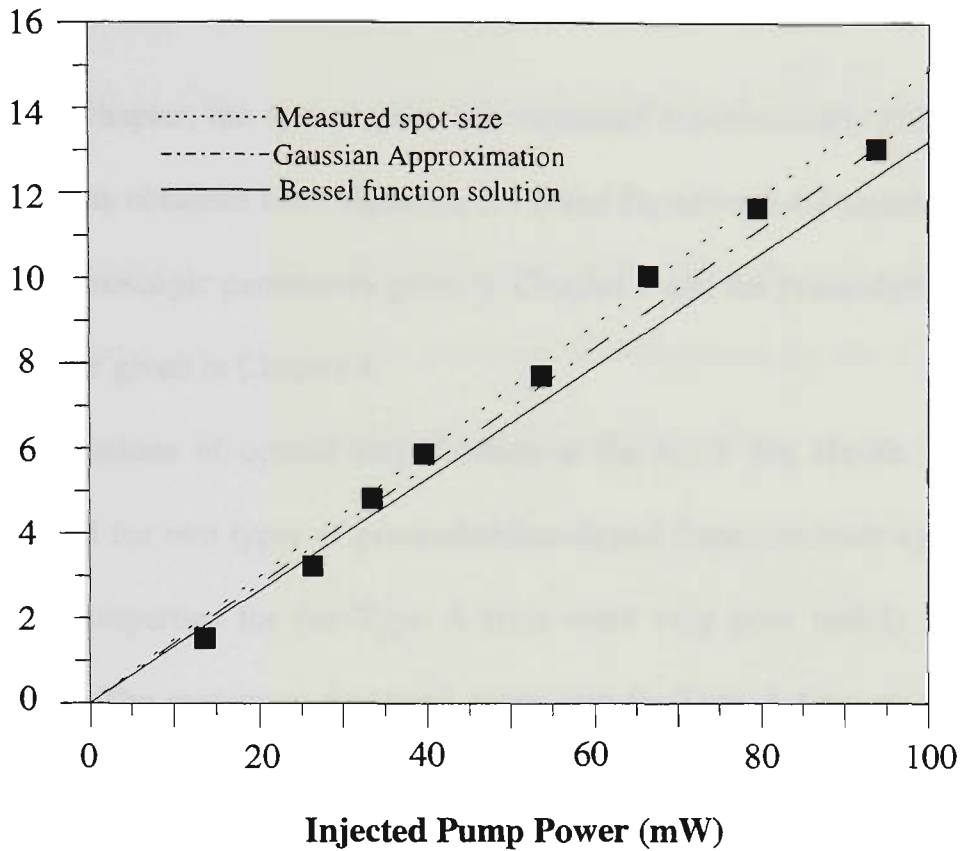


Figure 5.4.2

Comparison of the measured gain (squares) with the model described in Chapter 2 incorporating the measured spectroscopic parameters from Chapter 3. The gain was calculated with different values of the mode-field-radius. The mode-field-radius includes that calculated from the Bessel function solutions (full line), the Gaussian approximation or the Marcuse polynomial (dashed-dotted line) and that measured from near field experiments (dashed) calculated in Chapter 4.

5.5 CONCLUSION

In this chapter, the optical gain was measured experimentally and compared with calculations obtained from Equation 5.4.6 and Equation 5.4.7 together with the measured spectroscopic parameters given in Chapter 3 and the praseodymium-doped fibre parameters given in Chapter 4.

Investigations of optical amplification at the 632.8 nm He-Ne wavelength were conducted for two types of praseodymium-doped fluorozirconate optical fibre. The material properties for the Type A fibre were very poor mainly because of scattering loss. The maximum measured gross gain for Type A fibre was 10 dB for an injected pump power of up to 300 mW and a fibre length of 1.4 m. Net gain was achieved in this fibre by optimising the length to approximately 210 mm for which 1.4 dB net gain for an injected pump power of 80 mW was possible. The material properties for Type B fibre were much improved as compared to the Type A fibre. The background loss of the Type B fibre was less than 1 dB/m compared with approximately 18 dB/m in the Type A fibre. For the Type B fibre, the 635 nm transition was found to have such a high gain that, for pump powers greater than approximately 95 mW, lasing was easily achieved due to the 4 % Fresnel reflections at the bare cleaved ends. The highest gross gain achieved in Type B fibre was 14 dB for an injected pump power of 95 mW, since the maximum output power of the pump laser used in these experiments was approximately 100 mW.

Apart from experimental measurements the gain was also calculated by using Equation 5.4.6 and Equation 5.4.7 together with the measured spectroscopic parameters given in Chapter 3 and the praseodymium-doped fibre parameters given in Chapter 4.

As a comparison, the calculated gain compared very well with the gain measured for the Type B fibre. The gain was not calculated for the Type A fibre because of the complexities arising from the high scattering loss.

Chapter 6

CONCLUSION AND FUTURE WORK

6.1 Conclusion

6.2 Future work

6.1 CONCLUSION

Reported in this Thesis is an investigation of single-pass small-signal amplification at the 632.8 nm He-Ne wavelength using praseodymium-doped fluorozirconate optical fibre as the amplifying medium. The optical gain is fundamentally related to the spectroscopic characteristics of praseodymium-doped in a fluorozirconate glass host together with optical fibre parameters, that determine the physical characteristics of the waveguide. The spectroscopic parameters that influence the gain include, the branching ratio of ${}^3P_0 \rightarrow {}^3F_2$ transition (β_{32}), the fluorescence lifetime of the 3P_0 state (τ_3), the absorption cross-section at the pump wavelength and the emission cross-section at 632.8 nm on the ${}^3P_0 \rightarrow {}^3F_2$ transition. The optical fibre parameters that also influence the gain include the intensity spot-size of the fundamental mode of the He-Ne signal beam (ω_s) and the 476.5 nm pump beam (ω_p) propagating in the amplifying fibre and the radial distribution of the praseodymium ions. The work presented in this Thesis is divided into four main chapters including modelling of rare-earth-doped fibre amplifiers (Chapter 2), spectroscopic characterisation of praseodymium-doped fluorozirconate glass (Chapter 3), characterisation of optical fibre parameters (Chapter 4) and experimental determination of amplification at the 632.8 nm He-Ne wavelength (Chapter 5).

Modelling of rare-earth-doped optical fibre amplifiers is given in Chapter 2. This chapter steps back from considering specific amplifier systems and gives an outline of the essential methods used in the modelling of amplifiers. In particular, a set of coupled differential equations were derived for both a three- and four-level

atomic systems from which the evolution of the pump and signal power, and thus the gain along the length of the fibre, were determined in the low pump and high pump regimes. The gain coefficient for a four-level amplifier system in the low pump regime, as described in Chapter 2, is given by (Equation 2.4.2.7)

$$g_{coeff}^{low} \cdot L = \frac{\tau_3 \sigma_s^e P_{abs}(L)}{h\nu_p} \cdot \frac{\Gamma_{p,s}}{\Gamma_s}$$

where the ratio $\frac{\Gamma_{p,s}}{\Gamma_s}$ is given by Equation 2.4.2.8.

Experimental investigations of the spectroscopic parameters that influence the optical gain on the ${}^3P_0 \rightarrow {}^3F_2$ transition in praseodymium-doped fluorozirconate glass have been presented in Chapter 3. These parameters include, the branching ratio of ${}^3P_0 \rightarrow {}^3F_2$ transition (β_{32}), the fluorescence lifetime of the 3P_0 state (τ_3), the absorption cross-section at the pump wavelength and the emission cross-section at 632.8 nm on the ${}^3P_0 \rightarrow {}^3F_2$ transition. The branching ratio, β_{32} , was measured to be approximately 15% which compares well with the most recent measurements summarised in Table 3.4.2. The fluorescence lifetime of the 3P_0 state was measured for varying dopant concentrations ranging from 2.8×10^{25} ions/m³ to 67×10^{25} ions/m³. For these concentrations, the fluorescence lifetime was found to vary between 49 μ s and 33 μ s respectively. The radiative lifetime of the 3P_0 state decreases with increasing concentration mainly due to increasing cross-relaxation rates. The relaxation rate of the 3P_0 state is related linearly to the concentration by (Equation 3.8.3.7)

$$\frac{1}{\tau} = \frac{1}{\tau_6} + \frac{1}{2} \alpha_{cr} \rho$$

From fluorescence lifetime measurements and a rate equation analysis of the level dynamics, values for the cross-relaxation parameter (α_{cr}) and the lifetime of the 3P_0 state in the limit of zero concentration (τ_0) were also obtained. Indeed, the cross-relaxation parameter was measured for the first time and was calculated to be $2.6 \pm 0.1 \times 10^{-23} \text{ m}^3/\text{s}$ which was obtained from a least squares fit of Equation 3.8.3.7 to the measured lifetime as a function of concentration. From the same least squares fit, the lifetime in the limit of zero concentration was determined to be $49.8 \pm 0.3 \mu\text{s}$. Furthermore, the cross-relaxation parameter was used to calculate the extent to which the gain at 632.8 nm would be affected. From the fluorescence lifetime measurements and measurement of the branching ratio of the $^3P_0 \rightarrow ^3F_2$ transition, the absorption and emission cross-sections were calculated using Fuchtbauer-Ladenburg analysis. The emission cross-section at 632.8 nm was calculated to be $\sigma_e = 2.1 \pm 0.2 \times 10^{-24} \text{ m}^2$ and the absorption cross-section at the pump wavelength (476.5 nm) was calculated to be $\sigma_a = 0.14 \pm 0.02 \times 10^{-24} \text{ m}^2$. The branching ratio, the fluorescence lifetime, the cross-relaxation parameter, and the absorption and emission cross-sections of the $^3P_0 \rightarrow ^3F_2$ transitions are all key parameters required for accurate modelling and qualitative understanding of the optical properties of the amplifier material.

Experimental investigation of the optical fibre parameters that influence the overall performance of the 632.8 nm praseodymium-doped fibre amplifier have been presented in Chapter 4. These parameters include the intensity spot-size of the fundamental mode of the He-Ne signal beam (ω_s) and the 476.5 nm pump beam (ω_p) propagating in the amplifying fibre and the radial distribution of the praseodymium

ions. The intensity spot-size of the fundamental mode was determined from near field measurements of the 632.8 nm beam propagating in the praseodymium-doped fluorozirconate optical fibre. The experimentally determined value for the intensity spot-size of the fundamental mode was $\omega_s^{exp} = 1.6 \pm 0.1 \mu\text{m}$. This value compared well with that calculated from Gaussian approximations given by the Marcuse polynomial ($\omega_s^{Bessel} = 1.75 \mu\text{m}$) and that calculated from Bessel function solutions for the fundamental mode ($\omega_s^{Gaussian} = 1.67 \mu\text{m}$). The radial distribution of praseodymium ions in the fibre core is another parameter that was investigated in Chapter 4.3. Measurements of the concentration dependant relaxation rates of the 3P_0 state of praseodymium, spatially resolved by confocal microscopy, were analysed to give an absolute measure of the concentration profile in praseodymium-doped fluorozirconate optical fibre. The results obtained in Section 4.3 are consistent with experimental measurements recorded in Chapter 3.7 and indicate, to some extent, a radially constant dopant ion distribution. The measurements are novel in that they rely directly on concentration-dependent processes in the material and as a result do not require optical calibration. The intensity spot-size of the fundamental mode of the He-Ne signal beam (ω_s), the 476.5 nm pump beam (ω_p) propagating in the amplifying fibre and the radial distribution of the praseodymium ions are also key parameters required for accurate modelling of the praseodymium-doped fibre amplifier. At this point it is important to note that the spectroscopic and optical fibre parameters have been calculated independently of the gain. Since this is the case, a comparison can be made between the calculated gain, incorporating the measured parameters, and the measured gain.

Finally, in Chapter 5 the results of measurements of amplification at the 632.8 nm He-Ne wavelength in praseodymium-doped fluorozirconate optical fibre were given. Investigations of optical amplification at the 632.8 nm He-Ne wavelength were conducted for two types of praseodymium-doped fluorozirconate optical fibre. The material properties for the Type A fibre were very poor mainly because of scattering loss. The maximum measured gross gain for Type A fibre was 10 dB for an injected pump power of up to 300 mW and a fibre length of 1.4 m. Net gain was achieved in this fibre by optimising the length to approximately 210 mm for which 1.4 dB net gain for an injected pump power of 80 mW was possible. The material properties for Type B fibre were much improved as compared to the Type A fibre. The background loss of the Type B fibre was less than 1 dB/m compared with approximately 18 dB/m in the Type A fibre. For the Type B fibre, the 635 nm transition was found to have such a high gain that, for pump powers greater than approximately 95 mW, lasing was easily achieved due to the 4 % Fresnel reflections at the bare cleaved ends. The highest gross gain achieved in Type B fibre was 14 dB for an injected pump power of 95 mW, since the maximum output power of the pump laser used in these experiments was approximately 100 mW. The gain was also calculated by using Equation 5.4.6 and Equation 5.4.7 and the measured spectroscopic parameters given in Chapter 3 and the praseodymium-doped fibre parameters given in Chapter 4. Evidently the calculated gain compared well with the measured gain. Indeed, the agreement between the calculated gain, using the measured parameters, and the measured gain indicates that the important processes that influence the gain characteristics of the amplifier have been included.

It can be further concluded that the spectroscopic parameters measured in bulk samples transferred well to the doped fibre core, since measured and calculated gains compared well and the measured absolute concentration profile in the fibre core agreed well with the preform specifications. These conclusions suggest that the reported problems of this transfer [Dybdal K. *et al.*, 1989] may be due to inappropriate measurement techniques in optical fibre [Poole S.B. *et al.*, 1989; Urquhart P., 1988].

An optical fibre amplifier, such as that described here, is required because all optical systems suffer from the usual effects of attenuation and power division in multiport couplers. Optical amplifier technology can be applied to sensor systems where it is often preferable to use visible wavelength sources as they offer certain sensitivity advantages over infrared (IR) laser diodes and the convenience of lower cost silicon detectors. The 632.8 nm He-Ne laser is attractive and widely used because it is inexpensive and it offers good frequency and intensity stability and a high degree of coherence. An optical fibre amplifier that will increase the system power budget in such a system has been the subject of these investigations. No previous work has been reported on single-pass amplification of the 632.8 nm He-Ne wavelength in praseodymium-doped fluorozirconate optical fibre. The importance of the work presented in this Thesis is that much of the existing amplifier technology has been extended for possible application in the expanding field of optical fibre sensor systems. Nevertheless, the understanding achieved in this Thesis is sufficient for predictions regardless of the application.

6.2 FUTURE WORK

The work presented in this Thesis may be enhanced by firstly considering some of the more important aspects of the praseodymium-doped fibre amplifier. As outlined in this Thesis, there are three main areas to consider including

- the spectroscopic parameters,
- the optical fibre waveguide parameters,
- and characterising the performance of the amplifier.

There is some scope for further work in all three of these areas.

Although the spectroscopic parameters themselves cannot be controlled to any great extent, the pumping scheme used to populate the 3P_0 state can. In the work presented in this Thesis, the pumping scheme used to populate the 3P_0 state was suitable for experimental purposes only and is not considered to be a practical solution since an argon-ion laser is very large in size and expensive to purchase and maintain. Usually, laser diode based pumping schemes are considered practical because laser diode sources are small in size, consume little power and are relatively cheap compared to other laser systems. A high power laser diode source operating at a wavelength somewhere between 450 nm and 480 nm would be required for the pumping scheme discussed in this Thesis. However, since laser diodes at any of these wavelengths are unobtainable there is an obvious need to investigate alternative pumping schemes with a particular emphasis placed on a pumping scheme that takes advantage of laser diode sources that are currently available. One solution is to obtain frequency doubled output from an infrared laser diode source. An alternative to this

is to investigate possible stepwise pumping schemes. One such pumping scheme, shown in Figure 6.2.1, involves an initial excitation of ground state ions to the 1G_4 state with $1.01\ \mu\text{m}$ radiation and subsequently to the 3P_0 state with 835 nm pumping [Smart R. *et al.*, 1991; Tropper A.C. *et al.*, 1994; Zhao Y. and Poole S.B., 1994]. This pumping scheme requires two commonly available high power laser diode sources. Finally, another alternative is to sensitise praseodymium with ytterbium since it has been previously shown by other authors that a two ion absorption process using a pump wavelength of around 840 nm can be used to ultimately populate the 3P_0 state of praseodymium (Figure 6.2.2) through energy transfer mechanisms between praseodymium and ytterbium [Allain J.T. *et al.*, 1991]. Laser diode sources at around this wavelength are also commonly available.

It is expected that by optimising the fibre waveguide parameters of the praseodymium-doped fibre amplifier to ensure single-mode propagation of the 632.8 nm wavelength a significant increase in the gain and slope efficiency will be possible. In particular, the measured spectroscopic parameters together with the models presented in this Thesis can be employed to simulate a number of fibre designs that will result in optimal gain. Take for example, a $1\ \mu\text{m}$ core radius and $NA=0.24$, then according to the model presented in Chapter 2 and Chapter 5, for a pump power of 100 mW, 38 dB gain would be expected. Conversely, only 37 mW would be needed to reach the 14 dB gain obtained in Chapter 5. The modal noise encountered in Chapter 5, due to the multimode fibre, would also be significantly reduced.

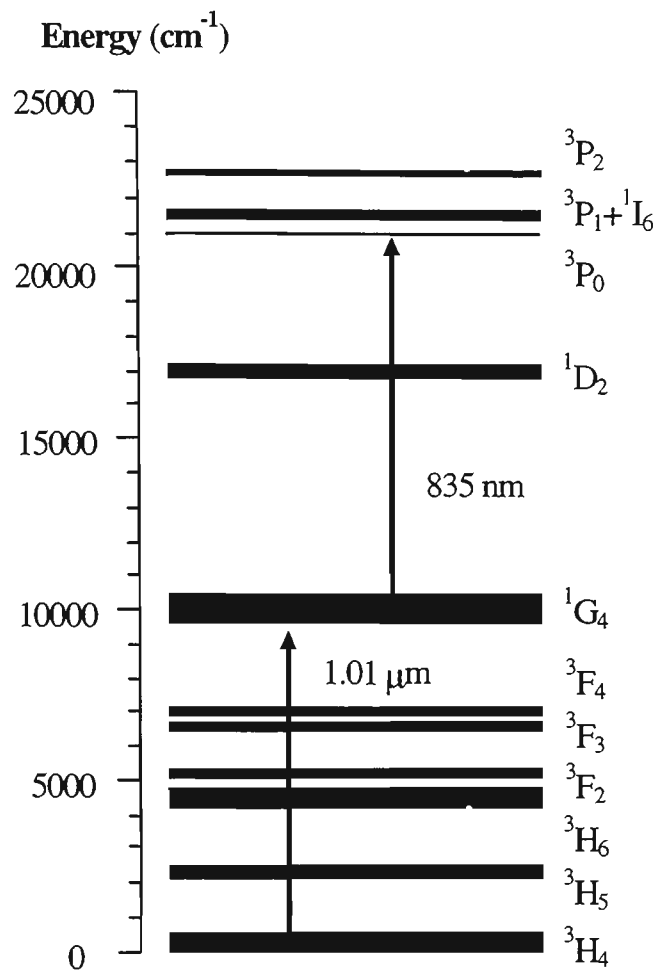


Figure 6.2.1

Pumping scheme used by other authors to populate the ³P₀ state [Smart R. et al., 1991; Tropper A.C. et al., 1994; Zhao Y. and Poole S.B., 1994].

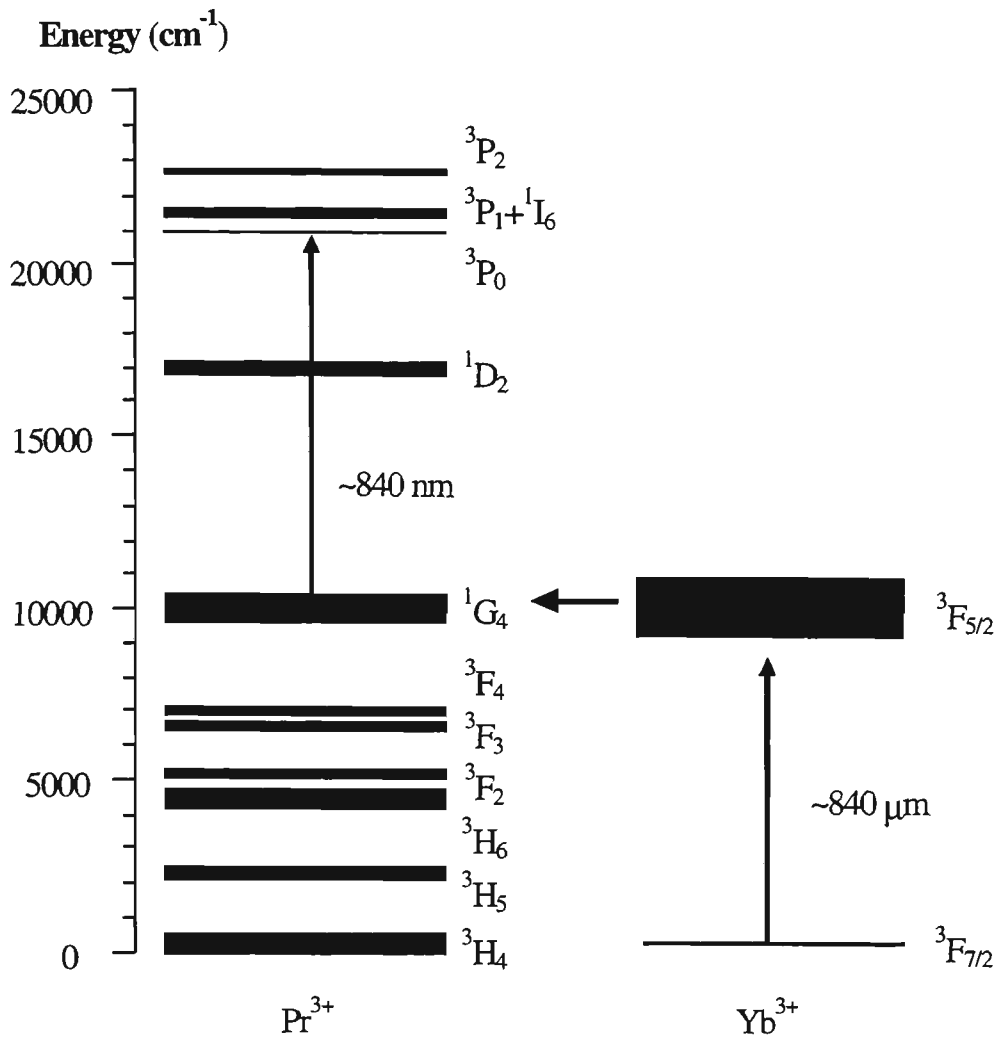


Figure 6.2.2 Pumping scheme used by other authors to populate the $^3\text{P}_0$ state [Allain J.T. et al., 1991].

Finally, the performance of an optical fibre amplifier must be characterised not only by the gain but by its noise performance as well. The noise performance, with specific reference to light in an optical fibre amplifier, is associated with the electric field, optical power, frequency, phase and polarisation [Desurvire E., 1994a & b]. Furthermore, in the case of a multimode fibre, noise is also associated with the random excitation in time of the transverse modes [Neumann E.G., 1988]. Since the noise is associated with many factors it is difficult to discuss the noise without

reference to a particular sensor system. However, in general terms energy fluctuation at the amplifier output can be attributed to spontaneous emission where a random or incoherent noise background builds up and is amplified along with the signal. This is referred to as amplified spontaneous emission (ASE). The noise in an amplifier consists of signal-spontaneous beat noise and spontaneous-spontaneous beat noise. The dominant noise in an amplifier is the beat noise between the signal and the spontaneous emission components since the spontaneous-spontaneous beat noise can be minimised by using a narrow-band optical filter. Other optical fibre amplifier systems have indicated good noise performance and it is expected that the amplifier discussed in this Thesis will have similar properties.

References

- Adam J. L., and Sibley W. A., "Optical Transitions of Pr³⁺ Ions in Fluorozirconate Glass," *J. Non-Cryst. Solids*, vol. 76, pp. 267-279, Apr. 1985.
- Aggarwal I. D., and Lu G., *Fluoride Glass Fiber Optics*, Academic Press, San Diego, 1991.
- Agrawal G. P., *Fiber-optic communication systems*, Wiley-Interscience, New York, 1992.
- Allain J. Y., Monerie M., and Poignant H., "Red Upconversion Yb-Sensitised Pr Fluoride Fibre Laser Pumped in 0.8 μm Region," *Electron. Lett.*, vol. 27, no. 13, pp. 1156-1157, Jun. 1991.
- Allain J. Y., Monerie M., and Poignant H., "Tunable CW Lasing Around 610, 635, 695, 715, 885, and 910 nm in Praseodymium-Doped Fluorozirconate Fibre," *Electron. Lett.*, vol. 27, no. 2, pp. 189-191, Jan. 1991.
- Ankiewicz A., and Peng G. D., "Generalized Gaussian Approximation For Single-Mode Fibers," *J. Lightwave Tech.*, vol. 10, no. 1, pp. 22-27, Jan. 1992.
- Ankiewicz A., and Ruhl F. F., "Effect of dopant distribution on optimization of Pr-doped fibre amplifiers," *Optical and Quant. Electron.*, vol. 26, pp. 987-993, Oct. 1994.
- Arauzo A. B., Cases R., and Alcalá R., "Optical Absorption, Photoluminescence and Cross-relaxation of Pr³⁺ Ions in Some Fluoride Glasses," *Physics and Chem. of Glasses*, vol. 35, no. 5, pp. 202-206, Oct. 1994.
- Armitage J. R., "Three-level Fiber Laser Amplifier: a Theoretical Model," *Applied Optics*, vol. 27, no. 23, pp.4831-4836, Dec. 1988.

- Atkins G. C., Cotter D., Smith D. W., and Wyatt R., "Application of Brillouin amplifier in coherent optical transmission," *Electron. Lett.*, vol. 22, no. 10, pp. 556-558, May 1986.
- Barnard C., Myslinski P., Chrostowski J., and Kavehrad, "Analytical Model for Rare-Earth-Doped Fiber Amplifiers and Lasers," *J. Quant. Electron.*, vol. 30, no. 8, pp. 1817-1830, Aug. 1994.
- Barnes W. L., Laming R. I., Tarbox E. J., and Morkel P. R., "Absorption and Emission Cross Section of Er^{3+} Doped Silica Fibers," *J. Quant. Electron.*, vol. 27, no. 4, pp. 1004-1010, Apr. 1991.
- Bjarklev A., Hansen S. L., and Povlsen J. H., "Large-signal modeling of an erbium-doped fibre amplifier," Proc. SPIE Conference on fiber laser sources and amplifiers, vol. 1171, pp. 118, Sep. 1989.
- Brierly M., and Millar C. A., "Amplification and lasing at 1350 nm in a neodymium doped fluorozirconate fibre," *Electron. Lett.*, vol. 24, no. 7, pp. 438-439, Mar. 1988.
- Brierly M., Carter S., France P., and Pedersen J. E., "Amplification in the 1300 nm telecommunications window in a Nd-doped fluoride fibre," *Electron. Lett.*, vol. 25, no. 5, pp. 329-330, Mar. 1990.
- Buck J. A., *Fundamentals of optical fibers*, Wiley-Interscience, New York, 1995.
- Carter S., Szebesta D., Davey S., Wyatt R., Brierly M. and France P., "Amplification at 1.3 μm in a Pr^{3+} -doped single mode fluorozirconate fibre," *Electron. Lett.*, vol. 27, no. 8, pp. 628-629, Apr. 1991.

Cheo P. K., *Fiber optics & optoelectronics 2nd edition*, Prentice Hall, New Jersey, 1990.

Cotter D., "Observation of stimulated Brillouin scattering in low-loss silica fibre at 1.3 μm ," *Electron. Lett.*, vol. 18, no. 12, pp. 495-495, Jun. 1982.

Culshaw B. and Dakin J., *Optical fibre sensors: Principles and components/ systems and applications*, vol. 1 & 2, Artech House, Inc., 1988/1989.

Davey S. T., and France P. W., "Rare Earth Doped Fluorozirconate Glasses for Fibre Devices," *B. T. Technol. J.*, vol. 7, no. 1, pp. 58-68, Jan. 1989.

Davey S. T., Carter S. F., Szebesta D. Whitley T. J., Wyatt R., Lobbett R., Brierly M. C., and Millar C. A., "Rare Earth-Doped Fluoride Fibres for Optical Amplification," *In Proc. SPIE : Fiber Laser Sources and Amplifiers III*, Boston, USA, Sep. 5-6, vol. 1581, pp. 144-154, 1991.

Desurvire E. and Simpson J. R., "Amplification of Spontaneous Emission in Erbium-Doped Single-Mode Fibers," *J. Lightwave Technol.*, vol. 7, no. 5, pp. 835-845, May 1989.

Desurvire E., "Analysis of Erbium-Doped Fiber Amplifiers Pumped in the $^4\text{I}_{15/2}$ - $^4\text{I}_{13/2}$ Band," *Applied Optics*, vol. 33, no. 24, pp. 5585-5593, Aug. 1994a.

Desurvire E., *Erbium-doped fibre amplifiers: Principles and applications*, Wiley-Interscience, New York, 1994b.

Desurvire E., Simpson J. R., and Becker P. C., "High-gain erbium-doped travelling-wave fibre amplifier," *Optics Lett.*, vol. 24, no. 11. pp. 888, Nov. 1987.

Dexter D.L., "A theory of sensitized luminescence in solids," *J. Chem. Phys.*, vol. 21, no. 5, pp. 836-850, May 1953.

- Dieke G. H., and Crosswhite H. M., "The spectra of doubly and triply ionized rare earths," *Appl. Opt.*, vol.2, no. 7, pp. 657-666, Jul. 1963.
- Digonnet M. J. F., "Closed-Form Expressions for the Gain in Three- and Four-Level Laser Fibers," *J. Quant. Electron.*, vol. 26, no. 10, pp 1788-1796, Oct. 1990.
- Digonnet M. J. F., and Gaeta C. J., "Theoretical Analysis of Optical Fiber Laser Amplifiers and Oscillators," *Applied Optics*, vol. 24, no. 3, pp. 333-342, Feb. 1985.
- Digonnet M. J. F., Ginzton E. L., and Hansen W. W., "Theory of Operation of Three- and Four-Level Fiber Amplifiers and Sources," *In Proc. SPIE Fiber Laser Sources and Amplifiers*, Boston. USA, Sep. 6-8, vol. 1171, pp. 8-26, 1989.
- Digonnet M. J. F., *Rare earth doped fibre lasers and amplifiers*, Marcel Dekker, New York, 1993.
- Durteste Y., Monerie M., Allain J. Y., and Poignant H., "Amplification and lasing at 1.3 μm in a Pr^{3+} -doped single mode fluorozirconate fibres," *Electron. Lett.*, vol. 27, no. 8, pp. 626-628, Apr. 1991.
- Dybdal K., Bjerre N., Pedersen J.E., and Larsen C.C., "Spectroscopic properties of Er-doped silica fibres and preforms," *Proc. SPIE Fibre laser sources and amplifiers*, Boston. USA, Sep. 6-8, vol. 1171, pp. 209-218, 1989.
- Edwards J. G., "Measurement of the Cross-Section for Stimulated Emission in Neodymium Glass," *Nature*, vol. 212, pp. 752-753, Nov. 1966.
- Eyal M., Greenberg E., Reisfeld R., and Spector N., "Spectroscopy of Preseodymium(III) in Zirconium Fluoride Glass," *Chem. Phys. Lett.*, vol. 117, no. 2, pp. 108-114, Jun. 1985.

- Fleming S. C., "Accurate analytic expressions for gain in a Pr^{3+} :ZBLAN fibre amplifier using modified Gaussian field functions," *IEEE J. Quantum Electron.*, vol. 30, no. 2, pp. 280-283, Feb. 1994
- Fleming S.C., Whitley T.J. and Millar C.A., "The effect of pump and signal field overlap with the ion distribution on the efficiency of an Er^{3+} -doped fibre amplifier," *Optics Communications*, vol. 83, no. 1,2, pp. 154-161, May 1991.
- France P. W. (Ed), *Optical Fibre lasers and amplifiers*, Blackie, London, 1991.
- France P. W., *Fluoride Glass Optical Fibres*, Blackie, London, 1990.
- Gambling W. A., "Fibre lasers and amplifiers in distributed sensors," *Proc. Optical Fibre Sensors Conference OFS'93*, Florence, Italy, May 4-6, pp. 49-54, 1993.
- German K. R., Kiel A., and Guggenheim H., "Radiative and Nonradiative Transitions of Pr^{3+} in Trichloride and Tribromide Hosts," *Phys. Rev. B.*, vol. 11, no. 7, pp. 2436-2442, Apr. 1975.
- Giles R. C., and Desurvire E., "Modelling Erbium-Doped Fiber Amplifiers," *J. Lightwave Technol.*, vol. 9, no. 2, pp. 271-283, Feb. 1991.
- Gloge D., "Weakly guiding fibres," *Appl. Optics*, vol. 10, no. 10, pp. 2252-2258, Oct. 1971.
- Goh S., "A Spectroscopic Study of the Best Pump Wavelength in the 800 nm Band for Erbium-Doped Fluorozirconate Fibre Amplifiers," *J. Non-Crystal. Solids*, vol. 140, no. 1-3, pp. 179-183, Jan. 1992.
- Hegarty J., Huber D. L., and Yen W. M., "Fluorescence Quenching by Cross Relaxation in $\text{LaF}_3:\text{Pr}^{3+}$," *Phys. Rev. B.*, vol. 25, no. 9, pp. 5638-5645, May 1982.

- Holst G. C., Snitzer E., and Wallace R., "High-coherence high-power laser system at 1.0621 μ ," *J. Quantum Electron.*, vol. 6, pp. 342, Jun. 1969.
- Horigichi M., Shimizu M., Yamada M., Yoshino K., and Hanafusa H., "Highly Efficient Optical Fibre Amplifier Pumped by a 0.8 μ m Band Laser Diode," *Electron. Lett.*, vol. 26, no. 21, pp. 1758-1759, Oct. 1990.
- Ippen E. P. and Stolen R. H., "Stimulated Brillouin scattering in optical fibers," *App. Phys. Lett.*, vol. 21, no. 11, pp. 539-541, Dec. 1972.
- Jeunhomme L., *Single-mode fibre optics : principles and applications. 2nd edition.*, Marcel Dekker, New York, 1990.
- Jha A., Naftaly M., Jordery S., Samson B. N., Taylor E. R., Hewak D., Payne D. N., Poulain M., and Zhang G., "Design and Fabrication of Pr³⁺-Doped Fluoride Glass Optical Fibres for Efficient 1.3 μ m Amplifiers," *Pure Appl. Opt.*, vol. 4, no. 4, pp. 417-424, Jul. 1995.
- Jones W. B., *Introduction to optical fibre communication systems*, Holt Rinehart and Winston Inc., New York, 1988.
- Kaminskii A.A., *Laser Crystals*, Springer-Verlag Berlin, Heidelberg, 1981.
- Kapron F. P., Keck D. B., and Maurer R. D., "Radiation losses in glass optical waveguides," *Appl. Phys. Lett.*, vol. 17, no. 10, pp. 423-425, Nov. 1970.
- Koechner W., *Solid-State Laser Engineering*, Springer-Verlag Berlin, Heidelberg, 1992.
- Koester C. J. and Snitzer A., "Amplification in a fiber laser," *Applied Optics*, vol. 3, no. 10, pp. 1182-1186, Oct. 1964.
- Kubodera K., and Otsuka K., "Single-Transverse-Mode LiNdP₄O₁₂ Slab Waveguide Laser," *J. Appl. Phys.*, vol. 50, no. 2, pp. 653-659, Feb. 1979.

- Lai S. T., Huang S., and Yen W. M., "Temporal Variation of the Fluorescence Line Shape and Relaxation Processes in $\text{LaF}_3:\text{Pr}^{3+}$," *Phys. Rev. B.*, vol. 26, no. 5, pp. 2349-2361, Sep. 1982.
- Lee L. S., Rand S.C., and Schawlow A. L., "Cooperative Energy Transfer Among Pr^{3+} Ions in LaF_3 ," *Phys. Rev. B.*, vol. 29, no. 12, pp. 6901-6906, Jun. 1984.
- Marcerou J. F., Fevrier H. A., Ramos J., Auge J. C., and Bousselet P., "General theoretical approach describing the complete behaviour of the erbium-doped fiber amplifier," *Proc. SPIE conference on fiber laser sources and amplifiers*, San Jose, USA, Sep. 18-19, vol. 1373, pp. 168, 1990.
- Marcuse D., "Loss Analysis of Single-Mode Fiber Splices," *Bell Syst. Tech. J.*, vol. 56, pp. 703-718, May/June. 1992.
- Marcuse D., *Principles of Quantum Electronics*, Academic, New York, 1980.
- Mears R. J., Reekie L., Jauncey I. M., and Payne D. N., "Low noise erbium-doped amplifier operating at $1.54 \mu\text{m}$," *Electron. Lett.*, vol. 23, no. 19, pp. 159-160, Sep. 1987.
- Mears R. J., Reekie L., Poole S. B. and Payne D. N., "Low threshold tunable CW and q-switched fibre laser operating at $1.55 \mu\text{m}$," *Electron. Lett.*, vol. 22, no. 3, pp. 159-160, Jan. 1986.
- Miniscalco W. J., Andrews L. J., Thompson B. A., Quimby R. S., Vacha L. J. B., and Drexhage M. G., " $1.3 \mu\text{m}$ Fluoride fibre laser," *Electron. Lett.*, vol. 24, no. 1, pp. 28-29, Jan. 1988.

- Miyajima Y., Komukai T., and Sugawa T., "1.31-1.36 μm optical amplification in Nd^{3+} -doped fluorozirconate fibre," *Electron. Lett.*, vol. 26, no. 3, pp. 194-195, Feb. 1990.
- Miyajima Y., Sugawa T., and Fukasaku Y., "38.3 dB Amplification at 1.3 μm and Possibility of 0.98 μm Pumping in Pr^{3+} -Doped Fluoride Fibre," *Electron. Lett.*, vol. 27, no. 19, pp. 1706-1707, Sep. 1991.
- Morkel P. R., and Laming R. I., "Theoretical modeling of erbium-doped fiber amplifiers with excited state absorption," *Optics Lett.*, vol. 14, no. 19, pp. 1062-1064, 1989.
- Morkel P. R., Farries M. C. and Poole S. B., "Spectral variation of excited state absorption in neodymium doped fibre laser," *Optics Communications*, vol. 67, no. 5, pp. 349-352, Aug. 1988.
- Nakazawa M., Kimura Y., and Suzuki K., "High Gain Erbium Amplifier Pumped by 800 nm Band," *Electron. Lett.*, vol. 26, no. 8, pp. 548-550, Apr. 1990.
- Neumann E. G., *Single-mode fibers: fundamentals*, Springer-Verlag Berlin, Heidelberg, 1988.
- Newhouse M. A., Bartholomew R. F., Aitken B. G., Button L. J., and Borrelli N. F., "Pr-Doped Mixed-Hallide Glasses for 1300 nm Amplification," *Photon. Technol. Lett.*, vol. 6, no. 2, pp. 189-191, Feb. 1994.
- Offenberger A. A., Thompson D. C., Fedosejevs R., Harwood B., Santiago J., and Manjunath H. R., "Experimental and modeling studies of a Brillouin amplifier," *J. Quantum Electron.*, vol. 29, no. 1, pp. 207-216, Jan. 1993.
- Ohashi M., "Design Considerations for an Er^{3+} Doped Fiber Amplifier," *J. Lightwave Technol.*, vol. 9, no. 9, pp. 1099-1104, Sep. 1991.

- Ohishi Y., Kanamori T., Kitagawa T., Snitzer E., and Sigel G., "Pr³⁺-doped fluoride fibre amplifier operating at 1.31 μm ," *Tech. Dig., Optical Fiber Communications OFC-91*, San Diego, CA, Postdeadline paper PD-2.
- Ohishi Y., Mitachi S., Kanamori T., and Manabe T., "Optical Absorption of 3d Transition Metal and Rare Earth Elements in Zirconium Fluoride Glasses," *Phys. Chem. of Glasses*, vol. 24, no. 5, pp. 135-140, Oct. 1983.
- Olshansky R., "Noise figure for erbium-doped optical fibre amplifiers," *Electron. Lett.*, vol. 24, no. 22, pp. 1363, Oct. 1988.
- Othonos A., Wheeldon J., and Hubert M., "Determining erbium distribution in optical fibres using phase-sensitive confocal microscopy," *Optical Engineering*, vol. 34, no. 12, pp. 3451-3455, Dec. 1995.
- Payne D. N. and Gambling W. A., "New silica-based low-loss optical fibre," *Electron. Lett.*, vol. 10, no. 15, pp. 289-290, Jul. 1974.
- Pedersen B., Bjarklev A., Povlsen J. H., Dybdal K., and Larsen C. C., "The Design of Erbium-Doped Fiber Amplifiers," *J. Light. Technol.*, vol. 9, no. 9, pp. 1105-1112, Sep. 1991a.
- Pedersen B., Bjarklev A., Vandeltorp-Pommer H., and Povlsen J. H., "Erbium Doped Fibre Amplifier : Efficient Pumping at 807 nm," *Opt. Comm.*, vol. 81, no. 1,2, pp. 23-26, Feb. 1991b.
- Pedersen B., Dybdal K., Hansen C. D., Bjarklev A., Povlsen J. H., Vandeltorp-Pommer H., and Larsen C. C., "Detailed theoretical and experimental investigation of high-gain erbium-doped fibre amplifier," *IEEE Photonics Tech. Lett.*, vol. 2, no. 12, pp. 863, Dec. 1990.

- Percival M. R., Phillips M. W., Hanna D. C., and Tropper A. C., "Characterisation of Spontaneous and Stimulated Emission from Praseodymium (Pr^{3+}) Ions Doped into a Silica-Based Monomode Optical Fibre," *J. Quant. Electron.*, vol. 25, no. 10, pp. 2119-2123, Oct. 1989.
- Peroni M., and Tamburrini M., "Gain in erbium-doped fiber amplifiers: a simple analytical solution for the rate equations," *Optics Lett.*, vol. 15, no. 15, pp. 842, Aug. 1990.
- Petreski B.P., Farrell P.M. and Collins S.F., "Cross-relaxation in praseodymium-doped fluorozirconate glass," *Optics Communications*, vol. 132, no. 1,2, pp. 39-43, Nov. 1996.
- Poole S.B., Townsend J.E., Payne D.N., Fermann M.E., Cowle G.J., Laming R.I., and Morkel P.R., "Characterisation of special fibers and fiber devices," *J. Lightwave Tech.*, vol. 7, no. 8, pp. 1242-1255, Aug. 1989.
- Quimby R. S. and Zheng B., "New excited-state absorption measurement technique and application to Pr^{3+} doped fluorozirconate glass," *Appl. Phys. Lett.*, vol. 60, no. 9, pp. 1055-7, Mar. 1992.
- Remillieux A., Jacquier B., Linares C., Lesegent C., Artigaud S., Bayard D., Hamon L., and Beylat J. L., "Upconversion mechanisms of a praseodymium-doped fluoride fibre amplifier," *J. Phys. D: Appl. Phys.*, vol. 29, no. 4, pp. 963-974, Apr. 1996.
- Saleh A. A. M., Jopson R. M., Evankow J. and D., Aspell J., "Modeling of gain in erbium-doped fiber amplifiers," *IEEE Photonics Tech. Lett.*, vol. 2, no. 10, pp. 714, Oct. 1990.

Sanghera J.S. and Aggarwal I.D., in Rare earth doped fibre lasers and amplifiers,
Chap. 10, pp. 474, Table 8, 1991.

Shimizu M., Yamada M., Horiguchi M., Takeshita T., and Oyasu M., "Erbium doped
fibre amplifiers with an extremely high gain coefficient of 11.0 dB/mW,"
Electron. Lett., vol. 26, no. 20, pp. 1641, Sep. 1990.

Smart R. G., Hanna D. C., Tropper A. C., Davey S. T., Carter S. F., and Szebesta D.,
"CW Room Temperature Upconversion Lasing at Blue, Green and Red
Wavelengths in Infrared-Pumped Pr³⁺-Doped Fluoride Fibre," *Electron. Lett.*,
vol. 27, no. 14, pp. 1307-1309, Jul. 1991.

Smart R., Carter J., Tropper A., and Hanna D., "Fluoride Fiber Lasers," *In Proc. SPIE
: Fiber Laser Sources and Amplifiers II*, vol. 1373, San Jose, USA, Sep. 18-19,
pp. 158-165, 1991.

Snitzer E., "Optical maser action of Nd³⁺ in barium crown glass," *Phys. Rev. Lett.*,
vol. 7, no. 12, pp. 444-446, Dec. 1961.

Snyder A. W. and Love J. D., *Optical waveguide theory*, Chapman and Hall, New York,
1983.

Stolen R. H. and Ippen E. P., "Raman gain in glass optical waveguides," *Appl. Phys.
Lett.*, vol. 22, no. 6, pp. 276-278, Mar. 1973.

Sugawa T., and Miyajima Y., "Gain and output-saturation limit evaluation in Pr³⁺-doped
fluoride fibre amplifier operating in the 1.3 μm band," *IEEE Photonics Tech.
Lett.*, vol. 3, no. 7, pp. 616-618, Jul. 1991.

- Suzuki K., Kimura Y., and Nakazawa M., "High gain Er³⁺-doped fibre amplifier pumped by 820 nm GaAlAs laser diodes," *Electron. Lett.*, vol. 26, no. 13, pp. 948, Jun. 1990.
- Trautman J. K., Betzig E., Welner J. S., DiGiovanni D. J., Harris T. D., Hellman F., and Gyorgy E. M., "Image contrast in near-field optics," *J. Appl. Phys.*, vol. 71, no. 10, pp. 4659-4663, May 1992.
- Tropper A. C., Carter J. N., Lauder R. D. T., and Hanna D. C., "Analysis of Blue and Red Laser Performance of the Infrared-Pumped Praseodymium-Doped Fluoride Fiber Laser," *J. Opt. Soc. Am. B.*, vol. 11, no. 5, pp. 886-893, May 1994.
- Urquhart P., "Review of rare-earth-doped fibre lasers and amplifiers," *IEE Proc. Pt. J.*, vol. 135, no. 6, pp. 385-407, Dec. 1988.
- Uttamchandani D., Othonos A., Alvie A. T., and Hubert M., "Determination of erbium distribution in optical fibers using confocal optical microscopy," *IEEE Photonics Tech. Lett.*, vol. 6, no. 3, pp. 437-439, Mar. 1994.
- Whitley T. J., "Laser Diode Pumped Operation of Er³⁺-Doped Fibre Amplifier," *Electron. Lett.*, vol. 24, no. 25, pp. 1537-1539, Dec. 1988.
- Whitley T. J., and Wyatt R., "Alternative Gaussian Spot Size Polynomial for Use with Doped Fiber Amplifiers," *Photon. Tech. Lett.*, vol. 5, no. 11, Nov. 1993.
- Whitley T. J., and Wyatt R., "Analytic Expression for Gain in an idealised 4-Level Doped Fibre Amplifier," *Proc. OSA Topical Meeting on Opt. Amps. Appl.*, Santa Fe, NM, paper WB2, 1992.

Yasuhiro A., "Properties of fiber Raman amplifiers and their applicability to digital optical communication systems," *J. Lightwave Tech.*, vol. 6, no. 7, pp. 1225-1239, Jul. 1988.

Zhao Y., and Poole S., "Efficient Blue Pr³⁺-Doped Fluoride Fibre Upconversion Laser," *Electron. Lett.*, vol. 30, no. 12, pp. 967-968, Jun. 1994.

Zhao Y., Fleming S., and Poole S., "22 mW Blue Output Power From a Pr³⁺ Fluoride Fibre Upconversion Laser," *Opt. Comm.*, vol. 114, pp. 285-288, Oct. 1994.

Appendices

- A.1 List of figure
- A.2 List of tables
- A.3 List of symbols

A.1 List of Figures

	Page
1.1.2.1 Power amplifier	1-4
1.1.2.2 In-line amplifier	1-5
1.1.2.3 Pre-amplifier	1-5
1.1.3.1 Typical optical fibre amplifier arrangement	1-9
2.2.1 An idealised four-level atomic model	2-5
2.2.2 An idealised three-level atomic model	2-7
2.3.1 An optical fibre	2-11
2.3.2 Schematic of an optical fibre amplifier	2-12
3.2.1 Periodic table indicating lanthanide series	3-6
3.2.2 Partial energy level diagrams for praseodymium, neodymium and erbium	3-7
3.3.1 Simplified energy level diagram of praseodymium	3-7
3.3.2 Experimental arrangement for attenuation measurements	3-10
3.3.3 The attenuation spectrum of praseodymium-doped fluorozirconate glass	3-13
3.3.4 The attenuation spectrum of praseodymium in a fluorozirconate glass measured for 500 ppm, 1000 ppm, 2000 ppm and 4000 ppm samples between 400 nm and 500 nm.	3-14
3.4.1 Experimental arrangement for measuring the emission spectrum	3-16

3.4.2	Emission spectrum of praseodymium in a fluorozirconate glass host	3-17
3.4.3	Simplified energy level diagram for praseodymium indicating radiative transitions relevant to the peaks shown in the emission spectrum	3-18
3.4.4	Fluorescence spectrum of transitions arising from the 3P_0 and 3P_1 states at 20°C and 145°C	3-20
3.4.5	Fluorescence spectrum of transitions arising from the 3P_0 and 3P_1 states at 20°C and 145°C	3-21
3.4.6	The $^3P_0 \rightarrow ^3F_2$ radiative transition	3-22
3.4.7	Fluorescence intensity of the $^3P_0 \rightarrow ^3F_2$ (635 nm) radiative transition as a function of pump intensity using 476.5 nm and 465.8 nm pump wavelengths	3-23
3.5.1	Non-radiative decay rates as a function of energy separation for fluorozirconate and silica glass hosts and for LaF ₃ crystal host.	3-28
3.6.1.1	Simplified energy level diagram for praseodymium indicating the levels and transitions for lifetime measurements.	3-29
3.6.2.1	Diagram of a blade cutting across a Gaussian spot.	3-33
3.6.2.2	Simulated plot of the relative population of the metastable level due to pump modulation as a function of time.	3-34
3.6.3.1	Experimental arrangement for lifetime measurements.	3-35
3.6.3.2	Fluorescence decay curves for 500 ppm, 1000 ppm, 2000 ppm,	3-37

	4000 ppm and 10000 ppm praseodymium doped samples	
3.6.3.3	Decay rate as a function of some time interval after pump turn-off.	3-38
3.6.3.5	Measured decay constants as a function of praseodymium concentration.	3-40
3.7.1	Calculated emission cross-section, using Fuchtbauer-Ladenburg analysis for the ${}^3P_0 \rightarrow {}^3F_2$ transition.	3-43
3.7.2	Calculated absorption cross-section, using Fuchtbauer-Ladenburg analysis for the ${}^3H_4 \rightarrow {}^3P_0$ transition.	3-45
3.8.1.1	An example of cross-relaxation.	3-47
3.8.1.2	An example of energy transfer.	3-48
3.8.2.1	Partial energy level diagram for praseodymium in a fluorozirconate glass host and the possible cross relaxation channels.	3-50
3.8.2.2	Cooperative energy transfer process for praseodymium in a fluorozirconate glass host.	3-51
3.8.3.1	Flow diagram showing the apparent circularity of the calculation of absorption cross-section, the concentration and determination of the lifetime in the limit of zero concentration.	3-57
3.8.4.1	Gain as a function of concentration calculated using Equation 3.8.4.3.	3-59
4.2.1.1	The first three modes propagating inside the core and in the cladding at 632.8 nm.	4-6

4.2.2.1	Experimental arrangement used to measure the mode profile of 632.8 nm light propagating through the praseodymium fibre.	4-8
4.2.2.2	Images of some typical mode profiles.	4-9
4.2.3.1	Comparison of the Bessel function solution for the LP ₀₁ mode with the Gaussian approximation.	4-12
4.2.3.2	Measurement of single-mode propagating in the amplifier.	4-13
4.3.1.1	The ratio of the population probability density, with and without cross-relaxation, as a function of pump rate and concentration.	4-17
4.3.2.1	Confocal system for concentration profile measurements.	4-20
4.3.2.2	Praseodymium concentration profile image.	4-21
4.3.2.3	Praseodymium fluorescence image.	4-21
4.3.2.4	Three dimensional fluorescence image.	4-22
5.2.1	Experimental arrangement used to measure the small signal gain.	5-5
5.2.2	Splitting characteristics of four-port coupler.	5-6
5.3.1	Gross gain as a function of injected pump power for Type A fibre.	5-11
5.3.2	Gross gain as a function of injected probe power.	5-12
5.3.3	Gross gain as a function of injected pump power for 260 mm, 210 mm, 162 mm and 115 mm fibre lengths.	5-14
5.3.4	Gross gain as a function of fibre length for fixed pump powers of 10 mW, 20 mW, 40 mW and 80 mW.	5-15

5.3.5	Gross gain as a function of injected pump power.	5-17
5.4.1	Simplified energy level diagram of praseodymium indicating transitions central to the amplification process.	5-20
5.4.2	Comparison of the measured gain with the calculated gain	5-25
6.2.1	Up-conversion pumping scheme	6-10
6.2.2	Co-doped pumping scheme	6-11

A.2 List of Tables

3.3.1	Dimensions of the praseodymium-doped samples	3-12
3.3.2	Attenuation coefficient at 476.5 nm for all five samples.	3-15
3.4.1	Radiative transitions arising from the 3P_0 and 3P_1 states to lower lying levels.	3-19
3.4.2	Branching ratios for a ZBLA glass host, an InF_3 crystal host and for a ZBLAN host.	3-25
3.5.1	Material parameters for a fluorozirconate and silica glass and LaF_3 crystal.	3-27
3.6.3.1	Summary of the measured decay rate of the 3P_0 state with varying praseodymium concentration.	3-39
3.7.1	Values for the parameters in Equation 3.7.1 used to calculate the emission cross-section.	3-42

3.7.2	Values for the parameters in Equation 3.7.1 used to calculate the absorption cross-section.	3-44
4.2.1.1	Summary of praseodymium-doped fibre parameters as given by the manufacturer.	4-4
4.2.1.2	Cutoff conditions and designation of the first six LP modes in a step-index fibre.	4-5
5.2.1	Selected wavelengths and relative powers of argon-ion laser.	5-7
5.4.1	Summary of the parameters relevant to the gain	5-24

A.3 List of Symbols

Symbol

σ_s^a	Absorption cross-section at the signal wavelength
σ_s^e	Emission cross-section at the signal wavelength
σ_p^a	Absorption cross-section at the pump wavelength
σ_p^e	Emission cross-section at the pump wavelength
g_{coeff}^{low}	Small signal gain coefficient in the low pump power regime
g_{coeff}^{high}	Small signal gain coefficient in the high pump power regime
$\psi_c(r, \phi)$	Dopant ion intensity distribution function
$\omega^{Desuvire}$	Desurvire definition for the spot size
$\omega^{Marcuse}$	Marcuse definition for the spot size
ν_p	Pump frequency
ω_p	Pump spot-size

ω_p	Concentration spot-size
$\psi_p(r, \phi)$	Intensity distribution function for the pump
ν_s	Signal frequency
ω_s	Signal spot-size
$\psi_s(r, \phi)$	Intensity distribution function for the signal
α	absorption coefficient
a	core radius
A	area
A_{ij}	Spontaneous radiative transition rate from an initial level i to a final level j
α_p	absorption coefficient at the pump wavelength
α_s	absorption coefficient at the signal wavelength
Δn	Refractive index difference
G	Gain factor
Γ_c	Overlap between the concentration and the fibre core
g_{coeff}	Small signal gain coefficient
Γ_p	Overlap between the pump beam and the fibre core
Γ_{psc}	Three way overlap between the pump and signal beams and the fibre core
Γ_s	Overlap between the signal beam and the fibre core
h	Planck's constant
I_p	Pump intensity
I_s	Signal intensity

L	length
λ_c	Cut-off wavelength
λ_p	Pump wavelength
λ_s	Signal wavelength
n	refractive index
n_0	refractive index of air
n_1, n_{core}	refractive index of core
$n_2, n_{cladding}$	refractive index of cladding
NA	Numerical aperture
N_i	Population density of level $i=0,1,2,\dots,i$
P_{abs}	Absorbed pump power
P_{in}	Pump power in
P_{out}	Pump power out
$P_{out}(Pumped)$	Pump power out measured with the pump present
$P_{out}(Umpumped)$	Pump power out measured without pumping
P_p	Pump power
P_s	Signal power
ρ	concentration
R_{ij}	Pump rate from an initial level i to some higher energy state j
τ	Lifetime
$\tau(\rho \rightarrow 0)$	Lifetime in the limit of zero concentration
t	time
τ_i	Lifetime of level $i=0,1,2,\dots,i$

τ_{ij}	Lifetime of transition from an initial level i to some final level j
$V_{p,s}$	Normalised frequency at the pump p , or signal s
W_{ij}	Stimulated emission rate from an initial level i to some lower energy j

Publications

- P.1 Journal articles
- P.2 International conference publications
- P.3 National conference publications
- P.4 Other publications

P.1 JOURNAL ARTICLES (ATTACHED)

Amplification in Pr³⁺-Doped Fluorozirconate Optical Fibre at 632.8 nm

Petreski B. P., Schilders S. P., Farrell P. M., Gu M.,

Electronics Letters, vol. 33, no. 10, pp. 889-891, May 1997.

ABSTRACT

Measurements are analysed of the concentration dependent relaxation rate of the ³P₀ state of praseodymium, spatially resolved by confocal microscopy, to give an absolute measure of the concentration profile in praseodymium-doped fluoro-zirconate optical fibre

Cross-Relaxation in Praseodymium-Doped Fluorozirconate Glass

Petreski B. P., Farrell P. M., and Collins S. F.,

Optics Communications, vol. 132, no. 1/2, pp. 39-43, Nov. 1996.

ABSTRACT

The lifetime of the ³P₀ state in praseodymium-doped fluoro-zirconate in bulk glass was measured for varying dopant concentrations. From these measurements and a rate equation analysis of the dynamics, values for a cross-relaxation parameter ($\alpha_{cr1}=7.1\pm 0.7\times 10^{-23}$ m³/s) and the lifetime in the limit of zero concentration of praseodymium (50 ± 1 μ s) are obtained. These parameters are essential for the understanding and modelling of optical processes which involve the ³P₀ state.

Amplification in Pr³⁺-Doped Fluorozirconate Optical Fibre at 632.8 nm

Petreski B. P., Murphy M. M., Collins S. F., and Booth D. J.,

Electronics Letters, vol. 29, no. 16, pp. 1421-1423, Aug. 1993.

ABSTRACT

Amplification in Pr³⁺-doped fluorozirconate optical fibre is reported at the 632.8 nm He-Ne wavelength. Gross gains up to 11 dB have been achieved in a 1.4 m length using a launched pump power of 315 mW at 476.5 nm. Measurements of extinction at the pump and signal wavelengths indicate that significantly improved performance can be expected using a much shorter length of fibre.

P.2 INTERNATIONAL CONFERENCE PUBLICATIONS

Determination Of The Concentration Profile Of Praseodymium Doped Optical Fibre By Confocal Microscopy

Petreski B. P., Schilders S. P., Farrell P. M., Gu M.,

International Quantum Electronics Conference, IQEC'96, Sydney, NSW, Australia,

14-19 July 1996.

ABSTRACT

Measurements of the concentration dependent relaxation rate of the 3P_0 state of praseodymium, spatially resolved by confocal microscopy, are analysed to give an absolute measure of the concentration profile in praseodymium doped fluorozirconate optical fibre.

An optical amplifier for the 632.8 nm He-Ne Wavelength

Petreski B. P., Farrell P. M., Murphy M. M., and Collins S. F.,

Proc. SPIE annual meeting, In-Situ Optical Sensors, Doped Fibre Devices, Denver,

CL, USA, 4-9 Aug. 1996, paper 2841-16.

ABSTRACT

Optical amplification at the 632.8 nm He-Ne wavelength has been investigated in praseodymium-doped fluorozirconate fibre. A slope efficiency of 0.15 dB/mW was realised with up-to 14 dB gain reported which is a significant improvement on previously reported results. A rate equation approach is used to model and understand the gain dynamics. The lifetime of the 3P_0 state was measured to be

46.5±0.9 μs. Using Fuchtbauer-Ladenburg analysis, the absorption cross-section at the pump wavelength (476.5 nm) and the emission cross-section at the signal wavelength (632.8 nm) were calculated to be 0.39±0.03 pm² and 1.65±0.15 pm² respectively. These parameters were used in a four-level amplifier model for comparison with our experimental measurements.

Optical Fibre Amplifier at the 632.8 nm He-Ne Wavelength for Sensor

Networks

Petreski B. P., Farrell P. M., Baxter G. W., and Collins S. F.,

*Proc. Optical Fibre Sensors OFS-11, Sapporo, Japan, May 21-24 1996, pp. 510-513,
paper Th3-23.*

ABSTRACT

Optical amplification at the 632.8 nm He-Ne wavelength has been investigated in praseodymium-doped fluorozirconate fibre. A maximum net gain of 13 dB was realised.

P.3 NATIONAL CONFERENCE PUBLICATIONS

Imaging Concentration Profiles Of Rare Earth Doped Optical Fibres

Petreski B. P., Schilders S. P., Farrell P. M. and Gu M.

Proc. Australian Conference On Optical Fibre Technology ACOFT-21, Broadbeach, Queensland, Australia, Dec. 1-4 1996.

ABSTRACT

Measurements of the concentration dependent relaxation rate of the 3P_0 state of praseodymium, spatially resolved by confocal microscopy, are analysed to give an absolute measure of the concentration profile in praseodymium doped fluorozirconate optical fibre. Techniques are described to image erbium concentrations in silica and fluorozirconate hosts.

Cross-Relaxation In Praseodymium-Doped ZBLANP

Petreski B. P., Farrell P. M., and Collins S. F.,

Proc. Australian Conference On Optical Fibre Technology ACOFT-20, Coolum Beach, Queensland, Australia, Dec. 3-6 1995, pp. 212-215.

ABSTRACT

The lifetime of the 3P_0 state in praseodymium-doped fluorozirconate in bulk glass was measured for varying dopant concentrations. We also investigated the $^3P_0 \rightarrow ^1G_4$ and $^3H_4 \rightarrow ^1G_4$ cross-relaxation process which reduces the fluorescence lifetime of the 3P_0 state with increasing dopant concentration. A rate equation model and lifetime data enabled quantification of the cross-relaxation parameter.

Fibre Amplifiers At The 632.8 nm And 543.5 nm He-Ne Wavelengths

Petreski B. P., Murphy M. M., Clarke K., and Collins S. F.,

Proc. Australian Conference On Optical Fibre Technology ACOFT-18, Wollongong, NSW, Australia, Dec. 1-4 1993, pp. 113-116.

ABSTRACT

Net amplification for two He-Ne wavelengths is reported in Pr³⁺- and Er³⁺-doped ZBLAN optical fibres. Envisaged applications of these amplifiers would be in optical systems, using these wavelengths, which employ multiplexed sensors.

P.4 OTHER PUBLICATIONS

Blue Led-Pumped Point Temperature Sensor Based On A Fluorescence

Intensity Ratio In Pr³⁺:ZBLAN Glass

Maurice E., Monnom G., Baxter G. W., Wade S. A., Petreski B. P., and Collins S.

F., Proc. Optical Fibre Sensors OFS-11, Sapporo, Japan,

May 21-24 1996, pp. 188-191, paper We3-4.

Temperature Sensing Using The Thermalisation Of The ³P₀ And ³P₁ Levels Of

Praseodymium

Wade S. A., Maurice E., Petreski B. P., Collins S. F., and Baxter G. W.,

Proc. Australian Conference On Optical Fibre Technology ACOFT-20, Coolum

Beach, Queensland, Australia, Dec. 3-6 1995, pp. 331-334.

Imaging concentration profiles of praseodymium-doped optical fibres

B.P. Petreski, S.P. Schilders, P.M. Farrell and M. Gu

Indexing terms: Optical fibres, Rare-earth doped fibres

Measurements are analysed of the concentration dependent relaxation rate of the 3P_0 state of praseodymium, spatially resolved by confocal microscopy, to give an absolute measure of the concentration profile in praseodymium-doped fluorozirconate optical fibre.

Introduction: A detailed understanding of rare-earth-doped optical fibre lasers and amplifiers requires a knowledge of the absolute concentration and dopant ion distribution in the fibre core [1]. Previous attempts to determine the concentration profile optically have assumed that the fluorescence intensity is proportional to the local dopant concentration [2 - 4]. However, for high concentrations, this assumption may be mistaken, since concentration-dependent co-operative processes can alter relaxation processes in the dopants and hence alter the fluorescence intensity. In this Letter, measurements of the concentration dependent relaxation rate of the 3P_0 state of praseodymium, spatially resolved by confocal microscopy, are analysed to obtain the absolute concentration profile.

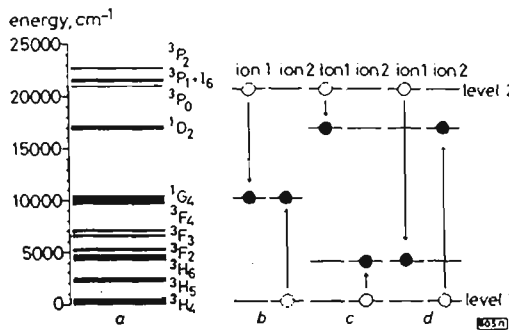


Fig. 1 Partial energy level diagram for praseodymium in fluorozirconate glass host with cross-relaxation processes
 a: Partial energy level diagram
 b, c and d: Cross-relaxation processes

Cross-relaxation in praseodymium: The partial energy level diagram of praseodymium, Fig. 1a, shows three main channels for cross-relaxation of the 3P_0 state. One possible path, Fig. 1b, has a donor ion in an excited state (3P_0) de-exciting to 1G_4 by transferring its energy to a ground state ion, with the acceptor ion being raised to 1G_4 . Another channel, Fig. 1c, has a donor ion in the 3P_0 state de-exciting to 1D_2 , while transferring its energy to another ground state, which is thus raised to the 3H_4 state. The third process, Fig. 1d, involves the 3P_0 state relaxing to 3H_4 and transferring energy to a ground state ion which is raised to 1D_2 ; this is possible since the energy differences between the appropriate transitions are nearly equal.

In Fig. 1a, the ground state (3H_4) multiplet is labelled level 1 and the metastable state (3P_0) is level 2. Using this scheme, the rate equation for the 3P_0 state with cross-relaxation included is given by [5]

$$\frac{dn_2}{dt} = R_{12}n_1 - \frac{n_2}{\tau_2} - \frac{1}{2}\alpha_{cr}\rho n_1 n_2 \quad (1)$$

where n_1 and n_2 are the normalised population probability densities of the ground state (3H_4) and the 3P_0 state, respectively; ρ is the concentration, R_{12} is the pump rate, τ_2 is the lifetime of the 3P_0 state and α_{cr} is a cross-relaxation parameter incorporating all three cross-relaxation processes. Since the decay rates of the intermediate states are relatively fast, a significant accumulation of population is unlikely, so it can be assumed that $n_1 + n_2 = 1$. An analytic solution to the lowest order in ρ of eqn. 1 for steady-state conditions for n_2 , is given by

$$n_2 = \frac{R_{12}}{R_{12} + A_2} \left(1 - \frac{\alpha_{cr} A_2}{2(R_{12} + A_2)^2 \rho} \right) \quad (2)$$

where $A_2 = 1/\tau_2$. This equation clearly indicates that the population probability density of the 3P_0 state decreases as a function of increasing concentration. Thus, the assumption that the fluorescence is linearly related to the concentration is often unwarranted, particularly for high concentrations. Consequently, fluorescence intensity is not a reliable method for determining the relative concentration profile of a doped optical fibre, nor is it a means for measuring the absolute concentration.

However, praseodymium offers a particularly simple means of overcoming this problem of obtaining an absolute measure of concentration and dopant profile, since it has been shown that the

relaxation rate of the 3P_0 state varies linearly with concentration according to [5]

$$\Gamma = \frac{1}{\tau_2} + \frac{1}{2}\alpha_{cr}\rho \quad (3)$$

where Γ is the measured relaxation rate, τ_2 is the lifetime of the 3P_0 state in the limit of zero dopant concentration, and ρ is the praseodymium concentration. This relation was determined by calibrating the fluorescence lifetime of the 3P_0 state as a function of concentration. The values of τ_2 and α_{cr} , in eqn. 3 are $50 \pm 1 \mu s$ and $(7.1 \pm 0.7) \times 10^{-23} m^3/s$, respectively, for the glass composition considered here [5]. Clearly, measurement of a spatially resolved relaxation rate directly gives an absolute measure of the local dopant concentration.

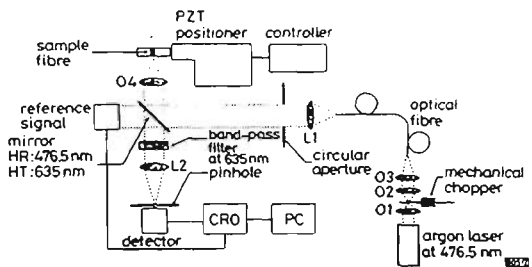


Fig. 2 Schematic of confocal microscope and lifetime measuring apparatus

Imaging of concentration profile: The confocal microscope used to measure the intensity and time resolved fluorescence is shown schematically in Fig. 2. Light from an argon-ion laser at 476.5 nm was launched into an optical fibre of 4 μm diameter using a microscope objective (O3). Prior to this, the beam was modulated using a mechanical chopper at the focal points of O1 and O2. The laser beam was focused to a spot and then, after the second objective, re-established at close to the original beam diameter. By placing the mechanical chopper at the focal point, the effect of the system response was minimised. The response time of the detection circuitry was in the order of 10 ns and was considered to not significantly affect the measurement. A lens (L1) collimated light from the output end of the fibre and the beam size was adjusted by a circular aperture. The pump light was reflected using a mirror which had a high reflectance at 476.5 nm and high transmission at 635 nm. The pump light was focused onto the fibre sample using objective O4. Fluorescence from the fibre was also collected by O4 and transmitted back through the mirror. A 635 nm band-pass filter ensured that no pump light entered the detector. The lens (L2) was used to focus the red light through a pinhole and onto a silicon detector. The time resolved fluorescence intensity was

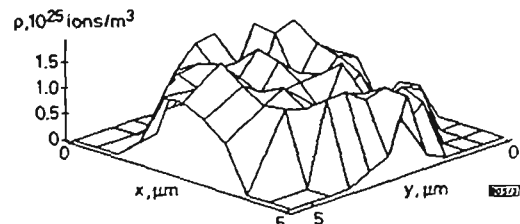


Fig. 3 Image of praseodymium concentration in fluorozirconate fibre core

recorded, at many different positions on the fibre core, on an oscilloscope (CRO) and the decay curves were stored on a PC for further processing.

The lifetime data were related to the local concentration using eqn. 3. The concentration profile of the fibre core thus obtained is shown in Fig. 3. The image for this particular fibre is reasonably consistent with a constant praseodymium concentration over the fibre core.

Conclusion: We have demonstrated that high resolution images of the absolute concentration profile of rare-earth-doped optical fibres can be obtained by taking advantage of concentration

dependent relaxation processes in the material. This novel technique has the advantage that no optical calibration is required and it may be readily extended to rare-earth-doped waveguide devices.

© IEE 1997

1 April 1997

Electronics Letters Online No: 19970579

B.P. Petreski, S.P. Schilders, P.M. Farrell and M. Gu (*Optical Technology Research Laboratory, Department of Applied Physics, Victoria University, PO Box 14428 MCMC, Melbourne 8001, Australia*)

E-mail: petbp@cougar.vut.edu.au

References

- 1 ANKIEWICZ, A., and RÜHL, F.F.: 'Effect of dopant distribution on optimisation of Pr-doped fibres', *Opt. Quantum Electron.*, 1993, 26, pp. 987-993
- 2 UTTAMCHANDANI, D., OTHONOS, A., ALVIE, A.T., and HUBERT, M.: 'Determination of erbium distribution in optical fibres using confocal optical microscopy', *IEEE Photonics Technol. Lett.*, 1994, 6, pp. 437-439
- 3 OTHONOS, A., WHEELDON, J., and HUBERT, M.: 'Determining erbium distribution in optical fibres using phase-sensitive confocal microscopy', *Opt. Eng.*, 1995, 34, pp. 3451-3455
- 4 TRAUTMAN, J.K., BETZIG, E., WELNER, J.S., DIGIOVANNI, D.J., HARRIS, T.D., HELLMAN, F., and GYORGY, E.M.: 'Image contrast in near-field optics', *J. Appl. Phys.*, 1992, 71, pp. 4659-4663
- 5 PETRESKI, B.P., FARRELL, P.M., and COLLINS, S.F.: 'Cross-relaxation in praseodymium-doped fluorozirconate glass', *Opt. Commun.*, 1996, 132, pp. 39-43
- 6 PETRESKI, B.P., SCHILDERS, S.P., FARRELL, P.M., and GU, M.: 'Imaging concentration profiles of rare earth doped optical fibres'. ACOFT'96, 1996, pp. 113-116

Cross-relaxation in praseodymium-doped fluorozirconate glass

Bill P. Petreski, Peter M. Farrell, Stephen F. Collins

*Optical Technology Research Laboratory, Department of Applied Physics, Victoria University of Technology,
P.O. Box 14428, MCMC, Melbourne, VIC 8001, Australia*

Received 16 January 1996; accepted 28 March 1996

Abstract

The lifetime of the 3P_0 state in praseodymium-doped fluorozirconate in bulk glass was measured for varying dopant concentrations. From these measurements and a rate equation analysis of the dynamics, values for a cross-relaxation parameter ($\alpha_{cr1} = (7.1 \pm 0.7) \times 10^{-23} \text{ m}^3/\text{s}$) and the lifetime in the limit of zero concentration of praseodymium ($(50 \pm 1) \mu\text{s}$) are obtained. These parameters are essential for the understanding and modelling of optical processes which involve the 3P_0 state.

1. Introduction

Praseodymium-doped fluorozirconate glass has potential for use in fibre amplifiers, fibre lasers and bulk glass lasers operating at visible wavelengths [1,2]. Recent interest in blue lasers for optical data storage purposes has led to further investigation of transitions originating from the 3P_0 state of praseodymium [3–5].

It is well known that the quantum efficiency of a lasing transition and the fluorescence lifetime of some levels decreases as the concentration of praseodymium increases [6]. Reported here are measurements of the lifetime of the praseodymium 3P_0 state as a function of concentration. From these measurements and a rate equation analysis of the dynamics, values for a cross-relaxation parameter ($\alpha_{cr1} = (7.1 \pm 0.7) \times 10^{-23} \text{ m}^3/\text{s}$) and the lifetime in the limit of zero concentration ($(50 \pm 1) \mu\text{s}$) are obtained. These parameters are essential for the un-

derstanding and modelling of optical processes which involve the 3P_0 state.

2. Energy transfer processes and rate equation model for the 3P_0 state

An ion in any level may decay at a rate determined by the sum of the radiative, non-radiative and energy transfer rates. The radiative and non-radiative relaxation rates are measures of the photon and phonon emission rates respectively, neither of which are concentration dependent. Energy transfer is a cooperative effect where one ion will change state by donating energy to a nearby acceptor ion at a rate which will depend on the separation of the interacting ions, and thus the process is concentration dependent. Two examples of energy transfer which are important at relatively low dopant concentrations are cross-relaxation and cooperative up-conversion.

According to the theory of Förster [7] and Dexter [8], the transition probability for an electric dipole process in which a donor ion transfers energy to an acceptor is proportional to the overlap integral between the emission band corresponding to the donor transitions and the absorption band of the acceptor ion and may be written in terms of the product of the fluorescence line-shape or emission cross-section of the donor transition and the absorption line-shape or the absorption cross-section of the acceptor.

A partial energy level diagram of praseodymium is shown in Fig. 1(a). There are two main channels for cross-relaxation of the 3P_0 state [9]. One possible path for cross-relaxation is depicted in Fig. 1(b) and is assigned the parameter α_{cr1} . In this case a donor ion in an excited state (3P_0) may de-excite to 1G_4 by transferring its energy to an ion in the ground state. The acceptor ion is subsequently raised to 1G_4 . Another channel for cross-relaxation, assigned the parameter α_{cr2} , is shown in Fig. 1(c). For this energy transfer process, a donor ion in the 3P_0 state may de-excite to 1D_2 by transferring its energy to another ion in the ground state. The ground state acceptor ion is thus raised into the 3H_6 state. Cross-relaxation is possible since the energy difference between the 3P_0 – 1D_2 and 3H_4 – 3H_6 transitions, and between the 3P_0 – 1G_4 and 3H_4 – 1G_4 transitions, are nearly equal.

Another mechanism which has been observed and which may also deplete the 3P_0 state is an up-conversion process attributed to a cooperative energy transfer from a pair of praseodymium ions in the 3P_0 state to a nearby ion in the same state [10]. The energy transfer process is a three-ion interaction in which the two donor ions and the participating acceptor ion are all praseodymium in the same excited state (3P_0). Through this interaction process the two donor ions can de-excite to the 1G_4 and 3F_2 states while releasing sufficient energy to up-convert the acceptor ion to the 1S_0 state at about 47000 cm^{-1} . The cross-relaxation and the cooperative up-conversion processes are described by the following rate equation for the 3P_0 state:

$$\frac{dN_6}{dt} = R_{16}(N_1 - N_6) - \frac{N_6}{\tau_6} - \frac{1}{2}\alpha_{cr1}N_1N_6 - \frac{1}{2}\alpha_{cr2}N_1N_6 - \frac{1}{3}\beta_{et}N_6^3, \quad (1)$$

where N_i is the population density of state i as labelled in Fig. 1, τ_6 is the lifetime of state 6 in the limit of zero concentration, the first term describes the pumping while the second term is the spontaneous decay of the 3P_0 state, the third and fourth terms are the cross-relaxation rates and the last term is the energy transfer rate characterised by the pa-

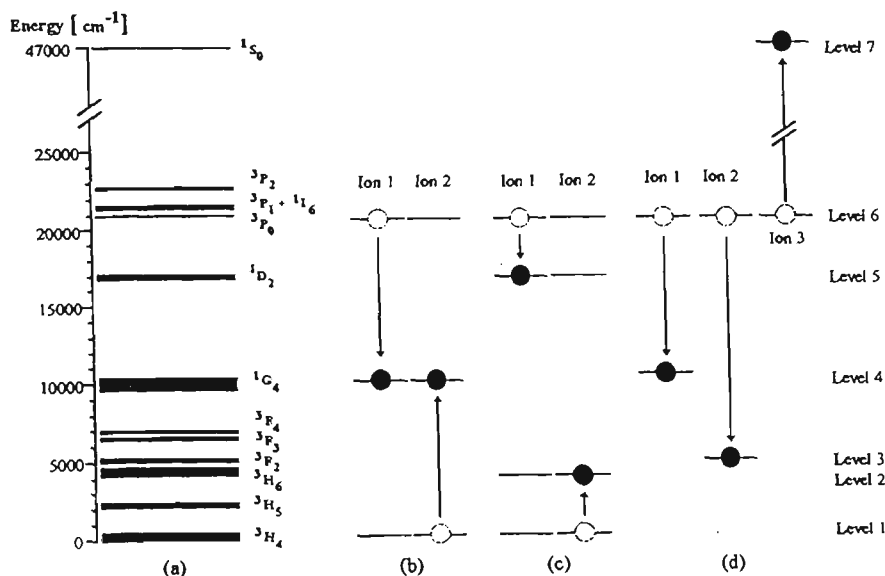


Fig. 1. (a) Partial energy level diagram for praseodymium in a fluorozirconate glass host, (b) and (c) cross-relaxation processes, (d) cooperative up-conversion.

parameter β_{et} . For simplicity, it is assumed that the pump absorption and emission cross-sections are equal and all other intermediate levels decay quickly back to the ground level.

To make the concentration dependence explicit in the rate equation, we can normalise the population densities of the levels by writing $N_i = \rho n_i$, where ρ is the concentration of the dopant ions (ion/m³) and n_i is the normalised population density of level i . The consequent decay of the 3P_0 state in the absence of pumping is then given by

$$\frac{dn_6}{dt} = -\frac{n_6}{\tau_6} - \frac{1}{2}(\alpha_{cr1} + \alpha_{cr2})\rho n_1 n_6 - \frac{1}{3}\beta_{et}\rho^2 n_6^3. \quad (2)$$

In the experiments described here, relatively low powers of the exciting laser were used so that the fraction of ions in the 3P_0 state was always small. Under these conditions the final term in Eq. (2) may be neglected since it depends on the cube of a small quantity and thus Eq. (2) simplifies to

$$\frac{dn_6}{dt} = -\frac{n_6}{\tau_6} - \frac{1}{2}(\alpha_{cr1} + \alpha_{cr2})\rho n_1 n_6. \quad (3)$$

3. Experimental arrangement, results and discussion

The decay of fluorescence intensity was observed using the experimental arrangement shown in Fig. 2. An argon ion laser emitting at 476.5 nm, modulated by a mechanical chopper, was used to excite ground state ions into the 3P_0 state of praseodymium. The fluorescence intensity decay was monitored with a PIN photodiode coupled to a Tektronix TDS-320 oscilloscope. A 635 nm band pass filter was used to

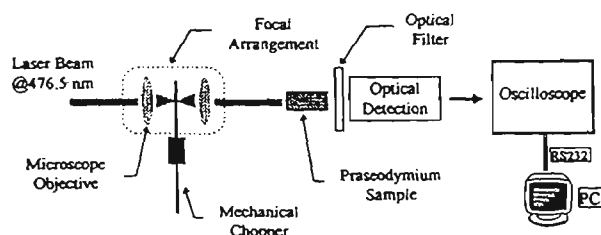


Fig. 2. Experimental arrangement.

block pump light from entering the detector. The samples used in all experiments were 40 mm in length and 8 mm in diameter. The data was stored on a personal computer for further processing.

When a mechanical chopper is used to modulate a laser beam (having a Gaussian intensity distribution) the rise and fall time of the modulation should be ideally very much faster than the fluorescence lifetime. However, the fall time of the modulation obtained in this work was about 6 μ s, which is significant compared to the lifetimes measured here (between 30 and 50 μ s). As the blade of the mechanical chopper covers a Gaussian spot, the leading and falling edge produces a time-dependent pump intensity and consequently a time-dependent population density in the 3P_0 state, distorting the fluorescence decay. This is normally dealt with by discarding fluorescence decay data which occurs too soon after the pump turn-off. It may be shown that the intensity of the pump as a function of time follows

$$I(t) = I_0 \left[\frac{1}{2} \operatorname{erfc}(t/t_0) \right]. \quad (4)$$

Here I_0 is the initial intensity, t_0 is the turn-off time of the chopper given by $\omega r_1/r_0$, r_0 is the beam radius, r_1 is the radius of the point where the laser strikes the chopper, and ω is the angular velocity. This was used to describe the rise and fall of the pump in accordance with the experimental conditions. For a four-level system [11], the distortion of the fluorescence decay time is obtained from the solution of the following rate equation at steady-state:

$$dN_6/dt = I(t) R_{16}(1 - 2N_6) - N_6/\tau_6. \quad (5)$$

Numerical modelling of this equation allows the calculation of the time at which pump modulation ceases to affect the fluorescence decay. This was determined for each decay curve.

The laser beam was focused to a spot and then, after the second objective, re-established close to the original beam diameter (Fig. 2). By placing the mechanical chopper at the focal point the system response was minimised. The response time of the detection circuitry was of the order of 10 ns and was considered to not affect the measurement significantly.

Measurement of the fluorescence decay lifetime was obtained for five different samples having dopant

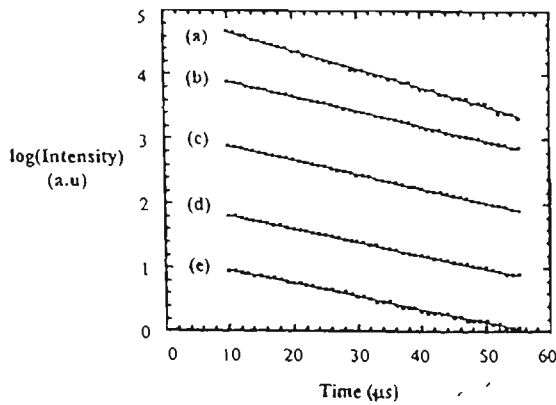


Fig. 3. Fluorescence decay curves for praseodymium-doped samples, (a) 1.0×10^{25} , (b) 2.3×10^{25} , (c) 4.5×10^{25} , (d) 8.9×10^{25} and (e) 24.0×10^{25} ions/ m^3 .

concentrations of (1.0 ± 0.1) , (2.3 ± 0.2) , (4.5 ± 0.5) , (8.9 ± 0.9) and $(24 \pm 2) \times 10^{25}$ ions/ m^3 . The logarithm of the fluorescence intensity as a function of time for these concentrations is shown in Fig. 3. The concentration (ρ) is related to the absorption coefficient $\alpha(\lambda)$ and to the absorption cross-section $\sigma_a(\lambda)$ at the pump wavelength by $\alpha(\lambda) = \sigma_a(\lambda)\rho$. The absorption coefficient was measured using a white-light absorption technique while the absorption cross-section was calculated using Fuchtbauer-Ladenberg (FL) analysis. The FL analysis relates the fluorescence linewidth, the branching ratio and the lifetime of the level (measured in the realm of low concentration) to the absorption cross-section [12]. However the validity of the FL relation has been questioned by other authors [13] who suggest the cross-sections may be up to 20% too low. Adjustments were made by multiplying the calculated cross-section by 1.10 and allowing for an error of $\pm 10\%$. The error in the absorption coefficient was $\pm 8\%$ so that the error in the concentration is $\pm 13\%$. Fig. 4 shows the resultant decay constant ($1/\tau$) as a function of concentration.

As the pump rate to the $^3\text{P}_0$ state is dependent on pump intensity, the diameter of the pump beam was kept relatively large at the sample, ensuring minimal depletion of the ground level population density. As is evident in Fig. 3, no deviation from exponential decay, for all data, was observed which justifies the validity of the previous statement. This also indicates that the energy up-conversion process (term 5 in Eq.

(1)) is relatively small. Since the ground state is minimally depleted, the normalised population density of the ground level can be approximated to unity and Eq. (3) no longer depends on n_1 . This allows Eq. (3) to be written as

$$dn_6/dt = -n_6 \left[1/\tau_6 + \frac{1}{2}(\alpha_{cr1} + \alpha_{cr2})\rho \right]. \quad (6)$$

This has a solution of the form

$$n_6(t) = n_6(0) \exp(-t/\tau), \quad (7)$$

where

$$1/\tau = 1/\tau_6 + \frac{1}{2}(\alpha_{cr1} + \alpha_{cr2})\rho. \quad (8)$$

From Eq. (8) τ is the measured lifetime, $1/\tau_6$ is the sum of the radiative and non-radiative rates and $\frac{1}{2}(\alpha_{cr1} + \alpha_{cr2})\rho$ is the energy transfer rate, and $n_6(0)$ is the population density at level 6 at the end of the pump pulse. Eq. (8) indicates the relationship between the lifetime of level 6 and the dopant concentration. Using this relationship we applied a least squares fit to the data in Fig. 3 to relate the measured lifetime of level 6 with dopant concentration. The sum of the cross-relaxation parameters ($\alpha_{cr1} + \alpha_{cr2}$) was determined to be $(7.1 \pm 0.7) \times 10^{-23}$ m^3/s . Furthermore, in the limit of zero concentration, the lifetime of the $^3\text{P}_0$ state was determined to be (50 ± 1) μs .

Both cross-relaxation processes involve an ion in the $^3\text{P}_0$ excited state interacting with a ground state ion. From our experiments and rate equation models we are unable to distinguish between the two cross-relaxation processes as we have quantified only their

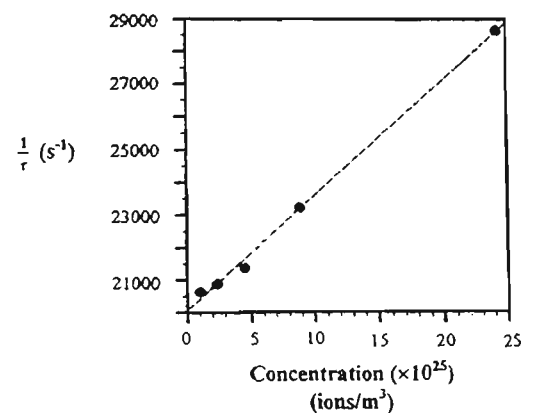


Fig. 4. Measured decay rates as a function of praseodymium concentration.

sum ($\alpha_{cr1} + \alpha_{cr2}$). For the purposes of modelling the system in a laser or amplifier configuration this sum of cross-relaxation parameters is all that is required. However, the relative contributions of the respective cross-relaxation processes depend on the radiative transition rates and branching ratios for the respective transitions. The radiative transition rates for the ${}^3P_0 \rightarrow {}^1G_4$ and ${}^3P_0 \rightarrow {}^1D_2$ are approximately 55.8 and 0.352 s^{-1} respectively [9]. The branching ratio for the ${}^3P_0 \rightarrow {}^1D_2$ transition is negligible [9] and about 1.8% for the ${}^3P_0 \rightarrow {}^1G_4$ transition. As a consequence we may conclude that the (${}^3P_0 \rightarrow {}^1G_4$) and (${}^3H_4 \rightarrow {}^1G_4$) cross-relaxation process is significantly greater than the (${}^3P_0 \rightarrow {}^1D_2$) and (${}^3H_4 \rightarrow {}^3H_6$) process. Thus the cross-relaxation parameter may be attributed to α_{cr1} only.

4. Summary

We have measured the fluorescence lifetime of the 3P_0 state of praseodymium-doped fluorozirconate glass for different concentrations. From these measurements we determined the cross-relaxation parameter, a key parameter required for accurate modelling and qualitative understanding of the optical properties of the material.

Acknowledgements

The authors wish to thank the members of the Photonics Section, at Telstra Research Laboratories, for access to rare-earth doped glass samples.

References

- [1] B.P. Petreski, M.M. Murphy, S.F. Collins and D.J. Booth, *Electron. Lett.* 29 (1993) 1421.
- [2] J.Y. Allain, M. Monerie and H. Poignant, *Electron. Lett.* 27 (1991) 189.
- [3] Y. Zhao, S. Fleming and S. Poole, *Optics Comm.* 114 (1995) 285.
- [4] A.C. Tropper, J.N. Carter, R.D.T. Lauder, D.C. Hanna, S.T. Davey and D. Szebesta, *J. Opt. Soc. Am. B* 11 (1994) 886.
- [5] S.C. Goh, R. Pattie, C. Byrne and D. Coulson, *Appl. Phys. Lett.* 67 (1995) 768.
- [6] Y. Ohishi, T. Kanamori, T. Nishi, S. Takahashi and E. Snitzer, *Photon. Techn. Lett.* 4 (1992) 1338.
- [7] T. Förster, *Ann. Phys.* 2 (1948) 55.
- [8] D.L. Dexter, *J. Chem. Phys.* 21 (1953) 836.
- [9] M. Eyal, E. Greenberg, R. Reisfeld and N. Spector, *Chem. Phys. Lett.* 117 (1985) 108.
- [10] L.S. Lee, S.C. Rand and A.L. Schawlow, *Phys. Rev. B* 29 (1984) 6901.
- [11] M.J.F. Digonnet, *IEEE J. Quantum Electron.* 26 (1990) 1788.
- [12] W.L. Barnes, R.L. Laming, E.J. Tarbox and P.R. Morkel, *J. Quantum Electron.* 27 (1991) 1004.
- [13] B. Pedersen, A. Bjarklev, P. Hedegaard, K. Dybdal and C.C. Larsen, *J. Lightwave Techn.* 9 (1991) 1105.

AMPLIFICATION IN Pr³⁺-DOPED FLUOROZIRCONATE OPTICAL FIBRE AT 632.8 nm

B. P. Petreski, M. M. Murphy, S. F. Collins and D. J. Booth

Indexing terms: Optical fibres, Fibre lasers

Amplification in Pr³⁺-doped fluorozirconate optical fibre is reported at the 632.8 nm He-Ne wavelength. Gross gains up to 11 dB have been achieved in a 1.4 m length using a launched pump power of 315 mW at 476.5 nm. Measurements of extinction at pump and signal wavelengths indicate that significantly improved performance can be expected using a much shorter length of fibre.

Introduction: Pr³⁺-doped fluorozirconate optical fibres have been identified as promising candidates for optical amplification in the second communications window around 1.3 μm , where significant gains have been observed [1, 2]. Pr³⁺ in the fluorozirconate host has a number of other useful transitions and CW lasing has been reported at visible and near infra-red wavelengths [3, 4]. In particular, efficient lasing has been possible on the ³P₀ → ³F₂ transition (Fig. 1) around 635 nm, where the tuning range is broad enough to offer the possibility of useful amplification at the 632.8 nm He-Ne wavelength. Such an amplifier could have applications in optical fibre sensing systems based on this wavelength.

This Letter reports initial data on the gains achieved at 632.8 nm in a Pr³⁺-doped fluorozirconate fibre pumped with 476.5 nm radiation from a CW argon ion laser. Gross gains of

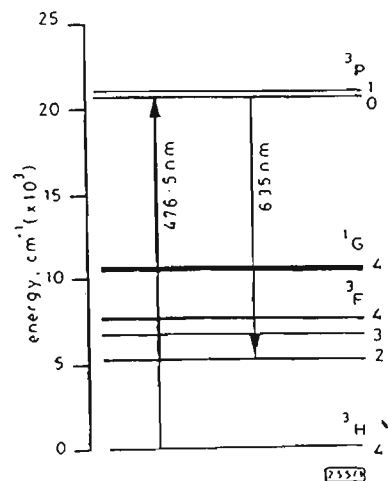


Fig. 1 Energy level diagram for Pr³⁺-doped fluorozirconate fibre

up to 11 dB were realised despite the fact that the amplifier length was not optimised.

Experimental measurements: A range of Pr^{3+} -doped fluoro-zirconate optical fibres with different dopant concentration and core diameter were investigated with specific results reported for 1000 ppm/ $4\ \mu\text{m}$ fibre of length 1.4 m. Absorption, fluorescence and gross signal gain were investigated using the experimental arrangement given in Fig. 2. The 476.5 nm line from the argon ion laser was used as the pump, because it was found that this wavelength best matched the $^3\text{P}_0$ absorption band and resulted in maximum fluorescence at 635 nm. The experimental fluorescence spectrum for this fibre is shown in Fig. 3. The pump radiation and He-Ne probe beam were

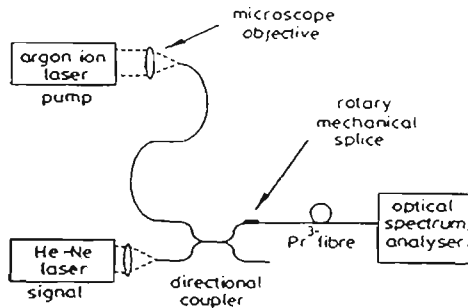


Fig. 2 Experimental arrangement

[25572]

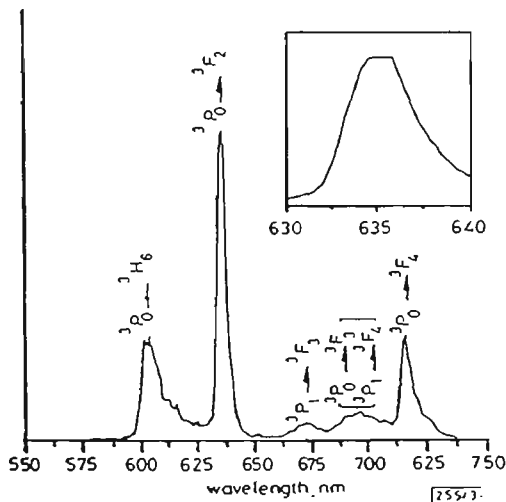


Fig. 3 Experimental fluorescence spectrum for Pr^{3+} doped fluoro-zirconate fibre

coupled into the Pr^{3+} fibre using a $4\ \mu\text{m}$ diameter silica fibre directional coupler, with a splitting ratio of 50 : 50 at 632.8 nm and 96 : 4 at 476.5 nm. The spare arm of this coupler was used to monitor either the signal or pump power injected into the amplifier. An optical power meter or a spectrum analyser was used at the output end of the fibre to measure the exit power and spectrum, respectively. An AT&T rotary mechanical splice enabled low loss injection from the directional coupler into the Pr^{3+} fibre core.

Fig. 4 shows gross gain against pumping power and indicates an amplifier efficiency of 32 dB/W for the 632.8 nm signal. The highest gain achieved at 315 mW was 11 dB, but as this was not easily reproduced the highest repeatable gain of 9.8 dB is indicated in the Figure. The measurement of Fig. 4 corresponds to small-signal gain because it was found that the gains remained constant for input signal powers between 0.5 and 50 μW .

The extinction at the signal wavelength was measured on a number of samples to be between 17 and 20 dB/m. The total attenuation of the pump radiation in the 1.4 m length of fibre was measured to be 63 dB. With 25 μW input signal power, the signal level at the output was measured to be 35 μW without pumping and 334 nW with 315 mW of injected pump power (9.8 dB gross gain)

Discussion: Obtaining representative data for extinction and absorption per metre of the Pr^{3+} fibre proved difficult due to

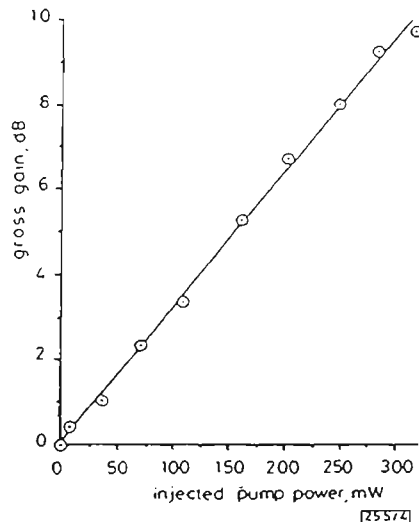


Fig. 4 Gross gain against injected pump power for Pr^{3+} -doped fluoro-zirconate fibre

the variable quality of its core. This was evident from observation of non-uniform fluorescence and scattering along the length of the fibre.

In any fibre amplifier the gain efficiency is dependent on the overlap of pump and signal modes and is optimised by ensuring singlemode operation for both. The Pr^{3+} amplifying fibre was multimoded at both pump and signal wavelengths with normalised frequencies of 4.35 and 5.75, respectively. It is believed that this modal mismatch contributed to instability in the gain measurements, because it was noted that the gain varied with mechanically induced modal changes in either the pump arm of the 3 dB coupler or the amplifying fibre.

It is important to note that only gross gains were achieved in this fibre rather than net gains because the fibre was considerably longer than required for this application. The measured extinction at the pump wavelength of 45 dB/m indicates that the pump radiation was reduced to ~5% of its input value after ~0.3 m of fibre. This is consistent with the observed fluorescence which was negligible beyond the first 0.4 m of fibre. Thus the final 1 m of amplifying fibre contributed little to the pumping and merely attenuated the signal by ~20 dB. If allowance is made for this attenuation then it would appear that a net gain would be achieved in a fibre length of 0.3–0.4 m. The figure quoted here would imply a net gain of ~5.4 dB/m for a 0.4 m length of fibre.

Conclusions: This Letter reports the first measurements of amplification at the 632.8 nm He-Ne laser wavelength in Pr^{3+} -doped fluoro-zirconate optical fibre. Gross gains of up to 11 dB were achieved in a 1.4 m length. Measured extinction at the pump and signal wavelengths indicate that significantly better performance, and possibly net gain, can be expected from a much shorter fibre.

Acknowledgment: The authors acknowledge the Telecom Australia Research Laboratories for the supply of Pr^{3+} -doped fluoro-zirconate optical fibre and K. Clarke for technical advice. The assistance of A. Shelamoff is also appreciated.

© IEE 1993

3rd June 1993

B. P. Petreski, M. M. Murphy, S. F. Collins and D. J. Booth (Optical Technology Research Laboratory, Department of Applied Physics, Victoria University of Technology, PO Box 14428, MMC, Melbourne, Victoria 3000, Australia)

References

- OHISHI, Y., KANAMORI, T., KHAGAWA, T., TAKASHI, S., SNITZER, E., and SIGEL, G. H., JUN.: ' Pr^{3+} doped fluoride fibre amplifier operating at 1.31 μm '. Proc. OEC '91, San Diego, CA, 1991, PD?

- 2 CARTER, S. L., SZABUNIA, D., DAVEY, S. T., WYATT, R., BRIBLEY, M. G., and FRANCEL, P. W.: 'Amplification at $1.31\ \mu\text{m}$ in a Pr^{3+} -doped single-mode fluorozirconate fibre', *Electron. Lett.*, 1991, 27, pp. 628-629
- 3 DURTESTE, Y., MONERIE, M., ALLAIN, J. Y., and POIGNANT, H.: 'Amplification and lasing at $1.3\ \mu\text{m}$ in praseodymium-doped fluorozirconate fibres', *Electron. Lett.*, 1991, 27, pp. 626-628
- 4 ALLAIN, J. Y., MONERIE, M., and POIGNANT, H.: 'Tunable CW lasing around 610, 636, 695, 715, 885, and 910 nm in praseodymium-doped fluorozirconate fibre', *Electron. Lett.*, 1991, 27, pp. 189-190